UNIVERSIDADE FEDERAL DO RIO DE JANEIRO

REBECCA RODRIGUES MATOS

PHASE II METABOLISM STUDY OF STANOZOLOL THROUGH ZEBRAFISH WATER TANK (ZWT) EXPERIMENTAL SETUP AND LIQUID CHROMATOGRAPHY COUPLED WITH HIGH-RESOLUTION MASS SPECTROMETRY (LC-HRMS/MS)

RIO DE JANEIRO

2021

REBECCA RODRIGUES MATOS

PHASE II METABOLISM STUDY OF STANOZOLOL THROUGH ZEBRAFISH WATER TANK (ZWT) EXPERIMENTAL SETUP AND LIQUID CHROMATOGRAPHY COUPLED WITH HIGH-RESOLUTION MASS SPECTROMETRY (LC-HRMS/MS)

Dissertação de Mestrado apresentada ao Programa de Pós-graduação em Química (PGQu), da Universidade Federal do Rio de Janeiro, como parte dos requisitos necessários à obtenção do título de Mestre em Ciências (Química).

Universidade Federal do Rio de Janeiro - UFRJ
Instituto de Química - IQ
Programa de Pós-Graduação em Química - PGQu

Supervisor: Henrique Marcelo Gualberto Pereira

Rio de Janeiro
2021

CIP - Catalogação na Publicação

Matos, Rebecca Rodrigues
MM433p PHASE II METABOLISM STUDY OF STANOZOLOL THROUGH ZEBRAFISH WATER TANK (ZWT) EXPERIMENTAL SETUP AND LIQUID CHROMATOGRAPHY COUPLED WITH HIGH-RESOLUTION MASS SPECTROMETRY (LC-HRMS/MS) / Rebecca Rodrigues Matos. -- Rio de Janeiro, 2021.
125 f.

Orientador: Henrique Marcelo Gualberto Pereira.
Dissertação (mestrado) - Universidade Federal do Rio de Janeiro, Instituto de Química, Programa de Pós Graduação em Química, 2021.

1. Química analítica. 2. Controle de dopagem. 3. Cromatografia Líquida (LC). 4. Espectrometria de Massas de alta resolução (HRMS/MS). I. Gualberto Pereira, Henrique Marcelo, orient. II. Título.

Elaborado pelo Sistema de Geração Automática da UFRJ com os dados fornecidos pelo(a) autor(a), sob a responsabilidade de Miguel Romeu Amorim Neto - CRB-7/6283.

PHASE II METABOLISM STUDY OF STANOZOLOL THROUGH ZEBRAFISH WATER TANK (ZWT) EXPERIMENTAL SETUP AND LIQUID CHROMATOGRAPHY COUPLED WITH HIGH-RESOLUTION MASS SPECTROMETRY (LC-HRMS/MS)

Rebecca Rodrigues Matos

Orientador: Henrique Marcelo Gualberto Pereira

Dissertação de Mestrado submetida ao Programa de Pós-Graduação em Química (PGQu), da Universidade Federal do Rio de Janeiro, como parte dos requisitos necessários à obtenção do título de Mestre em Ciências (Química)

Aprovada por:

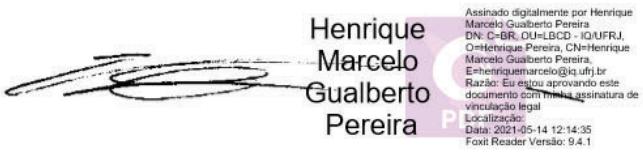

_____

Presidente, Prof. Dr. Henrique Marcelo Gualberto Pereira

_____

Prof. Dra. Cláudia Rezende Moraes

_____

Prof. Dr. José Luís da Costa

Rio de Janeiro – RJ, Brasil

Maio de 2021

For all the curious and brave women out there,
that may be afraid but do it anyway

Acknowledgements

Verdade seja dita, a primeira pessoa a ser grata é a mim mesma. Por ter me aberto a tantas as experiências novas, não ter desistido mesmo quando assoberbada e por meditar lembrando a cada momento que o mais importante é o processo e não o fim.

Em segundo, ao meu orientador Henrique, por ter me adotado como filha acadêmica, dividido comigo seu amor pela profissão e pela ciência de dopagem e embarcado nas minhas mais diversas ideiais. Ao Vinícius, sem cujo o qual não teria chegado aqui até hoje, só pra começar. Seu amor pela ciência acendeu uma pequena chama idêntica em mim. Hoje ela é labareda.

À Minha mãe, por ter desbravado de caminhos inóspitos à florestas densas para tornar minha caminhada mais leve. Por ter me mostrado pelo exemplo que a educação é um fim em si mesma. E ao meu pai, por me lembrar diariamente da minha força interior e que o brilho da minha estrela é mais que suficiente para iluminar meu próprio caminho.

À minha rede de apoio: Jéssica que é desde um ouvido amigo à solucionadora de problemas sempre costurando momentos com risadas, tornando tudo mais leve por onde passa. Mais que isso, é uma das pessas que mais admiro na vida. Sua ética, alegria genuína e compaixão ao próximo me fazem querer ser uma pessoa melhor. Rachel, irmã de alma e agora de casa, cuja demonstrações de paciência e amor também me fazem querer ser uma pessoa mehor. Rafael, meu amor e amigo, quem segurou meu choro algumas ~muitas~ vezes sempre com uma palavra de compaixão.

À amigas de longa data: Carol e Débora, por terem compartilhado comigo tantos momentos.

Aos novos membros do laboratório, Laryssa, Renan, Beatriz e Vanessa que me fazem reviver tão felizmente a surpresa de ver um braço mecânico em movimento e o medo de manusear um orbitrap de muitos dólares. Isso sem contar a felicidade que é ter com quem discutir problemas de pesquisa e planejar experimentos.

À todos os professores do IQ-UFRJ que fizaram parte dessa jornada na UFRJ. Em especial à Marciela.. À toda equipe do LADETEC, desde funcionários da limpeza, administração à TI por fazerem da minha segunda casa um lugar mais acolhedor.

“primeiro,
peguei minhas palavras
cada não posso. *não vou*. *não sou boa o bastante*.
fiz uma fila e dei um tiro em todas
depois peguei meus pensamentos
invisíveis e dispersos
não dava tempo de reunir um por um
joguei água em tudo
transformei meu cabelo em tecido
deixei de molho com limão e menta
coloquei na boca e fui escalando
a trança até chegar na parte de trás da cabeça
fiquei de joelhos e comecei a limpar minha mente
demorou vinte e um dias
ralei os joelhos mas não me importei
não ganhei de presente o ar
do meu pulmão para depois sufocá-lo
esfreguei a falta de confiança até o osso
até o amor-próprio ficar exposto”

Rupi Kaur

Somewhere, something incredible is waiting to be known.

Carl Sagan

RESUMO

MATOS, Rebecca Rodrigues. Phase II metabolism study of stanozolol through zebrafish water tank (ZWT) experimental set up and liquid chromatography coupled with high resolution mass spectrometry (LC-HRMS/MS) Rio de Janeiro, 2021. Dissertação (Mestrado em Ciências) – Programa de Pós-Graduação em Química (PGQu), Instituto de Química, Universidade Federal do Rio de Janeiro, Rio de Janeiro, 2021.

O esteroide anabólico androgênico estanozolol (STAN) é um dos esteroides androgênicos anabólicos mais frequentemente detectados em testes antidopagem em humanos. Por esta razão, seu extenso metabolismo foi exaustivamente estudado. O diagnóstico de seu uso indevido em humanos é alcançado principalmente pelo monitoramento de metabólitos de fase II intactos, conjugados com ácido glucurônico ou sulfato, através da cromatografia líquida acoplada a espectrometria de massas. Os estudos metabólicos são um elemento chave na toxicologia forense, auxiliando no melhor entendimento dos processos biológicos. Como resultado, obtém-se o aumento das janelas de detecção por meio de biomarcadores de longa excreção urinária. No entanto, os estudos de administração em humanos de substâncias tóxicas ou com toxicidade não determinada enfrentam um importante gargalo ético que foi contornado pelo uso de modelos *in vitro* e *in vivo*. Desta forma, o zebrafish (*Danio rerio*) water tank (ZWT) tem emergido como um modelo *in vivo* para o estudo do metabolismo de substâncias não aprovadas para uso em humanos principalmente porque seu genoma, que já foi sequenciado, apresenta importante homologia com mamíferos. Sabe-se que a configuração experimental do ZWT é capaz de produzir metabólitos de fase I do STAN. Portanto, no presente estudo, investigou-se o metabolismo de fase II *in vivo* de STAN por meio do modelo ZWT para determinar se este é capaz de produzir metabólitos relevantes para o controle de dopagem. Para isso, STAN foi adicionado a um recipiente de 200 mL contendo oito peixes a 32 ± 1 ° C, em triplicata. As amostras não invasivas (água do recipiente) foram analisadas com e sem pré-tratamento usando Cromatografia Líquida acoplada a Espectrometria de Massa de Alta Resolução (LC-HRMS/MS) nos modos de ionização positivo e negativo. Como resultado, o metabólito de fase I epímero, 17epi-STAN, e mais dez metabólitos de fase

II foram detectados. Desses, quatro metabólitos hidroxilados na forma sulfatada e outros quatro metabólitos hidroxilados glicoconjugados foram observados, sendo dois dos últimos identificados como 3'OH-STAN-Glucuronídeo e 16β-OH-STAN-Glucuronídeo. Dois derivados STAN-glicuronídeos foram produzidos: um confirmado como STAN-*N*-glicuronídeo e o outro foi identificado como o STAN-*O*-glicuronídeo. Após oito horas de experimento, STAN-*O*-glicuronídeo foi o metabólito de fase II mais produzido. As curvas de bioacacumulação sugerem que altas concentrações de peixes e substrato na água são necessárias para formar os metabólitos da fase II. Além disso, pelas curvas de bioacumulação prevê-se que com o aumento do tempo de experimento, a biossíntese de metabólitos de longa excreção também aumenta. Dessa forma, a partir dos resultados aqui obtidos, novos estudos almejando a obtenção de metabólitos de longa excreção de esteroides poderão ser elaborados. Pelos resultados, infere-se que o estudo estrutural dos metabólitos de fase II por espectrometria de massas requer a utilização de diferentes energias de colisão (baixas e altas) de forma a obter perfis de fragmentação mais diagnósticos.

Palavras-chave: Stanozolol. Zebrafish water tank, LC-HRMS/MS.

ABSTRACT

MATOS, Rebecca Rodrigues. Phase II metabolism study of stanozolol through zebrafish water tank (ZWT) experimental set up and liquid chromatography coupled with high resolution mass spectrometry (LC-HRMS/MS) Rio de Janeiro, 2021. Dissertação (Mestrado em Ciências) – Programa de Pós-Graduação em Química (PGQu), Instituto de Química, Universidade Federal do Rio de Janeiro, Rio de Janeiro, 2021.

The growth-promoting anabolic-androgenic steroid stanozolol (STAN) is one of the most frequently detected anabolic androgenic steroids in sports drug testing. Thus, its extensive metabolism has been exhaustively studied. Its misuse in humans is mainly detected by monitoring intact phase II metabolites as conjugated with glucuronic acid or sulfate moiety by liquid chromatography-tandem mass spectrometry. Metabolic studies are a crucial element in forensic toxicology that aids the better understanding of biological processes, increasing the detection windows through additional biomarkers. However, administration studies in humans of non-approved substances face an essential ethical bottleneck that has been circumvented using *in vitro* and *in vivo* models. In this way, the zebrafish (Danio rerio) water tank has been emerging as an in vivo model for studying non-approved drugs' metabolism mainly because zebrafish's genome, which has already been sequenced, presents substantial homology with mammals. The Zebrafish Water Tank (ZWT) experimental setup can produce phase I STAN metabolites. In the present study, the *in vivo* phase II metabolism of STAN was investigated through the ZWT model to determine whether the ZWT produces metabolites relevant for doping control. To achieve that, STAN was added to a 200 mL recipient containing eight fish at 32 ± 1°C. The noninvasive samples (recipient water) were analyzed both with and without pretreatment using Liquid Chromatography coupled with High-Resolution Mass Spectrometry (LC-HRMS/MS) in positive and negative ionization modes. As a result, four hydroxylated-sulfate and four hydroxylated-glycoconjugate metabolites were formed, two of the last ones being 3'OH-STAN-Glucuronide and 16β-OH-STAN-Glucuronide. Additionally, two STAN-Glucuronide derivatives were produced: one was confirmed to be STAN-*N*-

Glucuronide, and the other was presumed to be STAN-*O*-Glucuronide. After eight hours of the experiment, STAN-O-Glucuronide was the most intense phase II metabolite produced. The accumulation curves suggest that high concentrations of fish and substrate in water are required to form phase II metabolites. In addition, it is possible to predict by the bioaccumulation curves that by increasing the experiment time, the biosynthesis of long-excreted metabolites will also increase. Thus, from the results obtained here, further studies aiming at obtaining metabolites of long steroid excretion may be elaborated. It is also possible to infer that to understand the fragmentation profile of phase II metabolites it is necessary to use low and high collision energies in order to obtain a comprehensive fragmentation profile.

Keywords: Stanozolol. Zebrafish water tank, LC-HRMS/MS.

SUMMARY

LIST OF FIGURES

LIST OF TABLES

LIST OF ABBREVIATIONS AND ACRONYMS

IOC	International Olympic Committee
WADA	World Anti-Doping Agency
AAS	Anabolic-androgenic steroids
AAF	Adverse analytical findings
STAN	Stanozolol
IOC	International Olympic Committee
LTM	Long-term metabolites
GC-MS	Gas chromatography-mass spectrometry
HPLC	High-performance liquid chromatography
TMS	Trimethyl silyl group
HRMS	High-resolution mass spectrometry
16β-OH-STAN	16β-hydroxy-stanozolol
3'-OH-STAN	3'-hydroxy- stanozolol
4β-OH-STAN	4β-hydroxy- stanozolol
LC-MS	Liquid chromatography-mass spectrometry
ESI	Electrospray ionization
3′-OH-STAN-G	3′-OH-STAN-glucuronide
SPE	Solid phase extraction
HSO_4^-	Monohydrogensulfate
STAN-17S	STAN-17-sulfate
3'-OH-STAN-17S	3'-OH-STAN-17-sulfate
16-OH-STAN-S	16-OH-STAN-sulfate
HLM	Human liver microsomes
CYP450	Cytochrome P450
UGT	5'-diphospho-glucuronosyltransferase
ZWT	Zebrafish water tank
UDP-5'	Uridine-5'-diphosphate
PAPS	3'- phosphoadenosine-5'-phosphosulfate
SULT	Sulfotransferases
KT	ketotestosterone
SIB	Sibutramine

IS	Internal standard
EI	Electron impact
ITP	Initial testing procedure
DS	Dilute-and-shoot
TF	Fourier Transform
FWHM	Full Width at Half Maximum
NO_2^-	Nitrite ion
NH_4^+	Ammonium ion
Cl^-	Chlorine ion
MSX	Multiplexing count
NCE	Normalized collisional energy
E_{lab}	Energy plots with the laboratory energy
AnhydroGlcA	Anhydroglucuronic acid

1. Introduction

1.1. Society, sport and the fair play spirit – Why we do what we do?

The sport reflects how society organizes itself, considering differences among States, people, and social classes. The sports institution's importance and prestige have increased through the years and adapted according to the world's reality (RUBIO, 2002). For instance, in Greece's first Summer Olympic Games in 1896, 250 athletes from 13 nationalities competed in 9 different sports. In the last one, Rio de Janeiro's Summer Olympic Games in 2016, over 11.000 athletes from 209 nationalities participated in 28 different sports (PEREIRA et al., 2017). Because of the sports institution's expansion, it is also possible to understand its significance from an economic, social, and political perspective (DIAS; DE SOUSA, 2012; DUVAL, 2017; FOGEL, 2014; HOBERMAN, 1995; RUBIO, 2002).

Since that first competition, the Modern Olympic Movement evolved from an amateur gymnastic regime to a pos-modern professionalized and commercialized element of the contemporary cultural industry (HOBERMAN, 1995; RUBIO, 2002; SEGRAVE, 2007). That shift, driven mainly by mass communication technology's development, created an extraordinary global audience, raising billions of dollars in mega-events as Olympics Games and World Cup. In addition, the money injection of serious corporate sponsorship turned these events into extended extravaganzas of promotional opportunities (HORNE, 2007). Thus, with these need to live with sponsors, commercial space, and new regulations came the *fair play spirit*, the ethical and moral commitment that assures the competition's suitability and the "spirit of sports" (SERRANO-DURÁ; MOLINA; MARTÍNEZ-BAENA, 2020).

Despite fair play being considered the moral nucleus of sport activity, its conception is not simply engaging in good behavior or following the rules. Instead, it has to do with noble but also fair behavior. It must be associate more with justice (related to equal opportunities) than with good behavior itself (SERRANO-DURÁ; MOLINA; MARTÍNEZ-BAENA, 2020). This concept is intrinsically related to sports competition, which reflects values wrapped up in the capitalist system's performance ideology. This may be observed from two different perspectives. On the one hand, winning may be more important than anything, and achieving victory legitimizes any

approach taken to obtain it. On the other hand, developing a fair competition means that sports people must comply with rules and regulations and commit to the ethical principles on which such competition is based (SERRANO-DURÁ; MOLINA; MARTÍNEZ-BAENA, 2020).

Either way, the International Olympic Committee (IOC), World Anti-Doping Agency (WADA), and International Sports Federations assure the fair play spirit mainly through a zero-tolerance drug policy, inhibiting the use of performance-enhancing substances and methods by competitors by testing them (SHARMA, 2017; SMITH; STEWART, 2015). This act of using a prohibited substance or method, called doping, creates unfair advantages, distorting the level of equality in sports competition (WADA, 2014; SERRANO-DURÁ; MOLINA; MARTÍNEZ-BAENA, 2020). With more significant risks involved, such distortions create negative externalities not only at the individual level (permanent damage to health, for example) but also at the aggregate level (such as loss of interest in the mass media), and erode the principle of sport (RENSON, 2009). Thus, according to these global-sport authorities, drug use, which is considered cheating, must be eliminated by imposing severe punishments (SMITH; STEWART, 2015).

It is noteworthy that athletes' reasons to dope are far more complex than the "free-will." The sport represents a fast and legal chance of social and economic ascension. In addition to the cash prizes, the rising prestige related to the search for self-realization is a strong incentive for an athlete to win (AQUINO NETO, 2001). Besides, the intense social pressure, irresponsible coaches, greedy sponsors lead them to exceed their limits. Such incentives can cause athletes to cross legal boundaries to create a cutting edge (AQUINO NETO, 2001). Elite athletes already made it clear that they would try any performance-enhancing substance as long as it is not banned by sports organs (SMITH; STEWART, 2015). Thus, according to the current zero-tolerance politics proposed by the sports legislation organs, there are two main reasons to support the fight against doping that must be considered. First, the potentially harmful effects on athletes' health due to the usual lack of knowledge on certain drugs' toxicity. Second, unfair competition breaks the fair play idealism.

1.2. Stanozolol and its mass spectrometry detection through the years

Anabolic agents represent the most frequently detected class of prohibited substances in doping control. Indeed, from the last WADA statistical data, 44% of the adverse analytical findings (AAFs) were attributed to this class of substances. Within this drug class, 17% of the AAF's were attributed to the misuse of the anabolic androgenic steroid (AAS) stanozolol (STAN) (WADA, 2018). This class of substances has been banned from sports since 1976 by the IOC, as well as by National and International Sports Federations. Due to their long-lasting effects, AAS are mainly misused during training periods, and their use is usually discontinued at some point before the competition (SCHÄNZER; OPFERMANN; DONIKE, 1990). Hence, they are prohibited all times, in –24 h before competition– and out – during training period– of competition, by WADA (WADA, 2020).

That the athletes usually discontinued AAS's misuse before competition hindered AAS's detection by Doping Control laboratories mainly because the analytical procedures at that time did not have high sensitivity and specificity as today. To overcome this dilemma, two non-analytical strategies were proposed. Out-of-competition testing and unannounced tests were introduced during training periods (SCHÄNZER; OPFERMANN; DONIKE, 1990). In addition, the search for new metabolites that may increase an AAS's window of detection opportunity has received particular interest. These metabolites, called long-term metabolites (LTM), are found in urine for a much longer time than the original drug itself (THEVIS; WALPURGIS; THOMAS, 2019; SCHÄNZER et al., 1996).

Hence, dedicated research into the metabolic fate of all times prohibited drugs as AAS, targeting LTM's have been extensively presented in the past. Their implementation into routine sports drug testing combined with improved instrumental sensitivity eventually resulted in a significant increase in AAFs, changing the detectability paradigm for steroids. For instance, the number of AAF's for dehydrochloromethyltestosterone quadrupled in 2013 probably due to the implementation of a new LTM first described in 2012 (THEVIS; WALPURGIS; THOMAS, 2019;SOBOLEVSKY; RODCHENKOV, 2012). In addition, for mesterolone, the phase II metabolite sulfo-conjugate of 1α- methyl-5α-androstan-3,6,16-triol-17-one

was found to be traceable up to 15 days after enzymatic hydrolysis using GC-MS/MS analysis. Thus, given the importance of these and other LTMs for routine doping controls, substantial effort was invested into their chemical synthesis to corroborate the initially putative analyte's structures (POLET; EENOO; COPPIETERS, 2019).

STAN (Figure 1), a 17β-hydroxy-17α-methyl AAS with a pyrazole moiety (*N*-ring) condensed to an androstane backbone, became popularly known through the positive doping case of the Canadian sprinter Ben Johnson, at the 1988 Olympic Games in Seoul after winning the gold medal in the 100 m run (MASSÉ et al., 1989; SCHÄNZER; OPFERMANN; DONIKE, 1990). This historical fact led to extensive and dedicated research on the metabolic fate and urinary excretion of this AAS in order to improve its detection window using urine as the analyzed matrix. At that time, gas chromatography-mass spectrometry (GC-MS) was the primary analytical tool used to monitor the AAS abuse.

In 1990, Schänzer, Opfermann, and Donike performed the first documents STAN human excretion study after an oral administration, isolated the outcome by preparative high-performance liquid chromatography (HPLC), and identified its hydroxylated metabolites by GC-MS after derivatization with trimethyl silyl group (TMS). In this work, the authors observed that STAN is metabolized to a large extent. Since GC-MS is not the proper tool to directly detect phase II metabolites due to their high polarity, the authors observed by indirect means that less than 5% of STAN metabolites are excreted in the unconjugated urine fraction, which means that STAN's metabolites occur majorly as conjugated form.

In 1996, Schänzer *et al*. improved that analysis of this steroid's metabolites using GC coupled with high-resolution mass spectrometry (HRMS). The use of GC-HRMS at 3000 resolution increased the AAFs due its higher sensitivity and specificity when compared to GC-MS. In 116 positive cases for AAS misuse, 75 were identified using only HRMS screening with a general select ion monitoring (SIM) procedure. Thus, the authors defined the phase-I metabolites 16β-hydroxy-STAN (16β-OH-STAN), 3'-hydroxy-STAN (3'-OH-STAN), and 4β-hydroxy-STAN (4β-OH-STAN) (Figure 1) as targets that enlarge the window of opportunity to detect this steroid (SCHÄNZER et al., 1996; SCHÄNZER; OPFERMANN; DONIKE, 1990).

Figure 1 – STAN and its phase I metabolites 16β-OH-STAN, 3'-OH-STAN, and 4β-OH-STAN chemical structures, targets for doping control analysis first described by SCHÄNZER; OPFERMANN; DONIKE, 1990. STAN's rings' names are highlighted in blue, carbon, nitrogen, and stereochemistry positions in bold, orange, and gray, respectively.

The detection of this easily ionized steroid shifted from GC-MS to liquid chromatography-MS (LC-MS) due to the advent of electrospray ionization (ESI) in the turn of the century (POELMANS et al., 2002; POZO et al., 2009a; THEVIS et al., 2005). This amenable ionization technique made it possible to detect the original drug (STAN), its phase I metabolites, and the intact phase-II metabolites such as glucuronides and sulfates that were usually cleaved using β-glucuronidase from *Escherichia coli* and Helix Pomatia (BALCELLS; VENTURA, 2017; SCHÄNZER et al., 2013; TUDELA; DEVENTER; VAN EENOO, 2013).

The primary motivation to detect the intact phase II metabolites without cleaving the glucuronide and/or sulfate moiety is that hydrolysis with β-glucuronidase from *E. Coli* or *Helix Pomatia* could have limitations that may result in the underestimation of some conjugates. None of the enzyme preparations provides complete hydrolysis (FABREGAT et al., 2013; GRAEF; FURUYA; NISHIKAZE, 1977). Thus, the analysis's sensibility may increase by analyzing long-term metabolites, and the detection window would enlarged.

The primary stanozolol metabolites are excreted in urine as glucuronide conjugates. 3′-OH-STAN-glucuronide (3′-OH-STAN-G, Figure 2) is one of the most

relevant target metabolites in human urine, and historically, the most relevant target to be detected after cleavage by GC-MS. In this context, a LC-MS's fast and straightforward procedure using urine as sample was presented by Tudela *et al*. in 2013. Solid-phase extraction (SPE) was used for sample preparation, and no hydrolysis step was required. As a result, the authors observed the intact 3′-OH-STAN-G in positive and negative ionization, what can be explained by the pyrazole ring's basic character and the acid character of glucuronic acid. Besides, the limit of detection for the 3′-OH-STAN-G was 25-50 pg mL^{-1}, which is much lower than any previously described methods. This method extended the detection window of this steroid to 10 days after the single dose ingestion.

It was, however, the phase II epimerized metabolite 17-epimerized STAN-*N*-G (17epiSTAN-*N*-G, Figure 2) described as the most favorable long-term metabolite for doping control purposes by Schänzer et al. in 2013. 17epiSTAN-*N*-G was observed up to 28 days post-administration of 5 mg single dose of the drug to a human volunteer. This was the first time that *N*-glucuronides metabolites of STAN (17epiSTAN-*N*-G, and STAN-*N*-Glucuronide, STAN-*N*-G) were described in their intact form by LC-HRMS/MS and confirmed by reference material means. Interestingly, the *N*-glucuronidation linkage is not cleaved by the β-glucuronidase enzyme. Only β-*O*-glucuronic acid conjugates are reportedly cleaved (GRAEF; FURUYA; NISHIKAZE, 1977; SCHÄNZER et al, 2013). Hence, the combination of hydrolysis and non-hydrolysis experiments can be used as additional confirmation procedures for the presence of *N*-glucuronides metabolites. However, STAN's pyrazole ring possesses two feasible N-atoms (1'N/2'N). Even though the authors confirmed the presence of STAN-N-G and 17epiSTAN-N-G against reference material, the specific nitrogen the glucuronide is linkage was not specified.

To improve the characterization of these LTMs by mass spectrometry, the authors signalized that the *N*-glucuronide loses its glucuronide moiety in collision energy of 35 eV. In comparison, the *O*-glucuronide takes up to 45 eV to lose the same moiety. In this work, the authors also identified the four isomers of glucuronidation after hydroxylation being 3'-OH-STAN-*O*-G, 3'-epiOH-STAN-*O*-G, 16β-OH-STAN-*O*-G, and 4β-OH-STAN-*O*-G. However, no mass spectrometry information was provided concerning the OH-STAN-G metabolites.

In 2015, Thevis et al. performed experiments with collision cross-section computation and suggested the existence of both 1'N- and 2'N-stanozolol-glucuronides. The authors could not unequivocally confirm the position of the N-glucuronides, though. It was not until last year that GÖSCHL et al., 2020 develop and validated an on-line SPE procedure to detect and identify STAN-1'*N*-G and STAN-2'*N*-G. Thus, by using the same excretion urines Schänzer et al used in 2013, Göschl confirmed that 17epiSTAN-1'*N*-G is the main metabolites that extends the detection as described by Schänzer.

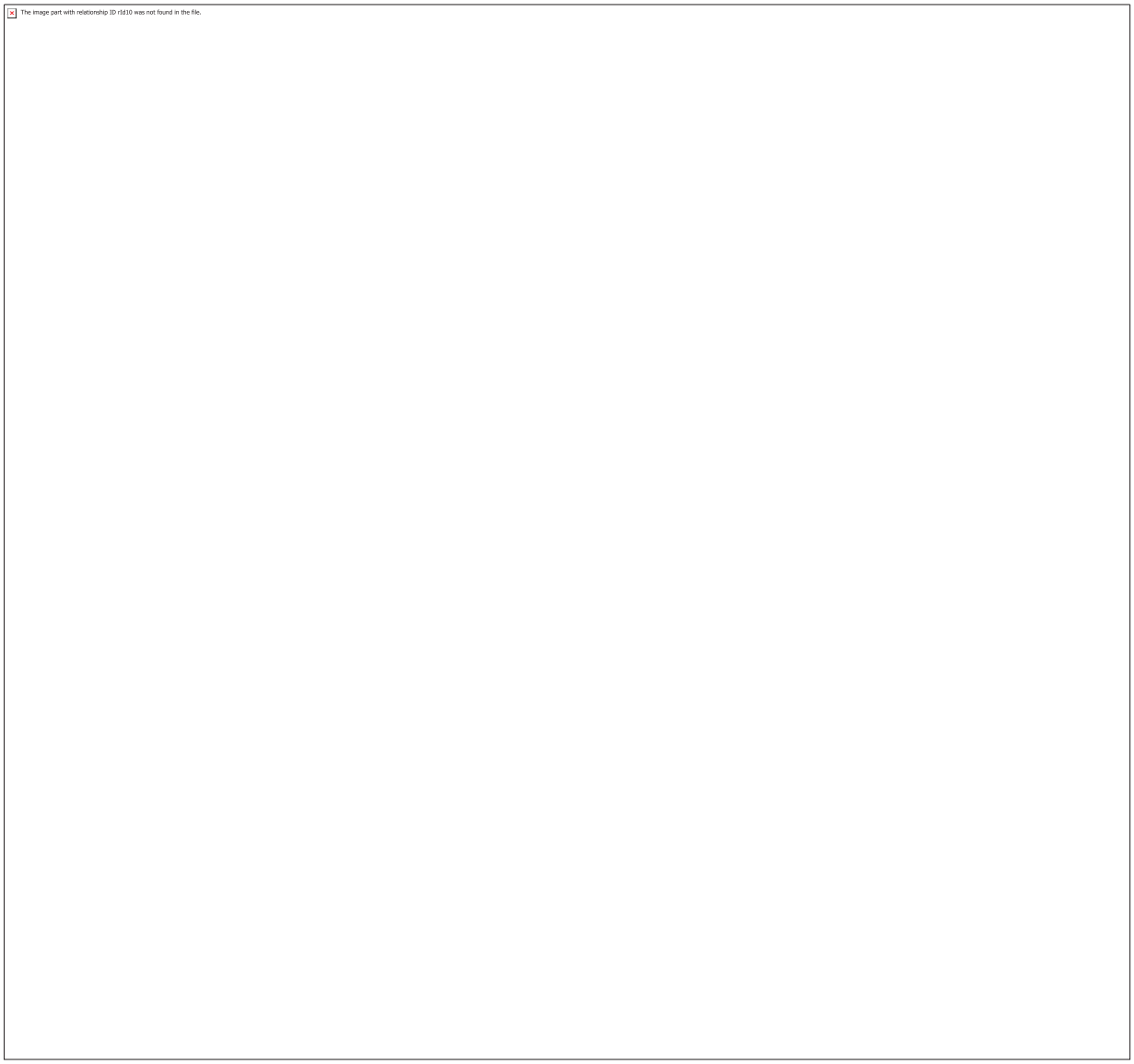

Figure 2 – STAN, and its phase II metabolites 3'-OH-STAN-*O*-G, and 17-epiSTAN-*N*-G chemical structures, targets for doping control analysis first described by TUDELA et al. 2013, and SCHÄNZER et al. 2013, respectively.

Recently, eleven sulfate metabolites (*O*-conjugates and *N*-conjugates) were shown as additional markers to detect STAN misuse (BALCELLS; MATABOSCH; VENTURA, 2017). As expected, the authors observed that sulfation at the 17β-hydroxy of a 17β-hydroxy-17α-methyl steroid is unstable and spontaneously decomposes, undergoing a loss of HSO_4^- resulting in reactive electrophilic carbocation intermediates, subsequently submitted to inversion of configuration producing mainly its epimerized form (Figure 3) (YI et al., 2006; SCHÄNZER; OPFERMANN; DONIKE, 1992). Among the unstable synthesized products, STAN-17-sulfate (STAN-17S) and 3'-OH-STAN-17-sulfate (3'-OH-STAN-17S) were detected immediately after the synthesis procedure, and, 24h later, the corresponded 17-epimerized product was also observed (Figure 4). 16-OH-STAN-sulfate (16-OH-STAN-S) was synthesized and evaluated as a stable product. Interestingly, the authors suggested most of the stable sulfoconjugation site at the pyrazole moiety of stanozolol, supported (among others) by the fact that ESI allowed only for deprotonation and not for protonation of the analyte (Figure 4). Nevertheless, none of these identified sulfoconjugated urinary metabolites allow further extending earlier accomplished detection windows (SCHÄNZER et al., 2013; BALCELLS; MATABOSCH; VENTURA, 2017). On the other hand, this study complemented the knowledge on the anabolic agent's metabolic pathway. Therefore, the comprehensive detection of phase-II metabolites for stanozolol has already been demonstrated as the correct strategy to be employed to characterize AAS misuses profiles in doping control.

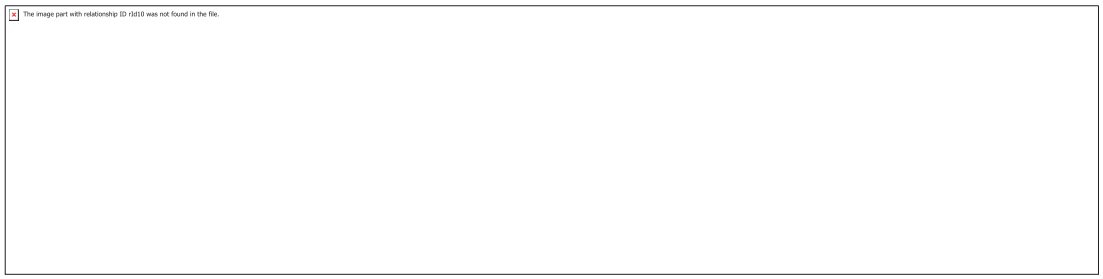

Figure 3 – Reaction scheme for the 17-epimerization of STAN. 1, 17β-hydroxy-17α-methyl STAN, 2. Sulfation of STAN, 3. Loss of sulfate moiety yield a tertiary carbocation; 4. Hydroxylation (adapted from: SCHÄNZER; OPFERMANN; DONIKE, 1992).

Figure 4 – Sulfate STAN metabolites first described by BALCELLS et al. 2017. From left to right: STAN undergo phase I reaction adding a hydroxyl group at 16β carbon (16β-OH-STAN), and further is sulfataded on this same position generating a stable phase II metabolite (16β-OH-STAN-S); Sulfated moiety is directedly added to STAN in 1N position hindering the protonation of the molecule, generating a stable metabolite (STAN-1N-S); Direct sulfation (phase II reaction) of the original molecule at 17β oxygen is also possible generating an unstable sulfate metabolite (STAN-17S) that decomposes to its epimerized form (epiSTAN); STAN undergo phase I reaction adding a hydroxyl group at 3' carbon (3'OH-STAN), and is further sulfated on 17β hydroxy position generating an unstable phase II metabolite (13'-OH-STAN-S) that is further decomposed to its epimerized form (3'-OH-epiSTAN).

Taking the abovementioned into consideration, STAN has a well-elucidated biotransformation behavior. Thus, it is an exciting choice of substance model to elucidate ZWT's capabilities to produce long-term phase II metabolites, as sultates, *O*-glucuronides and *N*-glucuronides.

Because of the increasing number of new drug candidates and therapeutical approaches available, the analytical testing methods of doping control laboratories need to be developed and improved constantly. Along with instrument improvement, physiology, and pharmacology knowledge refinement, methods of expanding the window of opportunity for detecting the illicit use of AASs have also been the subject of intense research in doping control analysis. Thus, new analytical targets, *e.g.,*

metabolites, are continually updated (PROTTI; MANDRIOLI; MERCOLINI, 2019; THEVIS et al., 2018). Using metabolites as targets reduces the risk of outside samples' contamination. Furthermore, it can potentially prolong the detection time of analysis. In this way, the LTMs used as analytical targets is one of the strategies that provide the testing authorities a high level of certainty on the anti-doping decision-making process (THEVIS; WALPURGIS; THOMAS, 2019).

Usually, WADA does not require accredited laboratories to adopt standardized analysis methods, which guarantees the laboratory's freedom to develop its analytical approaches. However, to ensure that the analyzes are carried out homogeneously, and the results are reproducible, WADA establishes a base of rules and criteria to be followed. Among them, it is determined that for molecules up to 800 Da, identification should be carried out using chromatography coupled with mass spectrometry (WADA, 2019).

In the '90s, before the popularization of the ESI interface that coupled liquid chromatography with mass spectrometry, the sample analysis of STAN and its metabolites was performed using GC-MS, then GC-HRMS, both with electron impact (EI) ionization (SCHÄNZER et al., 1996; SCHÄNZER; OPFERMANN; DONIKE, 1990). During this time, the analytical methods were drug-class dedicated. This fact means that, because of the drugs' closely related physical, chemical features within one class, it was possible to employ, to a certain extent, one sample preparation/derivatization and analysis protocol for each category of analytes. Thus, each drug class had its analysis protocols (THEVIS; WALPURGIS; THOMAS, 2019).

When Schänzer et al. 1990 established a reliable detection protocol for identifying the unconjugated hydroxylated stanozolol metabolites through a laborious derivatization procedure, the detection limit for metabolites 3'-OH-STAN and 3'-OH-17-epiSTAN reached 1 ng mL^{-1} using CG-MS. The phase II metabolites could not be detected intact by GC-MS. Therefore, the conjugated phase II urinary metabolites were subjected to enzymatic hydrolysis, with β-glucuronidase from *E. Coli* and *Helix Pomatia* juice, prior to the analysis to remove glucuronic acid and sulfate moieties. In addition, the phase II portion was usually estimated indirectly. This estimation involves obtaining the unconjugated metabolite to IS peak area ratio through two different sample preparations: with and without the hydrolysis step. If the metabolite has a conjugated moiety, it is expected that the metabolite peak area of the hydrolyzed sample is greater

than the metabolite peak area without hydrolysis. This fact occurs because the hydrolyzed sample's metabolite peak area comprises the unconjugated metabolite plus the conjugated portion that was cleaved because of the enzyme. Similarly, in the non-hydrolyzed sample, only the unconjugated metabolite is observed, and, therefore, its peak area is smaller than the corresponded hydrolyzed peak (Figure 5).

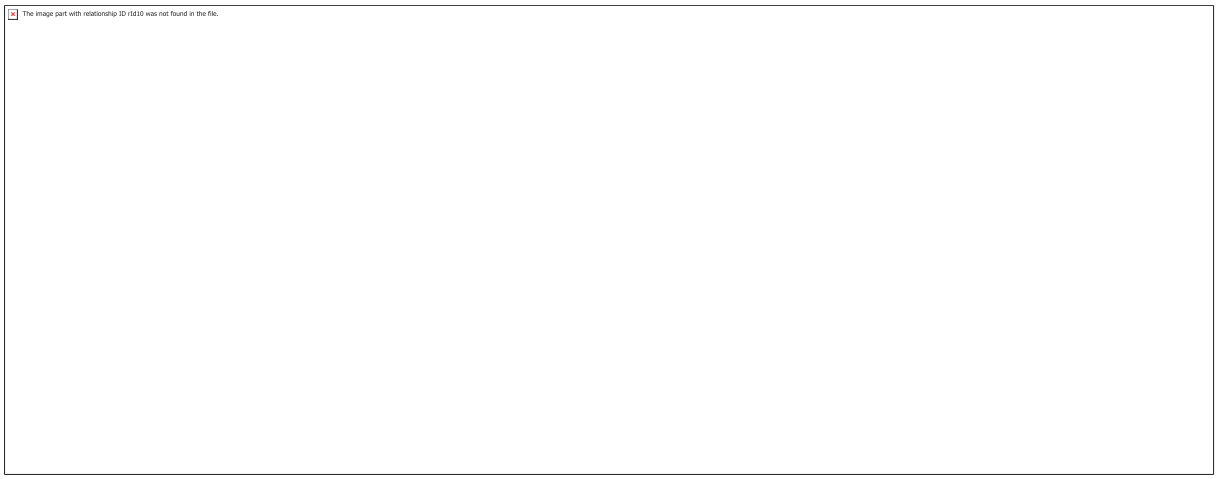

Figure 5 – Top: hydrolysis reaction of 3'OH-STAN-G by β-glucuronidase generating 3'OH-STAN and its glucuronic acid counterpart. GC-MS could measure only the unconjugated portion. Lower part: The hydrolyzed amount of 3'OH-STAN is considered 100%, and the amount of 3'OH-STAN in the non-hydrolyzed sample 5%. Hence, the estimated amount of 3'OH-STAN-G is estimated at 95% (adapted from SCHÄNZER et al. 1990).

Because of the fast-growing demand in routine sports drug testing, boosted by the need to enhance analytical comprehensiveness and sensitiveness as well as to handle swift turn-around analysis times, the drug class dedicated protocols have been replaced by methodology driven approaches since the beginning of the century (THEVIS et al., 2018; THEVIS; WALPURGIS; THOMAS, 2019). Interfacing LC facilitated these improvements to MS by soft ionization techniques, *e.g.*, ESI that transfers ions from the condensed phase to the gas phase at atmospheric pressure (FENN et al., 1989). That STAN has a pyrazole moiety condensed to the steroidal A-ring, aid this AAS and its structural analogs an efficient protonation making them suitable for LC/ESI-MS/MS analysis.

Among the methodology-driven analytical strategies adopted by anti-doping labs to detect prohibited substances, the initial testing procedure (ITP) is the first analytical procedure, encompassing a high-throughput sample preparation and

screening method to detect and identify a prohibited substance and/or a metabolite. In this way, Sardela et al. 2018 developed a comprehensive, straightforward, methodology-driven, targeted screening LC-HRMS/MS-based method to detect more than 450 substances among doping agents and their metabolites in 11 a minute chromatography run. A fast and easy cleanup procedure based on SPE sample preparation and hydrolysis with β-glucuronidase from *E. Coli* was employed.

This SPE sample preparation procedure is based on the use of a solid sorbent through which the sample, generally aqueous, in this case, the water tank (hydrolyzed or not), percolates, allowing the analytes to be selectively adsorbed from the matrix interferents. However, as the SPE usually provides inconsistent recoveries for some polar analytes, such as phase-II metabolites, direct injection of the in natura matrix in the analytical system, so-called dilute-and-shoot (DS), has been used (SCHÄNZER et al., 2013; TUDELA; DEVENTER; VAN EENOO, 2013). Despite the controversies involving this method due to the suppression of the ion signal and changes in the retention time of the analyzes caused by the matrix effects, it is a simple and robust solution for the detection of the wide range of analytes by LC-HRMS in a single injection (SARDELA et al., 2018a).

1.3. Why is it important to study a substance's metabolism for doping control purposes?

A laboratory accredited by WADA needs to cover a complex scope of standards, and requirements and, among these, monitor more than two hundred substances and methods prohibited by WADA (WADA, 2019). These substances are found in an updated and annually issued document and are separated according to their pharmacological activities, structural chemical, and physical-chemical characteristics (WADA, 2020).

In addition to prohibited substances, laboratories usually monitor one or more generated metabolites considering that many drugs are extensively and even completely metabolized before being excreted (THEVIS et al., 2018). Using metabolites as analytical targets can reduce the risk of outside contamination of the samples. Furthermore, their implementation in routine sports drug tests, especially

when combined with improved instrumental sensitivity, can potentially prolong the detection time, increasing AAFs (THEVIS; WALPURGIS; THOMAS, 2019).

An example of extending the detection window using metabolites as targets is the research concerning classics AASs conducted since the 1980s aiming for LTM (SCHÄNZER, 1996). In Figure 6, the AAFs reported by WADA-accredited laboratories for STAN between 2006 and 2018 are illustrated. The two main events to be highlighted are the all-time high of 337 AAFs in 2010, which almost doubled the numbers of 2009, followed by the second-high number of 329 AAFs in 2013. The last event coincides with implementing new LTMs first described by SCHÄNZER et al., 2013, which prolonged the detection window of this substance from 9-14 to 23-28 days after single-dose ingestion. Thus, this data summarizes the importance of metabolism studies of xenobiotics and improved instrumental sensitivity in the search for analytical targets that assist in detecting doping agents.

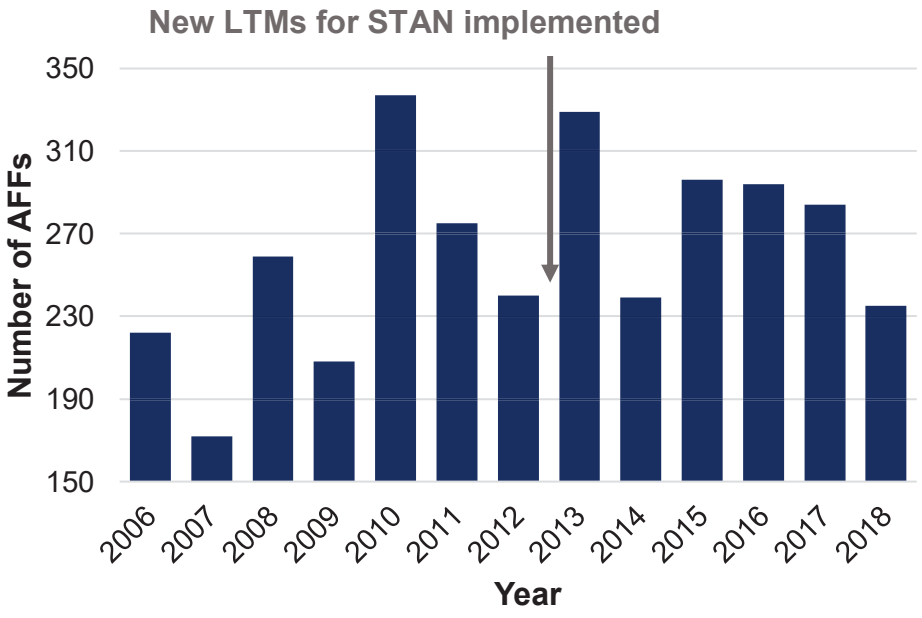

Figure 6 - AAFs reported for STAN between 2006 and 2018. A substantial increase in AAFs was enabled by extending the detection window for the anabolic-androgenic steroid by implementing a newly identified long-term metabolite of the drug.

Despite the recent study performed by SCHÄNZER et al., 2013 in which it was administrated a single oral dose of 5 mg of STAN on two healthy male volunteers and their urine samples analyzed by LC-HRMS/MS, metabolism studies usually present an ethical barrier in humans, especially for not approved substances for use. In this context, the anti-doping community has been switching over to use alternative *in vivo*

or *in vitro* models that can be considered predictive and reliable for metabolism studies (MCKINNEY et al., 2006; SCARTH et al., 2010). In this way, since the metabolism of STAN is well characterized in literature, it has been used to investigate the prediction and reliability of alternative and new metabolism models (REITER et al., 2009).

The liver is considered the primary organ for xenobiotics' metabolic transformations, although other tissues like the kidneys also play an essential role (ALMAZROO; MIAH, MOHAMMAD KOWSER RAMAN VENKATARAMANAN, 2016). Because of its importance, liver tissue is often used as *in vitro* models for human metabolism. The most popular in vitro system is human liver microsomes (HLM) and is a well-established method for investigating the biotransformation of drugs. HLM is easy to use and commercially available. Most of the enzymes present are from the Cytochrome P450 (CYP450) family, but they also contain uridine 5'-diphosphate-glucuronosyltransferase enzymes (UGT), which are the main enzymes involved in phase II metabolism. However, due to the lack of other phase II enzymes, liver microsomes mainly predict phase I metabolites. Since it is an incomplete metabolic system, the results cannot be directly translated to the *in vivo* situation, and the differences are both qualitative and quantitative (BRANDON et al., 2003). The liver can be used to prepare other metabolic models, such as hepatocytes or liver slices. Since these systems are more similar to the whole liver, they are supposed to result in more like the situation in vivo. The drawback is that these models are more complicated to use (ALMAZROO; MIAH, MOHAMMAD KOWSER RAMAN VENKATARAMANAN, 2016).

Due to the complexity of a whole organism compared to *in vitro* studies, *in vivo* models are often adopted for metabolic studies. In general, animals' phase I enzymatic machinery is similar to clinical ones, but metabolite formation's kinetics tend to be different (CHIEFFI et al., 2020). For example, POZO et al., 2009b studied the metabolism of anabolic steroids in mice transplanted with human hepatocytes. The authors have demonstrated some minority hydroxylated metabolites, in contrast to the *in vitro* model hepatocyte cells. Several *in vivo* models for metabolism studies are found in the literature, mainly using rats or mice. Since they are mammals and vertebrates, their genetic correspondence with humans is up to 85% (VAN CRUCHTEN et al., 2010). Flies such as drosophila are also used because they have a brief life span, generous offspring (100 eggs/day), 60% genetic similarity to humans,

and do not involve highly complex costs or logistics for maintenance (CHEN; FEANY, 2005).

1.4. The zebrafish in vivo model to assess xenobiotics' metabolism, and zebrafish water tank (ZWT) experimental setup application to anti-doping purposes

Zebrafish water tank (ZWT) is an experimental design that uses the water tank, instead of the body fluids or tissues from the animal itself. In this alternative *in vivo* model, the zebrafish (*Danio rerio*) excretes the metabolites of xenobionts, such as doping agents, and those can be assessed through highly sensitive mass spectrometry analysis. As other classic models, ZWT is very useful to avoid the expose humans to toxic or potentially toxic substances, circumventing ethical bottlenecks. (ANSELMO et al., 2017; PRADO et al., 2020; SARDELA et al., 2018b, 2020). The use of this small vertebrate is justified by the fact that zebrafish presents a genetic similarity with humans: its genome, which has already been sequenced, has shown that 70% of the human gene has a zebrafish ortholog (ANSELMO et al., 2018).

Zebrafish possess a plethora of phase I and II enzymes, being most of them cloned, expressed, and shown a high level of orthology with human enzymes (GOLDSTONE et al., 2010). Especially for phase II metabolic reactions, glucuronidation is the main detoxification pathway in humans and has shown to be an essential conjugation path in zebrafish (CHNG et al., 2012; JONES et al., 2010; KUROGI et al., 2013; LIU et al., 2010; MOHAMMED et al., 2013; TIERBACH et al., 2018; WANG; HUANG; WU, 2014). The conjugation with glucuronic acid occurs in animals with glucuronosyltransferase after activation of the acid to uridine-5'-diphosphate glucuronic acid (UDP-5'-glucuronic acid). The glucuronic acid is bound to the corresponding molecule by a glycosidic linkage (LEVSEN et al., 2005). Wang, Huang, and Wu (2014) studied the mechanisms by which zebrafish UGT enzymes metabolize endo and xenobiotics by determining their substrate specificity and catalytic activity toward several aglycone substrates, measuring mRNA levels of each of the 40 UGT genes in 11 different adult tissue, and observing if they are expressed in a tissue-specific manner. As a result, the authors observed that steroids, which in humans are predominantly glucuronidated by members of the UGT2 family, are mainly conjugated by members of the UGT5 family in particular UGT5A5, UGT5B2, and UGT5E1 in

zebrafish. Thus, this experimental design can perform phase I – oxidation, hydrolysis, and reduction –, and phase II –conjugation– metabolism.

Sulfation plays a vital role in the detoxification process as well. For instance, xenobiotics are readily conjugated with a sulfate group from the active sulfate (3'-phosphoadenosine-5'-phosphosulfate (PAPS) catalyze by sulfotransferases enzymes (SULTs) (LEVSEN et al., 2005). The presence of these enzymes superfamily have already been evaluated in zebrafish (KUROGI et al., 2013; LIU et al., 2010; MOHAMMED et al., 2013) sequences encoding Zebrafish SULTs gene sequences have been identified, cloned, expressed, purified, and characterized. The activity of SULT enzymes have been tested and SULT3 and SULT4 showed strong activity toward endogenous steroidal compounds such as dehydroepiandrosterone, pregnenolone, and 17β-estradiol (MOHAMMED et al., 2013)

In general, the ZWT experimental set up consists of three different types of tanks: (Figure 7.1.1) the treated tank added the doping agent previously solubilized in an appropriate solvent, preferably water, and the fish – in triplicate; two negative controls: (Figure 7.1.2) with fish, without substance, and (Figure 7.1.3) without fish, with substance. Thus, (Figure 7.2) the aquarium water is sequenced collected through a specific time course, (Figure 7.3) pretreated, and analyzed mainly by (4) chromatography coupled with mass spectrometry. The target metabolites, either previous described in the literature or rationalized by common metabolic reactions, can be characterized by their (Figure 7.5) retention time and (Figure 7.6) fragmentation pattern (Figure 7.6) (ANSELMO et al., 2017; CASTRO et al., 2020; MATOS et al., 2020, 2021; PRADO et al., 2020; SARDELA et al., 2018b, 2020).

The negative controls (Figure 7.1.2 and 7.1.3) are used to check any background activity. This is performed by comparing the metabolite's exact mass in both the negative controls chromatograms, with fish/without drug and with drug/without fish. If the searched metabolite is observed in the former – with fish/without drug – its productions may be justified by the fish's endogen metabolism –and not by the metabolism of the xenobiotic itself. If the aimed metabolite is observed in the last control - with drug/without fish – its presence may be due to a degradation of the molecule in water or its metabolization by biota microorganisms. If an increase in the metabolite production is observed in the treated tank compared to the negative controls, it can be associated with fish excretion.

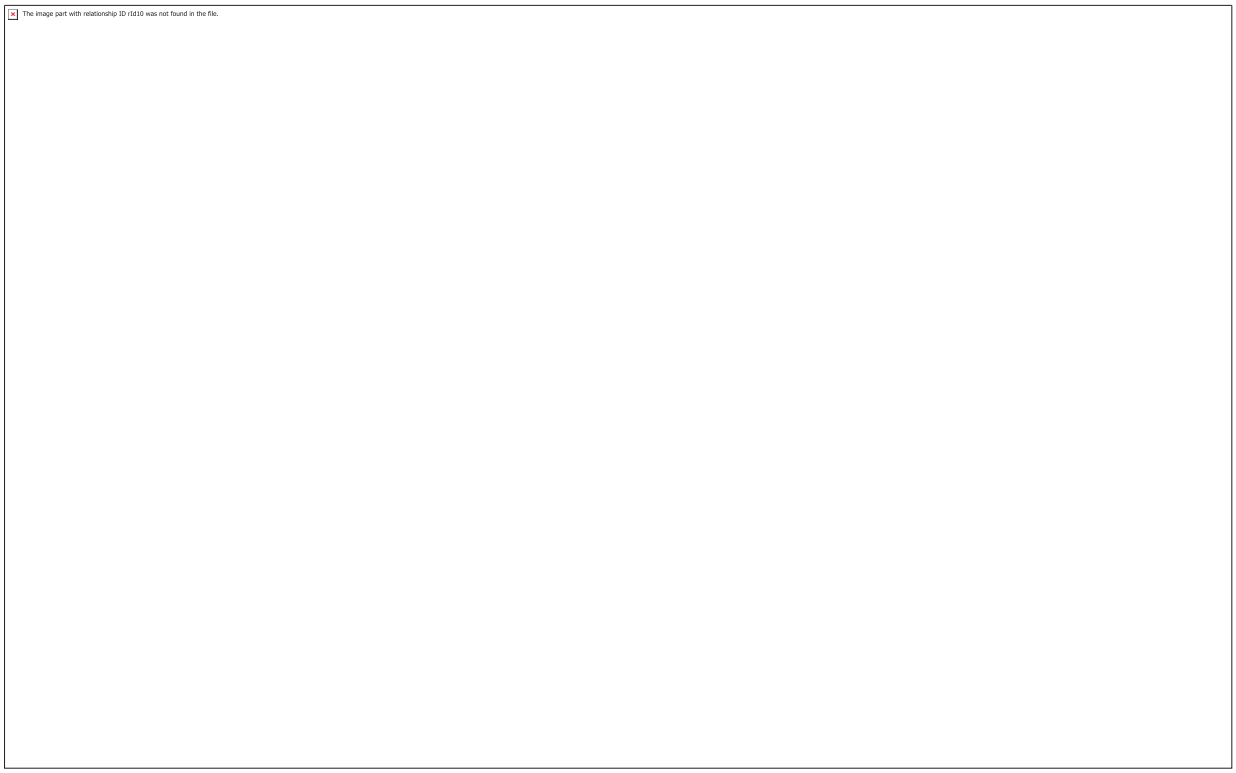

Figure 7 – Zebrafish water tank experimental set up consists of three different types of tanks: (1.1) treated tank – contains doping agent, and fish, in triplicate; two negative controls: (1.2) with fish, without substance, and (1.3) without fish, with substance. After the beginning of the experiment, the (2) aquarium water is sequenced collected through a specific time course. The (3) samples are pretreated and analyzed by (4) chromatography coupled with mass spectrometry. The target metabolites are characterized by their (5) retention time and (6) fragmentation pattern. Additional (7) bioaccumulation curves can be drawn.

Among the reasons to choose the water tank as the analyzed matrix is that the small body size of zebrafish makes blood sampling challenging to be performed, and the amount of blood per individual is small (FÉLIX et al., 2013). In addition, the use of whole-body homogenate, which implies sacrificing the animal, hampers sequential sampling. Hence, it is not possible to obtain an overall behavior of excretion through time. Besides, fish excrete xenobiotics and steroid hormones into the water either through the gills via passive diffusion or urine and feces (FÉLIX et al., 2013).

Taking this fact mentioned above into consideration, Félix et al. 2013 proposed and validated a non-invasive method to assay the steroid hormones cortisol and 11-ketotestosterone (KT) from zebrafish holding-water and compared with plasma levels. After pretreatment using SPE C_{18} and analysis via specific immunoassays, the authors

found that cortisol levels observed in plasma correlate with the observed in the holding water. However, there was a lack of correlation between plasma and water levels of KT. Furthermore, a significant sex difference when measuring KT levels, both in circulating levels, and released rates, was observed. Males release higher concentrations of androgen KT to water than females. In conclusion, although it is possible to infer some level of correlation between the circulating levels of metabolites and the aquarium water, it may depend on each drug's excretion pattern, its water-solubility, and its metabolites. Thus, to validate this experimental setup as an alternative *in vivo* model, the correlation between the amount of metabolites in the water tank and the circulated fish system should be measured for each drug studied. Furthermore, by identifying the metabolites in the fish's blood, its identification in the water can be attributed to fish production.

The ZWT experimental setup uses adult fish because their enzymatic machinery is completely developed. Besides, there is no need to build up a vivarium structure necessary when embryos and larvae are used. That the ZWT is less expensive, easier to handle, and has a higher reproductive rate makes it a viable alternative to the classic mammalian models (SARDELA et al., 2018). The matrix analyzed is cleaner than urine, tissues, or blood, which lowers the background noise, increases the specificity, and selectively. This fact makes easier the task of finding low concentrated metabolites.

Anselmo et al. 2017 demonstrated that 12 zebrafish kept in an aerated 4L tank water at (26 ± 2) °C (Figure 8.1 and 8.2) performed phase I and II metabolic reactions in STAN and Sibutramine (SIB) (Figure 8). The authors analyzed the aquarium water using liquid chromatography high-resolution mass spectrometry (LC-HRMS/MS). As a result, for STAN, the authors observed mono and di-hydroxylation metabolites at different positions on the androgen backbone, demethylation, hydroxyl reduction, and combination of these reactions after 24 h until 168 h of experiment. The authors confirmed the presence of 16β-OH-STAN by comparing the reference standard and depicted it as the major metabolite found after 168 h of the experiment. None of the metabolites were observed in the negative controls. Besides, the authors poorly observed STAN’s phase II metabolites. A much lower amount of glucuronide after mono, di-hydroxylation, methylation, and hydroxyl reduction was presented. However, the authors argued that the sample preparation which consisted in the dilution of a equal part of water tank in methanol was not appropriate to observe the phase II

metabolites. In addition, another hypothesis raised is that even if the ZWT set up produce the target metabolites it may be extremely diluted in the water tank since the authors used a low concentration of fish (3 fish L^{-1}) and amount of STAN (0.25 µg mL^{-1}). Hence, to this hypothesis be checked, a more appropriate ZWT experimental set up and sample preparation need to be used.

Figure 8 - Zebrafish water tank experimental set up applied by Anselmo et al. 2017 consisted of (1) 4 L water tanks containing 12 fish, and 0.25 µg mL^{-1} of STAN or 3.75 µg mL^{-1} of SIB displayed as the treated tank – contains doping agent, and fish, in triplicate; two negative controls: with fish, without substance, and without fish, with substance. After the beginning of the experiment, the (2) aquarium water is sequenced collected through 169 h. The (3) samples are pretreated and analyzed by (4) LC-HRMS/MS. 16β-OH-STAN and *nor*-sibutramine were characterized against reference material (5) retention time, and monohydroxilation, dihydroxylation of STAN and bis-demethylation, and monohydroxilation of SIB were elucidated according to their (6) fragmentation pattern (adapted from Anselmo et al. 2017).

Phase II metabolites of xylazine, a phenothiazine derivative, were indirectly observed by Matos et al., 2020 in a same manner as discussed in the item *"1.2. STAN detection through the years"*. The authors performed two different SPE sample preparation, with and without hydrolysis with β-glucuronidase and analyzed by LC-HRMS/MS. The aglycons to IS peak area ration were evaluated and, as a result, the

authors observed a higher amount of aglycon in the hydrolyzed sample than the non-hydrolyzed on. It was inferred that ZWT was capable of glucuronidation the model xenobiotic. However, no details concerning the identity of the phase II metabolites was provided.

One of the significant advantages of this setup is that it is highly versatile and modulable. In other words, the experimental setup may be adapted depending on the aimed experiment's outcome. For instance, Sardela et al. 2018 used a multivariate experimental design, Dohelert design, to evaluate how the number of fish, amount of drug, and time course of the experiment may interfere with the outcome of the experiment. As a result, the authors observed that 168 h, 18 fish and 15 mg of SIB are desirable to obtain the short and long excretion SIB metabolites. Another conclusion was that adapted experimental setups could be used as long as the model's response to the drug is known depending on the desirable outcome.

Prado *et al*. 2020 further adapted the previous experimental setup scaling it down using 200 mL of water, eight fish, eight h and 0.5 µg/mL during 8 hours of experiment to study the phase I metabolism of five different cathinones. The samples were collected, pre-treated analyzed using liquid chromatography high-resolution mass spectrometry (LC-HRMS/MS). As a result, phase I metabolism reactions as hydroxylation, oxidation, and reduction were observed. Thus, it could be concluded that the scaled down experimental set up used suited the need to obtain phase I metabolites of xenobionts. However, no phase II metabolite was evaluated.

Besides obtaining the retention time of metabolites and fragmentation spectrum of each metabolite, it is also possible to visually evaluate correlations of excretion rates in a graphic of bioaccumulation of the metabolites (Figure 7.7). In this graphic, the metabolite to the internal standard (IS) peak area ratio is plotted against the experiment's time course, and it is possible to evaluate the metabolite formation and/or consumption. In these graphics, it is possible to observe which metabolite is preferably excreted and which time course has a higher excretion rate. For instance, Sardela et al., 2020 studied the metabolic behavior of testolactone, a potent steroid aromatase (CYP19A1) inhibitor derived from progesterone in ZWT. The authors used the bioaccumulation graphics to track endogens modifications that the adding of testolactone may have caused to the fish. As a result, testolactone in the ZWT caused a rise in testosterone and androstenedione in the water tank, similar to that in human

serum. From these findings, the importance of elaborating a bioaccumulation curve is exemplified. This is only possible due to the sequential sampling of the aquarium water.

The potential of ZWT experimental set up to produce phase I and short term metabolites have extensively been proved (ANSELMO et al., 2017; DE SOUZA ANSELMO et al., 2018; MATOS et al., 2020; PRADO et al., 2020; SARDELA et al., 2018b, 2020). The knowledge surface concerning ZWT's ability to produce phase II metabolites has nearly been scratched, though (ANSELMO et al., 2017; MATOS et al., 2020). Therefore, it is of utmost importance to investigate the model metabolic behavior targeting these metabolic products due to the importance of phase II and LTMs metabolites to anti doping purposes. Hence, since the ZWT metabolism model has been systematically used to understand doping agents' biotransformation pathways, it is essential to rationalize its capabilities and applicability concerning the phase II metabolic reactions.

1.5. Analytical workflow for metabolite detection by LC-orbitrap-HRMS/MS

After the LC separation, the ions state switch from aqueous to gaseous at atmospheric pressure using ESI and continuously enter the hybrid Q-Exactive system, progressively traveling to a high vacuum (SARDELA et al., 2018a). ESI made it possible to analyze thermally labile low molecular substances (e.g. highly polar functionalized molecules as phase II metabolites of STAN) (DA CUNHA PINTO et al., 2016; LEVSEN et al., 2005). The ions are focused by the S-lenses to the first quadrupole type mass analysis, considered a mass filter with unit resolution. However, the instrument is versatile and capable of being coupled to high resolution analyzers as orbitrap (THEVIS et al., 2005).

Because ESI is a soft ionization method - which typically does not promote extensive fragmentation at source (except for the molecular ion) - it is commonly used in mass spectrometers equipped with collision cells to induce fragmentation (SARTORI et al., 2014; DA CUNHA PINTO et al., 2016). The collision cell generates an MS^2 (or HRMS/MS) spectrum where the generated fragmented ions are detected in the second analyzer, a high resolution like the orbitrap. Fragmentation is of utmost importance to generate structural information on molecules skeleton increasing reliability of its identity specially when no reference standard is available (DA CUNHA PINTO et al.,

2016; DEMARQUE et al., 2016). It is noteworthy that this work aimed to adapt and apply previously validated methods due to its readiness, simplicity, and robustness (SARDELA et al., 2018a; SCHÄNZER et al., 2013).

Before entering the orbitrap, the ions pass through the C-trap. This ion trap device reduces the ions' kinetic energy, store and accumulate a significant population of ions that can go either to ways: be readily injected into the orbitrap analyzer or go to a collision cell producing fragments traveling back to the C-trap and being subsequent injected into the orbitrap. The orbitrap consists of a central axial electrode and an outer electrode which traps the ions in an electrostatic field, allowing them to rotate around the inner (central) electrode in harmonic oscillations. After the central electrode's potential reaches its constant level, stable orbits are obtained, and detection begins by relating the frequencies of harmonic oscillations to the ions' *m/z* values. The angular velocity and radius of ions orbits are inversely proportional to *m/z*. Thus, larger masses have smaller angular velocity and larger orbits, while smaller *m/z* have higher velocities and smaller orbits. The detection of the orbitrap's signal is followed by a Fourier Transform (TF) to convert the signal into frequency and then into the *m/z* spectrum (MAKAROV; SCIGELOVA, 2010).

Given metabolic studies and structural characterization, using the high resolution of mass spectrometry (17,000 to 140,000 Full Width at Half Maximum, FWHM) is decisive since the mass accuracy of less than 5ppm allows assigning a single elemental composition given *m/z* candidate, therefore increasing the analysis sensitivity (CASTRO et al., 2020; SARDELA et al., 2018a). Among the practical experiments to elucidate the presence and identity of a substance, Full-MS dynamically acquire all protonated or deprotonated ions without filtering a specific one within a specified *m/z* range. The full-Ms chromatogram, called total ion chromatogram, makes it is possible to extract a specific protonated or deprotonated ion as a so-called extracted ion chromatogram. Multiple fragmentation (HRMS/MS) events may run in parallel to full-MS (SARDELA et al., 2018a).

The metabolic study workflow begins by inferring the putative metabolite's structure-elemental composition/*m/z* ratio based on classical CYP-mediated metabolic pathways and/or literature data (PRADO et al., 2020). Once this massive amount of data is obtained, each putative metabolite's exact mass is extracted from full-scan mode total ion current evidencing its presence or not. The treated tanks extracted ion

chromatogram are compared with the positive and negative control tanks to support this process. After a chromatography peak highlights a putative metabolite's presence, the targeted product ion scan HRMS/MS experiments on precursor ions of various (hypothesized) metabolites are obtained, allowing the fragment elemental composition and thus to infer structures by comparing with data from the literature. These data-independent acquisition experiments already demonstrated the improvement of the method sensibility (ANSELMO et al., 2017; MATOS et al., 2021; SARDELA et al., 2020).

2. Aim

The research presented in this dissertation aims to investigate the phase II metabolism of STAN using the *in vivo* model, zebrafish, through the experimental design zebrafish water tank (ZWT). To achieve this, liquid chromatography coupled to high-resolution mass spectrometry was used.

This dissertation specifically aimed to address the following pending questions:

- *Can the ZWT model produce phase II metabolites of STAN?* Since phase II metabolites usually extend the detection window of an AAS, it would be interesting to evaluate if this metabolic model can perform this type of reaction. STAN has an extensive and well-elucidated metabolism behavior in humans, generating *O*-glucuronides, *N*-glucuronides, *O*-sulfates and combining these to phase I reactions. Given the relevance of this prominent substance model, this study aims to characterize the ZWT's phase II metabolites of STAN by LC-HRMS/MS;

- *Is it possible to characterize STAN's biotransformation products employing LC-HRMS/MS*? Detailed knowledge concerning MS behavior of AASs and their structural analogs have gained more importance to provide important information on structural characteristics of analytes and allow utmost confidence in target analyte identification. In view of characterizing ZWT's phase II metabolites that do not have reference materials available, it would be useful to obtain their experimental fragmentation profile (E_{plots}) under the established conditions;

- *Can the kinetic behavior of STAN be inferred from phase II metabolites bioaccumulation curves are described, and the concentration of phase-II metabolites be estimated against reference material?* The bioaccumulation profile of ZWT's metabolites depends on the experimental setup used. In order to future works modulate the model to obtain a desirable outcome, it is crucial to obtain an accumulation curve for phase II metabolites of STAN.

3. Materials and Methods

3.1. Chemicals and reagents

STAN and the STAN metabolites 17epi-STAN-*N*-G, 16β-hydroxy-stanozolol (16β-OH-STAN), and 3'OH-STAN-*O*-G were purchased from the National Measurement Institute (Sydney, Australia). Methyltestosterone (internal standard; IS) was purchased from Sigma-Aldrich (São Paulo, Brazil). Formic acid, acetic acid, ammonium formate, sodium phosphate, acetonitrile, and methanol used were of analytical or HPLC grade and were purchased from Tedia, Fairfield, USA. β-glucuronidase from *Escherichia coli* was acquired from Roche (Rio de Janeiro, Brazil). Ultrapure water (18 MΩ/cm) was obtained from a Milli-Q Millipore water system (Burlington, MA, USA). Strata-X-CW, weak cation mixed-mode polymeric sorbent (30 mg, 3 mL) solid-phase extraction (SPE) cartridges from Phenomenex (São Paulo, Brazil) were used.

3.2. Zebrafish water tank (ZWT) model

Acclimation of zebrafish

Adult zebrafish (*Danio rerio*) of mixed-sex, from 3 to 5 months age were obtained from a local provider (Terra dos peixes ornamentais LTDA; CNPJ: 04.459.162/0001-43) and acclimatized to groundwater in tanks with circulatory pumps partially modified with the charcoal filter withdrawn (Atman Hf100 filter 160L/h; Guangdong, China) for a minimum of five days before the experiments. The fish were kept at a temperature of 28 ± 1 °C, in a 12h–12h circadian cycle (light/dark), fed three times a day with tetramin® fish food, composed of fish derivatives, vitamins, and minerals. The feeding stopped one day before the experimental phase started. To assure the fish's wellbeing before and during the experiments, the water's pH was tested every day. The presence of nitrite (NO_2^-), ammonium (NH_4^+), and chlorine (Cl^-) were also tested with LabconTest. The Ethics Committee on the Use of Animals of the Federal University of Rio de Janeiro approved the project under protocol 065/19.

ZWT setup for accumulation curve

The experiments were performed in 200 mL glass tanks, fitted with a heating device under a temperature of 32 ± 0.5 °C, as it follows:

1) Treated recipient: ZWT treated with the drug previously diluted in water with fish, in triplicate;
2) Positive control: ZWT treated with the drug previously diluted in water without fish;
3) Negative control: ZWT with fish without STAN.

STAN was previously diluted into MiliQ water at a final concentration of 1 µg mL^{-1}. A total volume of 3 mL was collected from all tanks at the following times: 0min (immediately after the drugs were added and mixed), 30min, 1h, 2h, 3h, 4h, 5h, 6h, 7h, and 8h.

3.3. Sample preparation of ZWT for metabolic studies by Liquid Chromatography coupled with High-Resolution Mass Spectrometry (LC-HRMS/MS)

Screening procedure and accumulation curve elaboration

To identify STAN and its phase II metabolites, the sample preparation method was based on Schänzer et al. (2013). Firstly, a methanol solution of IS methyltestosterone (concentration in the final extract: 100 ng mL^{-1}) was dried in a water bath at 40 °C, under N_2 flux, and the evaporated extract was resuspended in 90 µL of the *in natura* tank water and 10 µL of MeOH, 0.1% formic acid (mobile phase B). Lastly, the samples were analyzed through Liquid Chromatography coupled with High-Resolution Mass Spectrometry (LC-HRMS/MS). The human urine from a positive sample was prepared as described above.

Confirmatory analyses - Hydrolysis experiments

To substantiate STAN *N*-glucuronides and *O*-glucuronides' assignment, enzymatic hydrolysis experiments were conducted with and without β-glucuronidase

from *E. coli*. Therefore, as a first step, IS methyltestosterone was added to yield a concentration in the final extract of 100 ng mL^{-1} in 5 mL of ZWT sample 8h post-administration. Secondly, 75 µL of β-glucuronidase was added, and the mixture was incubated for 1h at 40 °C. After, the analytes' concentrations were measured by applying the hydrolyzed sample to an SPE cartridge (C18) preconditioned with 2 mL of water and 2 mL of methanol. After the sample passed through, the resin was washed with 2 mL of ultrapure water and 1 mL of a methanol and water (1:1) solution, and the analytes were removed with 3 mL of methanol: formic acid (95:5, v/v). Finally, the sample was analyzed through the LC-HRMS/MS. Additionally, the sample was extracted without the hydrolysis step (second step). As described above, the minor metabolites were analyzed by extracting 20 mL from the water tanks.

3.4. Instrumental analysis

Thermo Scientific Dionex Ultimate 3000 (Thermo Fisher Scientific, Waltham, USA) coupled to a Q Exactive™ Hybrid Quadrupole-Orbitrap mass spectrometer (Thermo Fisher Scientific, Waltham, USA) equipped with ESI was used to separate and detect the analytes in the water tank. The separation was performed in a reversed-phase column (Syncronis – Thermo, USA, C18, 1.7µm, 50 mm X 2.1 mm) at 40 °C and step-gradient elution. The mobile phases were composed of H_2O with 5.0 mM ammonium formate (A) and MeOH (B), 0.1% formic acid in both phases. The elution profile at a flow rate of 400 µL/min for 11min. The elution program was: 0 to 0.3min, 5% B; 0.3 to 0.5min, 5% to 10% B; 0.5 to 1.0min, 10% to 25% B; 1.0 to 6.0min, 25% to 90% B; 6.0 to 8.0min, 90% to 100% B; 8.0 to 9.0min, 100% B (column washing); 9.0 to 9.1min, 100% to 5% B; 9.1 to 11.0min, 5% B (to equilibrate the column to the starting conditions). The parameters were adapted from Sardela et al. (2018a). The Q Exactive mass spectrometer operated in positive ESI mode. To ensure mass accuracy below 5 ppm, the equipment was calibrated in positive mode with the manufacturer's calibration solution (Thermo Fisher Scientific, Bremen, Germany. The spray voltage was set to 3.9 kV, the capillary temperature to 380 °C, and the S-lens radio frequency level to 80 (arbitrary units). The nitrogen sheath and auxiliary gas flow rates were set at 60 and 20 (arbitrary units). Full-Scan data were acquired in a range of *m/z* 100-800 at a resolution of 70,000 FWHM with automatic gain control of 10^6. Additionally, the target

drugs and their target metabolites were fragmented and analyzed in the second stage of tandem mass spectrometry (Full-Scan/MS^2). The precursor ions were selected based on mass accuracy inclusion lists and a window at ±1.5min to the expected retention times. For these analyses, a resolution of 17,500 FWHM, loop count of 5, multiplexing (MSX) count of 1, and isolation window of m/z 2.0 were used. Normalized collisional energy (NCE) adapted for each substance and metabolite was obtained. Energy plots with the laboratory energy (E_{lab}) variation from 10 to 70 eV with the conditions described above were obtained. Data were evaluated using TraceFinder 3.2.512.0 software (Thermo Fisher Scientific, Waltham, USA).

3.5. Statistical analysis

For the accumulation curves, Grubbs statistical test was applied for the chromatography peak ($^{\mathrm{metabolite}}/_{IS}$) the ratio of each collection time of the three replicates to verify the presence of one outlier value in each edge. Then, the results were expressed with 95% confidence, and the curves plotted as the replicates' average value along with the standard deviation. All the data were analyzed in Microsoft Excel.

4. Results and discussion

4.1. Screening for STAN phase II metabolites

This study assessed the glucuronide and sulfate STAN metabolites using a ZWT experimental setup of 8 fish in 200 mL of water, at 32±1 °C, during 8h of experiment and compared the outcome with a brief overview of a human (elite athlete) metabolism of a post-STAN-administration urine sample. The samples were submitted to a screening preparation procedure and directly injected into LC-HRMS/MS system, *in natura*, without any pretreatment apart from its dilution in mobile phase B (MeOH, 0,1% formic acid) containing internal standard methyltestosterone (100 ng mL^{-1}, $[M+H]^+$ 303.2319).

Methyltestosterone is usually used as IS in the analysis of 17-alkyl substituted anabolic steroids such as STAN (GAMBELUNGHE et al., 2003; LEINONEN et al., 2004; SCHÄNZER et al., 2013) because it full fill the IS expected features of a chosen IS. Its retention time (8.51 min, Figure 9) is similar to STAN's (8.94 min, Figure 9) and its metabolites. The IS intensity presented the same order of magnitude ($\times 10^8$) in all samples (treated ZWT, negative and positive control; positive human sample and negative control Figure 9), discarding any matrix effects as suppression ionic effect even though the sample was injected *in natura* in the system.

Figures 9.a and 9.b present the extracted ion chromatogram of a ZWT sample after 8h of the experiment and a negative control sample (fish without the drug). Figures 9.c and 9.d show a comparison with the extracted ion chromatogram of a positive sample for STAN of human urine and blank (negative) control. While 3'OH-STAN-G and STAN-*N*-G were available as reference material, other metabolic products' characterization required the combined efforts of hydrolysis experiments, interpretation of product ion mass spectra by means of mass accuracy of intact protonated molecules, and loss of glucuronide moiety upon collisional dissociation and energy plots.

For STAN-G isomers ($[M+H]^+$ 505.29083), ZWT produced a minor peak at 7.79 min, confirmed as STAN-*N*-G a major one, two orders of magnitude greater. This latter

peak was not observed in the positive sample of human urine. The late eluting peak was assigned as STAN-*O*-G, described in detail later (refer to Subsection "*4.6. Characterization of STAN-G isomers*"). This *O*-position glucoconjugated metabolite was observed in human urine (SCHÄNZER et al., 2013), although not in the human positive sample used in this work for comparison purposes. When Schänzer et al., 2013 first described the *N*-Glucuronide metabolites of STAN after an excretion study by LC-HRMS/MS, the *O*-glucuronide was the less intense among the three glucuronides (17-epi-STAN-*N*-G, STAN-*N*-G, and STAN-*O*-G). In ZWT, the opposite was observed. STAN-*O*-G was 100-fold more intense than STAN-*N*-G, and 17-epi-STAN-*N*-G was not observed. These events are detailed discussed latter in "*4.7. Phase II metabolic pathway of STAN in ZWT*"

The ZWT treated sample extracted ion chromatogram of OH-STAN-G isomers ($[M+H]^+$ 521.28574) produced four significant peaks. The first two were unobserved in this human positive sample, and the last eluting peak (t_R 8.03 min, Figure 9) was confirmed as 3'OH-STAN-G by means of comparison with reference material. Schänzer et al., 2013 observed three different hydroxylated glucuronide peaks, confirmed employing comparison against reference standard as 16-OH-STAN-*O*-G, 3'-OH-STAN-*O*-G, and 3'-17-epi-OH-STAN-*O*-G. However, no fragmentation spectra were provided by the authors. In a similar way to Schänzer et al.'s 2013 findings, all four ZWT's OH-STAN-G metabolites were *O*-glucuronide (described in details in section "*4.4. Characterization of intact hydroxylated STAN glucuronide (OH-STAN-G) isomers metabolites*").

Figure 9 – Extracted ion chromatogram of a) post-administration ZWT sample collected 8 h after applying STAN to the aquarium water, b) negative control of ZWT model, c) positive human sample, and d) blank urine specimen obtained from screening procedure. The glucuronic acid conjugates, hydroxylated glucuronides, and hydroxylated sulfate metabolites were monitored by the precursor ions *m/z* 505.2908, 521.2857, and 425.2105, respectively in positive ionization mode using a mass tolerance of 5 ppm. The methyltestosterone (IS) was registered with the precursor ion pair *m/z* 303.2319. In comparison to reference standards, structures were assigned as indicated next to each peak.

From the extracted ion chromatogram in positive ionization mode corresponding to the hydroxylated sulfates (OH-STAN-S) isomers ($[M+H]^+$ 425.21046), it was found four peaks in the ZWT sample, three of them observed in the human urine positive urine (Figure 9). Balcells et al., 2018 observed three OH-STAN-S metabolites in positive ionization mode. As explained in detail in section "*4.5. Characterization of OH-STAN-S isomers,"* to be observed in positive ionization mode, the sulfate moiety must be linkage to oxygen, not nitrogen. However, the authors did not characterize them by means of comparison with reference material. Thus, the main phase II STAN

metabolites used as a target for doping control were readily observed in the water tank, even though the ZWT experimental setup was not tuned to increase the overall amount of metabolites (SARDELA et al., 2018b).

The sample is less diluted through the DS method presented in this work (90 µL sample is added to 10 µL of mobile phase B (9:1)) than the one presented by Anselmo et al. 2017 and, therefore, is more suitable to analyze the phase II metabolites. This affirmation is ratified by comparing the phase II STAN's metabolites extracted ion chromatograms (Figure 9) intensities (*i.e.* between 2.08E5 and 2.00E6) to Anselmo et al 2017 obtained intensities (*i.e.* 7.40E3 and 6.61E4). In addition to sample's preparation improvement, the experimental setup modification has also contributed to increasing the amount of phase II metabolites. However, the contribution of these ZWT's setup modification is discussed latter in *"4.6. Phase II metabolic pathways of STAN in ZWT".*

4.2. Complementing the characterization of ZWT's STAN phase I metabolites

Extracted ion chromatogram for STAN ($[M+H]^+$ 329.25874, Figure 10.a) in the treated ZWT sample showed two peaks. The first eluting peak at 8.94 min at an intensity of 1.99E8, and the last eluting peak at 9.22 min 100-fold less intense (2.47E6) (Figure 10.a). The same two peaks were observed the real urine sample but different intensities (Figure 10.c). None of the peaks were observed in the ZWT negative control and human negative control (Figure 10.b and 10.d). Methyltestosterone, the IS, can also be observed in all samples (Figure 10)

The first eluting peak was confirmed by means of comparison with reference material as STAN. The HRMS/MS spectra of STAN at 50 and 70 eV (Figure 10.e and 13.g, table 1) and the last eluting peak at 9.22 min (Figure 10.f and 10.h, table 1) showed the same product ions with similar intensities and with mass accuracy error of 5 ppm. Thus, while the first peak corresponds to STAN, the second smaller peak, named **M1** at 9.22 min, corresponds to the putative 17-epimerized metabolite (summarized in Appendix 1). The only difference between both spectra is the relative intensity of the pseudo-molecular ion $[M+H]^+$ at 70 eV. STAN $[M+H]^+$ 329.2590 intensity is 75% while for putative 17-epi-STAN $[M+H]^+$ 329.2589 is 60%.

Based on observations that 17-epimers of typical 17β-methyl-17α-hydroxy-steroids commonly represent the later eluting species on LC systems operated under conventional C_{18} reverse-phase conditions (SCHÄNZER et al., 2013), the peak at t_R 9.22 min (**M1**) was assigned to the unconjugated 17-epiSTAN. These chromatographic observations agree with Schänzer *et al*. 2013 work for the characterization of STAN-glucuronide and 17-epiSTAN-*N*-Glucuronide. The author has found that the epimerized metabolite of STAN elutes later than STAN-glucuronide. However, besides using the C_{18} reverse phase column, the authors used acetonitrile instead of methanol as the organic phase.

Lootens et al. 2009 studied methandienone's metabolism, a 17β-methyl-17α-hydroxysteroid, using uPA+/+-SCID mouse with humanized liver as metabolism model. The authors analyzed the samples by LC-HRMS/MS using C_{18} reverse-phase with 1 mmol L^{-1} ammonium acetate in water as aqueous phase and 1 mmol L^{-1} ammonium acetate in methanol as organic phase. Among other metabolites, the author has obtained the 17-epimer of methandienone eluting later than methandienone. Thus, it turns out that the 17-epimerized metabolites elute later than the non-epimerized isomer regardless of the elution force of the organic solvent used.

On the other hand, the hypothesis of this last eluting peak (Figure 10.a) corresponds to a phase II metabolite of STAN cleaved during the ESI process was discarded meanly because its retention time does not correspond to any other phase II glucuronide nor sulfoconjugated. Despite the fact that reference material of the 17-epimirized metabolite of STAN was not available, a positive urine sample (Figure 10.c) was used to compare the chromatography and HRMS/MS behavior to ZWT's sample.

The data from of a negative urine control sample was also used for comparison purposes (Figure 10.d). As a result, two peaks in the same retention time as the ones obtained in ZWT were observed. The first one, corresponding to STAN's at 8.94 min and a later eluting second one at 9.23 min, corresponding to the putative 17-epimerized STAN. The presence of an epimer on STAN implies that ZWT is capable of sulfating in Carbon 17, considering the spontaneous decomposition of 17-sulfates of STAN is a mechanism to form 17-epimers of some 17-methylated steroids (SCHÄNZER, 1996).

As expected, the mass accuracy deviations increased as the *m/z* ratio decreased regardless the collision energy employed (Table 1). This is so mainly

because the is more prominent masking effect of isobaric matrix interferences in the smaller mass range, thus contributing to a higher mass error.

Figure 10 – Up part: Extracted ion chromatogram of a) post-administration ZWT sample collected 8 h after applying STAN to the aquarium water, b) negative control of ZWT model, c) positive human sample,

and d) blank urine specimen. All chromatograms were obtained from the screening procedure sample pre-treatment. The STAN was monitored by the precursor ion *m/z* 329.2587, and methyltestosterone (IS) was registered with the precursor ion pair *m/z* 303.2319, both in positive ionization mode with a mass tolerance of 5 ppm. In comparison to the reference standard, the substance's name is assigned as indicated next to each peak. Down part: Product ion spectra of STAN and the putative 17epi-STAN, the last eluting peak at t_R 9.22 min, from a post-administration sample collected 8 h after application of stanozolol in the aquarium water at e) and f) 50 eV and g) and h)70 eV, respectively, using HCD mode and N_2 as collision gas

Table 1 - Elemental compositions of the $[M+H]^+$ ions of STAN and metabolites M1 (17-epiSTAN) and resulting diagnostic product ions obtained from high-resolution/high-accuracy MS/MS experiments from Orbitrap-HCD using positive ESI

Cmp.	Precursor ion (m/z)	Elemental comp. (exp.)	Error (ppm)	CE	Product ion (m/z)	Elemental comp. (exp.)	Error (ppm)
STAN	329.2580	$C_{21}H_{33}ON_2$	2.25	50	311.2481	$C_{21}H_{31}N_2$	0.24
Fig. 13.e					203.1538	$C_{13}H_{19}N_2$	2.34
RT:8.94					149.1070	$C_9H_{13}N_2$	1.91
					95.08591	C_7H_{11}	4.03
					81.0452	$C_4H_5N_2$	5.86
M1	329.2579	$C_{21}H_{33}ON_2$	2.40	50	311.2473	$C_{21}H_{31}N_2$	2.68
Fig. 13.f					201.1380	$C_{13}H_{17}N_2$	2.81
RT:9.22					135.1164	$C_{10}H_{15}$	3.09
					105.0699	C_8H_9	0.22
					81.0452	$C_4H_5N_2$	6.01
STAN	329.2590	$C_{21}H_{33}ON_2$	0.789	70	311.2486	$C_{21}H_{31}N_2$	1.36
Fig. 13.g					271.2166	$C_{18}H_{27}N_2$	0.97
RT:8.94					203.1545	$C_{13}H_{19}N_2$	1.11
					201.1392	$C_{13}H_{17}N_2$	3.11
					149.1073	$C_9H_{13}N_2$	0.17
					105.0703	C_8H_9	4.69
					95.0861	C_7H_{11}	6.00
					95.0609	$C_5H_7N_2$	5.73
					81.0450	$C_4H_5N_2$	3.40
M1	329.2589	$C_{21}H_{33}ON_2$	0.61	70	311.2484	$C_{21}H_{31}N_2$	0.85
Fig. 13.h					203.1544	$C_{13}H_{19}N_2$	076
RT:9.23					201.1387	$C_{13}H_{1]7}N_2$	0.67
					149.1074	$C_9H_{13}N_2$	0.97
					105.0703	C_8H_9	4.41
					95.0861	C_7H_{11}	6.03

Table 1 - Continuation

				95.0609	$C_5H_7N_2$	5.95
				81.0449	$C_4H_5N_2$	2.16

4.3. Indirect evaluation of hydroxylated glucuronide through hydrolysis experiments

Indirectly, the presence of 16β-OH-STAN-G in ZWT was identified. The appearance of a chromatographic peak at 8.23 min after enzymatic hydrolysis experiments was noticed, assigned as 16β-OH-STAN through comparison against reference standard (Figure 11.a). The glucuronide's contribution was estimated and represented as a bar chart (Figure. 11.b). The sum of metabolite peak area to IS ratio before and after hydrolysis was calculated (Figure. 11.c). Thus, the production of 16β-OH-STAN-G was estimated after 8h of the experiment as approximately 8 ng mL^{-1}. This estimative is reasonable, given the addition of the β-glucuronidase enzyme caused the specific cleavage of OH-STAN-G conjugates.

Interestingly, 16β-OH-STAN was the prevalent hydroxylated isomer in negative ionization mode observed in the hydrolyzed (t_R: 8.19 min, NL 8.68E5) and in the non-hydrolyzed sample (t_R: 8.19 min, NL 9.25E6), the last one in higher intensity. Thus, probably it presents a higher acidity character when compared to the other hydroxylated STAN isomers.

Figure 11 – a. Extracted ion chromatogram of a post-administration ZWT sample collected eight hours after applying STAN to the aquarium water treated a.1. without (dashed) and a.2. with (dot) β-glucuronidase. Upon enzymatic hydrolysis, a peak at 8.23 min appeared, and a comparison with a.3) standard of 16β-hydroxy-stanozolol (16β-OH-STAN) (at 8.24 min) confirmed the presence of 16β-OH-STAN. B. Estimation of glycoconjugate metabolite production by the difference in the chromatographic peak area of these hydroxylated metabolites from extraction with and without hydrolysis. The sum of peak areas 1, 2, and 3 increased upon enzymatic hydrolysis.

The indirect confirmation of glucuronide metabolites is usually done when the conjugated standard is not available (POZO et al., 2009b). Our study confirmed that 16β-OH-STAN-G used both hydrolysis and comparison with the reference standard of the unconjugated metabolite. This metabolite was already observed in human urine (SCHÄNZER et al., 2013), although without details of its characterization. From the E_{lab} variation, 16β-OH-STAN-G could be either **M3** or **M4**, peaks at t_R 7.37 and 7.71 min, respectively. It is hypothesized so because, as expected of 16β-OH-STAN, the **M3** and **M4** fragmentation pattern lacks specific ions, and both need the same amount

of energy to produce the fragments (Figure 13.e and 13.f). It is noteworthy that the phase I metabolite 16β-OH-STAN, only observed after enzymatic hydrolysis in this study, was the most intense hydroxylated metabolite after 168 h of experiment in ZWT (ANSELMO et al., 2017).

4.4. Characterization of intact hydroxylated STAN glucuronide (OH-STAN-G) isomers metabolites

The ZWT produced four OH-STAN-G metabolites, observed in positive and negative ionization mode (Figure 12.a and 12.b) (summarized in appendix 1). The late eluting peak at 8.07 min was confirmed as 3'OH-STAN-G by comparison with standard material (Figure 12, down part). The extracted ion chromatogram corresponds to the hydrolyzed sample (Figure 12, up part) and non-hydrolyzed ZWT sample (Figure 12, middle part). None of the peaks were observed in the hydrolyzed portion. This means that all four hydroxy-glucuronides were hydrolyzed under the influence of β-glucuronidase. Hence, since the glucuronides are hydrolysable, they correspond to *O*-glucuronides, not to *N*-glucuronides. However, since the molecules possess two oxygens (one at 17-position and the corresponding hydroxyl group from phase I biotransformation), it is not possible to which one the glucuronide is linkage unless it is confirmed by means of comparison with reference material. However, since the 17-sulfate metabolite usually decomposes, the sulfate moiety is probably linked to the phase I hydroxyl group.

To identify the other three peaks, accurate mass product ion spectra (Figure 13 .a, 13.b, 13.c, 13.d, table 2) were obtained under low to high collision energies. Then, the Ep_{lots} (Figure 13.e, 13.f, 13.g, 13.h) were depicted. For all four metabolites, only the loss of anhydroglucuronic acid (AnhydroGlcA) moiety was noticed under low E_{lab}. Under high E_{lab}, the product ion spectra were similar to the monohydroxylated metabolites (Appendix. 2 - 53).

Concerning **M2**, the first eluting OH-STAN-G isomer at t_R 6.75 min, the loss of the AnhydroGlcA moiety $[M+H-C_6H_8O_6]^+$ was observed up to 35 eV (Figure 13.a, table 2). Additionally, a consistent loss of one $[M+H-C_6H_8O_6-H_2O]^+$ or two $[M+H-C_6H_8O_6-2H_2O]^+$ molecules of water in medium E_{lab} was noticed. Interestingly, a small intensity

fragment ion at *m/z* 145.0762 ($C_9H_9N_2^+$) consistently appeared when E_{lab} from 30 to 40 eV was applied.

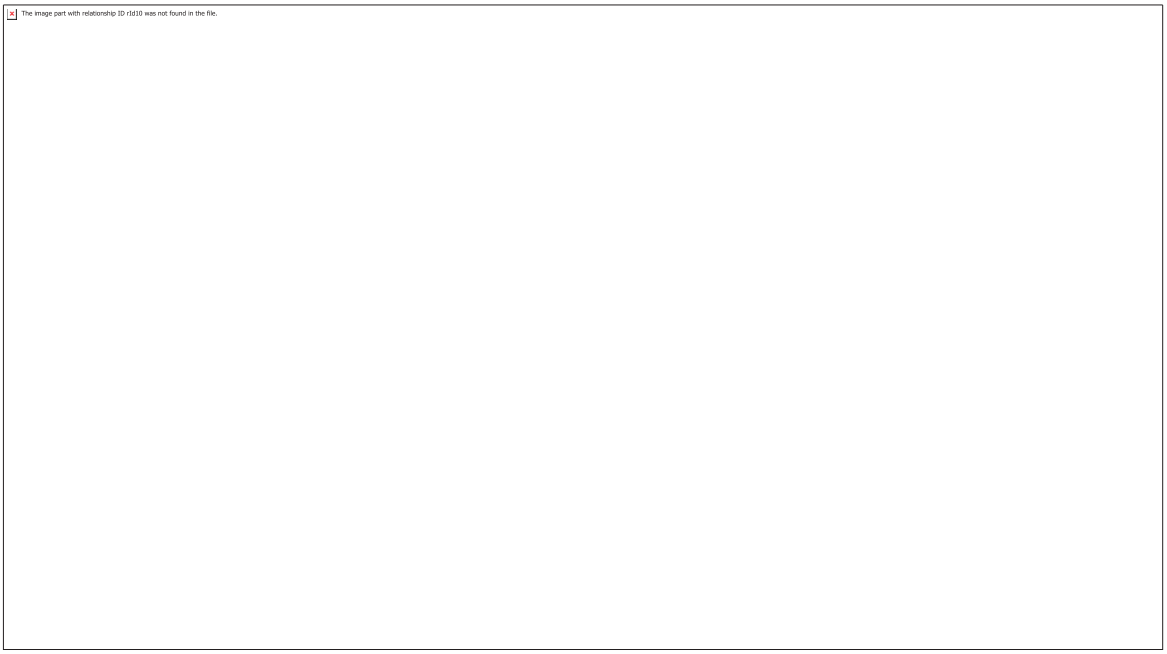

Figure 12 – Extracted ion chromatograms a) in positive ionization mode and b) negative ionization mode of in the up part a post-administration hydrolyzed sample collected 8 h after application of stanozolol in the aquarium water and the middle a non-hydrolyzed sample. The presence of 3'-OH-STAN-G (**M5**) at 8.07 min was corroborated with the standard reference at 50 ng mL^{-1} in the down part. 5 mL of sample was concentrated using SPE with and without hydrolysis

Figure 13 – Product ion spectra of OH-STAN-G isomers from a post-administration sample collected 8 h after application of stanozolol in the aquarium water a) **M1** b) **M2** c) **M3** d) **M4** and below each spectrum, e,f,g,h the correspondent peak energy-resolved plots of E_{lab} variation versus ion intensities between 10 and 65 eV using HCD mode and N_2 as collision gas.

Table 2 - Elemental compositions of the $[M+H]^+$ ions of OH-STAN-G metabolites M2 to M5 and resulting diagnostic product ions obtained from high-resolution/high-accuracy MS/MS experiments from Orbitrap-HCD using positive ESI

Cmp.	Precursor ion (m/z)	Elemental comp. (exp.)	Error (ppm)	CE	Product ion (m/z)	Elemental comp. (exp.)	Error (ppm)
M2	521.2857	$C_{27}H_{41}O_8N_2$	0.08	35	345.2535	$C_{21}H_{33}O_2N_2$	0.45
Fig. 13.a					327.2427	$C_{21}H_{31}ON_2$	1.19
					309.2324	$C_{21}H_{29}N_2$	0.41
					145.0762	$C_9H_9N_2$	1.21
M3	521.2842	$C_{27}H_{41}O_8N_2$	2.96	50	345.2528	$C_{21}H_{33}O_2N_2$	2.48
Fig. 13.b					327.2433	$C_{21}H_{31}ON_2$	0.64
M4	521.2855	$C_{27}H_{41}O_8N_2$	0.46	50	345.2528	$C_{21}H_{33}O_2N_2$	2.48
Fig. 14.c					81.0452	$C_4H_5N_2$	5.86
M5	521.2861	$C_{27}H_{41}O_8N_2$	0.67	20	345.2537	$C_{21}H_{33}O_2N_2$	0.13
Fig. 14.d							

Although ESI enabled the detection of intact sulfate and glucuronide metabolites, the fragmentation spectra provided by this technique lack structural information (LEVSEN et al., 2005). Also, the fragmentation spectra obtained from HCD are usually different from CID (VESSECCHI et al., 2020). Here, for the hydroxy-glucuronide metabolite **M2,** a small fragment at *m/z* 145.0762 was observed. Under CID conditions, this fragment has significant intensity and represents 4-OH-STAN. Two neutral water losses were also observed when 4-OH-STAN was fragmented under CID conditions (THEVIS et al., 2005). These neutral losses were also consistently observed in both spectra in this study. This finding indicates that **M1** could be 4-OH-STAN-G.

Interestingly, the ion *m/z* 81.0447, observed when high E_{lab} was applied in the HCD for **M2**, was not observed under CID for 4-OH-STAN. For a precise characterization of this metabolite, either its retention time should be compared with a reference material, or additional NMR experiments should be performed to locate its conjugation site. One of the ZWT's potential uses is concentrate liters of tank water going through an HPLC preparative, containing the target metabolite, which could later be characterized by other means.

There were no significant differences between **M3** and **M4** E_{lab} variations (Figure 13.b and 13.c). Both metabolites lost AnhydroGlcA up to 35 eV and high energies,

given their characteristics, but unspecific ion, *m/z* 81.0447 ($C_4H_5N_2^+$). Furthermore, a consistent loss of one molecule of water after AnhydroGlcA $[M+H-C_6H_8C_6-H_2O]^-$ was observed for both **M3** and **M4** from 35 to 70 eV. Additionally, both metabolites' spectra resembled STAN product ion spectra under high NCEs. The product ion spectra of metabolites where the hydroxylation site is far from the pyrazole ring also resembled STAN spectra. Thus, although the product ion spectra were uninformative, one of the metabolites could be 16β-OH-STAN-G, which was evaluated indirectly above. The other metabolite could be a stereoisomer of 16β-OH-STAN-G.

In the case of **M5**, 3'OH-STAN-G, the E_{plots} demonstrate that a small amount of energy was required to cleave the AnhydroGlcA moiety generating 3'-OH-STAN. The characteristic fragment at *m/z* 97.0396 was only observed when higher E_{lab} were applied (Figure 13.d). Throughout the chromatography peak, **M5**/IS area ratio, the concentration was approximately 5 ng mL^{-1}. In 1990, Schänzer et al. (SCHÄNZER; OPFERMANN; DONIKE, 1990) indirectly evaluated the presence of 3'OH-STAN-G by CG-MS and pointed out the instability of the glucuronidation site. Our study observed it takes up to 15 eV to break the glycosidic linkage, a considerably small amount of energy compared to the amount necessary to cleave the bond of the other three hydroxylated-glucuronide metabolites.

The E_{lab} variation showed that regardless of the metabolite, the glucuronide moiety is cleaved in low collision energy while the aglycon fragmentation occurs only in high collision energy. Thus, by mapping the isomers' fragmentation behavior through low to high collision energies, it is possible to understand the analytes comprehensively.

In order to unequivocally identify an analyte a series of identification criteria need to be full filed when the sample is compared to the reference material as describe by technical documents. According to the first criteria, the chromatographic peak, in this situation 3'OH-STAN-G at 8.07 min, should not differ (ΔRT) by more than 1% or ± 0.1 minutes from the reference material analyzed in the same batch. As observed in figure 13.a in the middle and down part, both peaks, M4 and 3'OH-STAN-G presented the same retention time with no variation, full filing, thus, the chromatographic criteria.

The second criteria, the mass spectrometry identification may be accomplished through the generation of the intact metabolite's substance-specific ions. Since tandem MS (HRMS/MS) was used, IDCR requires that at least the abundance

of two diagnostic ions, determinate by the chromatography peak areas, is monitored and compared to the standard material. The signal-to-noise (S/N) ratio of all diagnostic ions should be greater than three to one (3:1) and the relative intensities, used to infer the conformity evaluation, calculated by dividing the diagnostic peak area (in this sample *m/z* 97.040, 9.211E4) by the base peak area (*m/z* 345.254, 7.165E6) times 100% yielding a relative intensity of 1.29%.

Sample diagnostic ions relative intensities should not differ by more than the amount specified in Appendix 2 *"Maximum tolerance windows for relative ion intensities and RT"* from the reference material. The maximum tolerance windows for difference in relative ion intensity is of ±10 of the aglycon peak area and 5 of hydroxylated pyrazole peak area, both accomplished by the sample **M5** peak. Thus, the M4 was identified as 3'OH-STAN-G according to WADA's IDCR criteria. Besides extending the detection window of a prohibited substance, the use of a a phase II metabolites assemble confidence in the mass spectrometry identification criteria, since an addition fragment due to the glucuronic moiety loss can be used.

4.5. Characterization of OH-STAN-S isomers

Four intact hydroxylated sulfonate metabolites were observed in the ZWT samples. The four peaks observed in positive ionization mode (Figure 14.a) present similar retention time and intensity as in negative ionization mode (Figure 14.b). Each of the compounds has multiple potential sites of sulfation. In addition to the oxygen in 17 positions and the hydroxyl of phase I metabolism reaction, the two nitrogen atoms of the pyrazole ring are also potential sulfation sites. However, when the sulfate is conjugated through the nitrogen atom, the pyrazole ring cannot ionize in positive ionization mode (BALCELLS et al., 2017). Hence, since the four OH-STAN-S peaks were observed in both positive and negative ionization modes, it can be inferred that they are *O*-Sulfated (data summarized in Appendix 1).

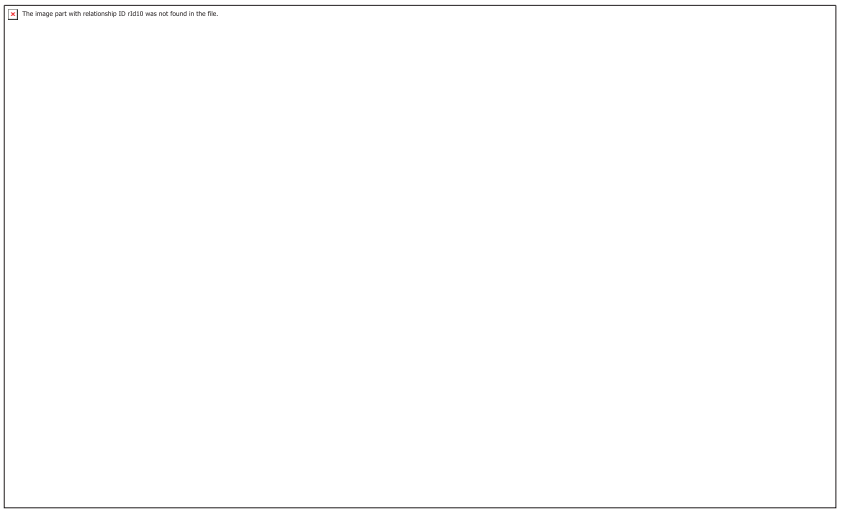

Figure 14 – Extracted ion chromatograms in a) positive ionization mode and b) negative ionization mode of OH-STAN-S in a post-administration non-hydrolyzed ZWT sample collected eight h after application of stanozolol in the aquarium water.

In positive ionization mode, the HRMS/MS product ion spectra of all four sulfate metabolites present in common fragment ions, with different intensities, regardless of the collision energy used (CE 25 eV, Figure 15, CE 30 eV Figure 16 and CE 40 eV Figure 17). In negative mode, in addition to the deprotonated ion $[M+H]^-$ 423.1948, all four OH-STAN-S metabolites yielded only one product ion (*m/z* 96.9590) at 45 eV (Figure 18).

M6 at t_R 6.80 min (Figure 15.a, 16.a, 17.a) showed the pseudo molecular ion at $[M+H]^+$ 425.2105. The neutral loss of SO_3 was noticed, yielding the elemental composition of OH-STAN (*m/z* 345.2537). Besides, a subsequent elimination of one molecule of water at *m/z* 327.2431 was observed as the major peak in higher collision energies, characteristic of a sulfate metabolite. A small but consistent fragment representing a second loss of water (m/z 309.2324) was observed in low to high collision energies. At 25 and 30 eV (Figure 15.a, 16.a), **M6** presented the fragment ion at *m/z* 145.0759 of $C_9H_9N_2^+$ and *m/z* 269.2015 of $C_{18}H_{25}N_2^+$ that are indicative of hydroxylation at Carbon 4, as explained in section *4.3.* Similarly, the small fragment at *m/z* 145.0759 and 269.2015 could be indicative of 4-OH-STAN-S.

M7, CE 25 eV at t_R 7.30 min, **M8** t_R 7.53 min **M9** at t_R 7.67 min (Figure 15.b, 16,c, 17,d, respectively) presented the same two product ions at *m/z* 345.2537 and *m/z* 327.2431 apart from the protonate $[M+H]^+$ 425.2105 but with different intensities. In low to high CE, **M7** was the only metabolite that presented a high-intensity loss of

one molecule of water after the sulfate moiety. In the low amount of energy, **M8** and **M9** (CE 25 eV, figure 15.c and 15.d) presented the loss of SO_3 as the major peak at *m/z* 345.2537. In higher energies (CE 30 and 40 eV, figure 16.c and 17.c), a small but consistent loss of one molecule of water consistently appeared. **M9** showed similar ion intensities to **M8,** with the most prominent peak in higher collision energies at *m/z* 345.2537. The second elimination of water was expected from a molecule with two hydroxylation sites. However, this behavior was only observed in the **M6**.

Balcells et al. 2017 identified 16STAN-S in human athlete urine by means of comparison with reference material. In addition to this finding, the author has observed two other OH-STAN-S isomers were hypothesized as 16-STAN-S stereoisomers due to similar fragmentation behavior in positive and negative ionization modes. The results obtained in the present work agree with Balcells et al. 2017 findings. Therefore, apart from **M6** at 6.80 min identified as the putative 4-OH-STAN-S of unknown stereochemistry, **M7**, **M8,** or **M9** is probably 16-STAN-S. However, since the fragmentation spectra are not informative and do not specify ions, it is not possible to identify the hydroxylation site's position and with which hydroxylation site the sulfate moiety is linked.

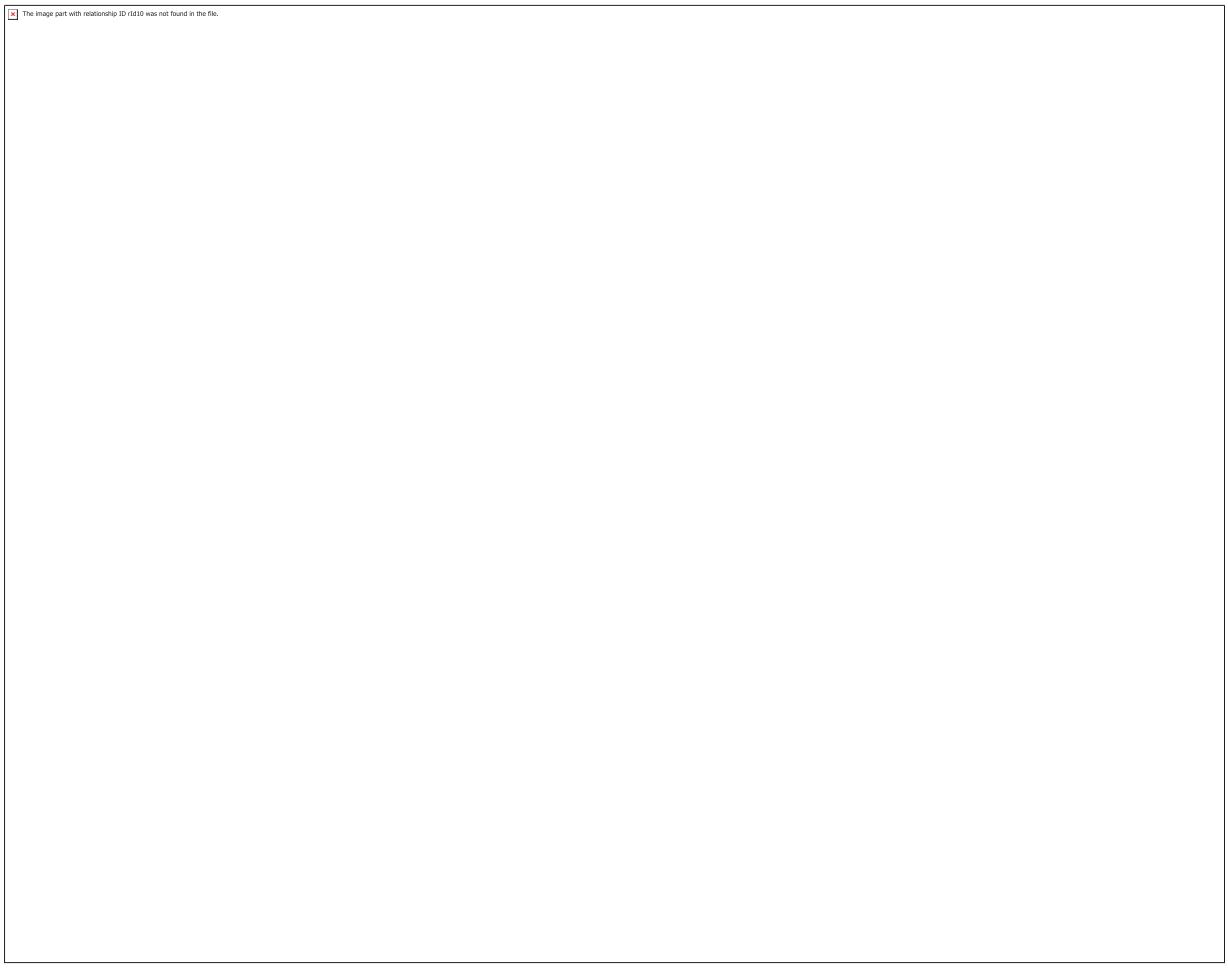

Figure 15 – Product ion spectra of OH-STAN-S isomers in positive ionization mode at CE 25 eV from a post-administration sample collected 8 h after application of stanozolol in the aquarium water a) **M6** b) **M7** c) **M8** d) **M9**

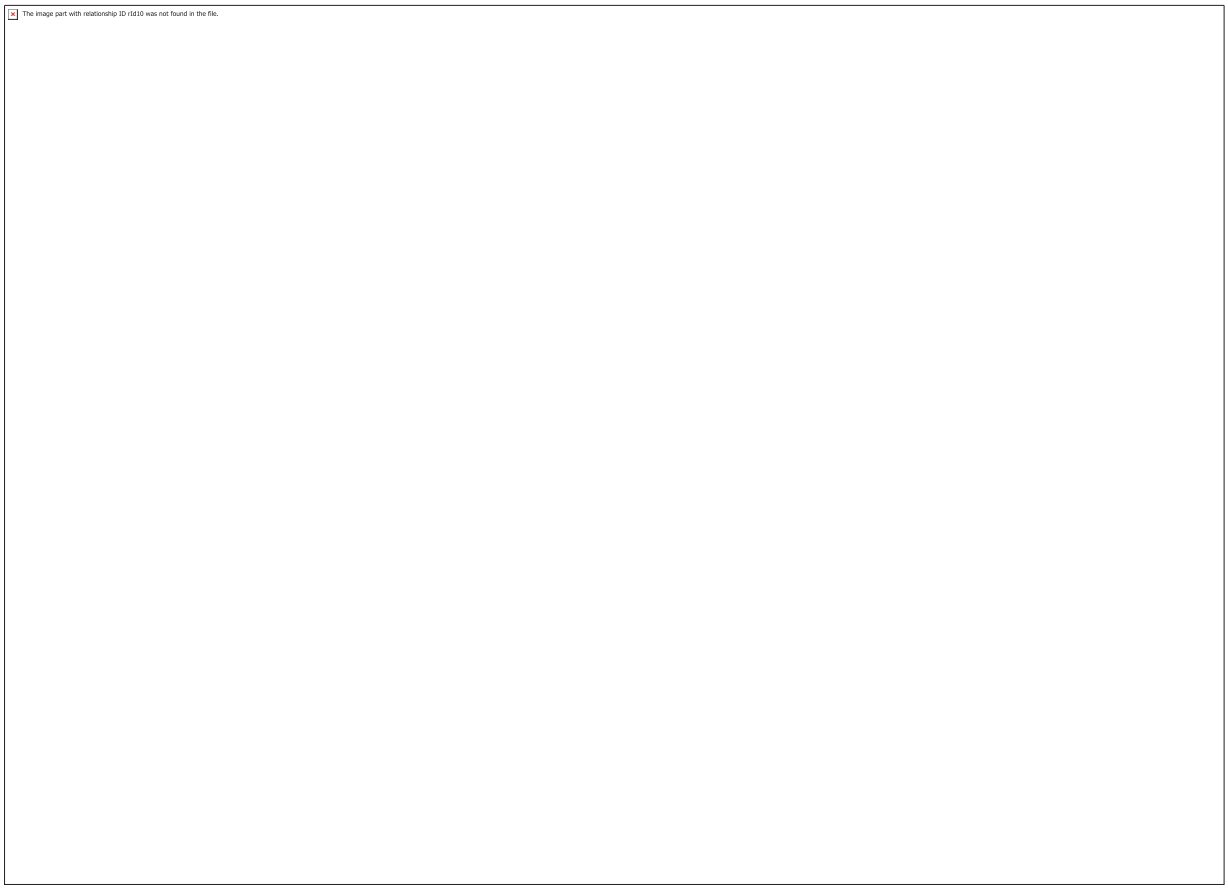

Figure 16 – Product ion spectra of OH-STAN-S isomers in positive ionization mode at CE 30 eV from a post-administration sample collected eight h after application of stanozolol in the aquarium water a) **M6** b) **M7** c) **M8** d) **M9**

Figure 17 – Product ion spectra of OH-STAN-S isomers in positive ionization mode at CE 40 eV from a post-administration sample collected eight h after application of stanozolol in the aquarium water a) **M6** b) **M7** c) **M8** d) **M9**

Figure 18 – Product ion spectra of OH-STAN-S isomers in negative ionization mode at CE 45 eV from a post-administration sample collected eight h after application of stanozolol in the aquarium water a) **M6** b) **M7** c) **M8** d) **M9**

Table 3 - Elemental compositions of the $[M+H]^+$ and $[M+H]^-$ ions of OH-STAN-S metabolites M2 to M5 and resulting diagnostic product ions obtained from high-resolution/high-accuracy MS/MS experiments from Orbitrap-HCD using positive and negative ESI

Cmp.	Precursor ion (m/z)	Elemental comp. (exp.)	Error (ppm)	CE	Product ion (m/z)	Elemental comp. (exp.)	Error (ppm)
M6	425.2109	$C_{21}H_{33}O_5N_2S$	1.01	25	345.2535	$C_{21}H_{33}O_2N_2$	0.45
Fig. 18.a	$[M+H]^+$				327.2430	$C_{21}H_{31}O_2N_2$	1.19
					309.2324	$C_{21}H_{29}N_2$	0.41
					269.2014	$C_{18}H_{25}N_2$	0.65
M7	425.2104	$C_{21}H_{33}O_5N_2S$	0.16	25	393.1879	$C_{25}H_{29}O_2S$	0.96
	$[M+H]^+$				345.2535	$C_{21}H_{33}O_2N_2$	0.45
Fig. 18.b					327.2430	$C_{21}H_{31}ON_2$	0.27
M8	425.2084	$C_{21}H_{33}O_5N_2S$	1.44	25	345.2535	$C_{21}H_{33}O_2N_2$	2.48

Table 3 – Continuation

Fig. 18.c	$[M+H]^+$				327.2428	$C_{21}H_{31}ON_2$	0.89
M9	425.2099	$C_{21}H_{33}O_5N_2S$	1.34	25	345.2532	$C_{21}H_{33}O_2N_2$	1.32
Fig. 18.d	$[M+H]^+$				327.2434	$C_{21}H_{31}ON_2$	0.95
M6	425.2108	$C_{21}H_{33}O_5N_2S$	0.78	30	345.2535	$C_{21}H_{33}O_2N_2$	0.49
Fig. 19.a	$[M+H]^+$				327.2428	$C_{21}H_{31}O_2N_2$	0.89
					309.2321	$C_{21}H_{29}N_2$	1.38
					269.2012	$C_{18}H_{25}N_2$	0.09
					145.0759	$C_9H_9N_2$	0.86
M7	425.2106	$C_{21}H_{33}O_5N_2S$	0.30	30	345.2534	$C_{21}H_{33}O_2N_2$	0.74
Fig.19.b	$[M+H]^+$				327.2427	$C_{21}H_{31}ON_2$	1.19
M8	425.2121	$C_{21}H_{33}O_5N_2S$	3.83	30	345.2535	$C_{21}H_{33}O_2N_2$	0.45
Fig. 19.c	$[M+H]^+$				327.2428	$C_{21}H_{31}ON_2$	0.89
M9	425.2100	$C_{21}H_{33}O_5N_2S$	1.10	30	345.2537	$C_{21}H_{33}O_2N_2$	1.31
Fig. 19.d	$[M+H]^+$				327.2432	$C_{21}H_{31}ON_2$	0.33
M6	425.2116	$C_{21}H_{33}O_5N_2S$	2.67	40	345.2536	$C_{21}H_{33}O_2N_2$	0.16
Fig. 20.a	$[M+H]^+$				327.2429	$C_{21}H_{31}O_2N_2$	0.58
					309.2321	$C_{21}H_{29}N_2$	1.38
					145.075	$C_9H_9N_2$	7.00
M7	425.2096	$C_{21}H_{33}O_5N_2S$	2.04	40	345.2534	$C_{21}H_{33}O_2N_2$	0.74
Fig.20.b	$[M+H]^+$				327.2428	$C_{21}H_{31}ON_2$	0.88
M8	-			40	345.2535	$C_{21}H_{33}O_2N_2$	0.45
Fig. 20.c	$[M+H]^+$				327.2430	$C_{21}H_{31}ON_2$	0.27
M9				40	345.2534	$C_{21}H_{33}O_2N_2$	0.74
Fig. 20.d	-				327.2428	$C_{21}H_{31}ON_2$	0.89
M6	423.1963	$C_{21}H_{33}O_5N_2S$	3.45	45	96.9588	HSO_4^-	2.12
Fig. 21.a							
M7	423.1963	$C_{21}H_{33}O_5N_2S$	3.45	45	96.9588	HSO_4^-	2.12
Fig.21.b							
M8	423.1963	$C_{21}H_{33}O_5N_2S$	3.50	45	96.9586	HSO_4^-	4.18
Fig. 21.c							
M9	423.1961	$C_{21}H_{33}O_5N_2S$	3.03	45	96.9584	HSO_4^-	6.00
Fig. 21.d							

4.6. Characterization of STAN-G isomers

To evaluate if one of these peaks corresponded to an *N*-glucuronide, the ZWT sample was concentrated through SPE with and without hydrolysis. Since *N*-glucuronides are not cleaved by β-glucuronidase, its intensity should remain the same regardless of the experiment. After hydrolysis, the first peak showed a similar magnitude before and after treatment with *E. coli* (Figure 19). STAN-*N*-G was unambiguously confirmed according to chromatographic IDCR criteria, since the retention time variation of the sample peak to reference material accounts for less than 1% (Figure 19.a). In addition, the sample peak mass spectrometry error is less the 5 ppm (table 4) contributing positively to the STAN-N-G identification. Hence, a rough comparison of chromatography peak areas of standard and ZWT indicates it was produced approximately five ng mL^{-1} after eight h of the experiment. The second peak (at 8.14 min) was hydrolyzable, indicating an *O*-Glucuronide of unknown stereochemistry (data summarized in Appendix 1).

The product ion spectra of both metabolites were almost identical (Figure 19.b and 19.c). At low E_{lab}, the intact glucuronide was observed at *m/z* 505.2910 and the neutral loss of AnhydroGlcA yielding its non-conjugated fragment at *m/z* 329.2587(Figure 19.d and 19.e). At high E_{lab} fragment ion at *m/z* 81.0447 appeared, and spectra were similar to STAN. The only difference between both spectra is that less energy is needed to produce the aglycon from STAN-*N*-G (35 eV) than from putative STAN-*O*-G (40 eV).

Figure 19 – Extracted ion chromatograms of a post-administration sample collected eight h after applying stanozolol in the aquarium water a) without and b) with enzymatic hydrolysis step. The presence of STAN-*N*-G (t_R 7.74 min) was corroborated with c) the standard reference at 50 ng mL^{-1}. Upon enzymatic hydrolysis, the first eluting peak intensity remained the same (NL:1.14E5) while the second disappeared, supporting the structural assignment as the 17-STAN-*O*-G of unknown stereochemistry (t_R: 8.06 min). Product ion spectra and E_{lab} variations of d) STAN-*N*-G and f) STAN-*O*-G from a post-administration sample collected eight h after applying stanozolol in the aquarium water. While STAN-O-G was dissociated with a collision energy of 40 eV, STAN-*N*-G was dissociated at 35 eV. The energy-resolved plots of E_{lab} variation versus ion intensities of e) STAN-*N*-G and g) STAN-*O*-G between 10 and 70 eV using HCD and N_2 as collision gas.

Table 4 - Elemental compositions of the $[M+H]^+$ ions of STAN-G metabolites resulting diagnostic product ions obtained from high-resolution/high-accuracy MS/MS experiments from Orbitrap-HCD using positive and negative ESI

Cmp.	Precursor ion (m/z)	Elemental comp. (exp.)	Error (ppm)	CE	Product ion (m/z)	Elemental comp. (exp.)	Error (ppm)
STAN-*N*-G Fig. 22.b	505.2892	$C_{27}H_{41}O_7N_2$	3.22	35	329.2587	$C_{21}H_{33}ON_2$	0.12
STAN-*O*-G Fig. 22.c	505.2910	$C_{27}H_{41}O_7N_2$	0.34	40	329.2586	$C_{21}H_{33}ON_2$	0.42

4.7. Phase II metabolic pathway of STAN in ZWT

The presence of sulfate and glucuronide metabolites were monitored in the recipient water throughout eight h of the experiment. The glucuronide metabolites were observed up to 2 h, whereas OH-STAN-S was observed up to 4h post-STAN-administration to the water tank (data not shown). Besides, the overall amount of putative 4-OH-STAN-G is higher than its respective 4-OH-STAN-S (Figure 20.a). The overall amount of glucuronide production was at least four times the sulfate production, indicating that glucuronidation constituted the majority of the studied phase II metabolic pathways of STAN in ZWT. Similarly, Lindholst et al. (2003) assessed the phase II metabolism of bisphenol A (BPA) in the holding water and tissue samples of zebrafish by adding 0.1 µg mL^{-1} of BPA to water. They discovered that the BPA-glucuronic acid level was much higher in bile and plasma than BPA-sulfate.

Interestingly, in humans, UGTs are low-affinity enzymes compared to SULTs, which implies that sulfation is usually faster than glucuronidation at low substrate concentrations (TESTA; KRÄMER, 2008). In our experiment, due to the STAN's hydrophobic character, a high substance concentration was applied to the recipient water to be sure that the fish ingest the drug. Therefore, if zebrafish UGTs' enzymes also have a lower affinity to the substrate than sulfotransferases, the sulfation pathways should be more pronounced in STAN's low concentrations.

After 8 h of the experiment, STAN-*O*-G was the most intense phase II metabolite monitored, whereas STAN-*N*-G was the less intense (Figure 20.b). Interestingly, Schanzer et al., 2013 findings are the opposite. The authors observed as STAN human excretion pattern that in *N*-glucuronides are more prevalent than *O*-glucuronides and inferred that glucuronidation of 17-hydroxy functions is sterically hindered in 17-alkylated steroids (such as, e.g., STAN and methyltestosterone), resulting in modest yields of 17-O-glucuronides of these compounds. However, in ZWT's, the opposite is observed (Figure 20.b). In addition, in ZWT it was not observed the main STAN's target analytes in humans, 17epiSTAN-1'N-G. However, as detailed described in this dissertation, ZWT's is both capable of perform *N*-Glucuronidation ("4.5. Characterization of STAN-G isomers") and epimerization ("*4.2. Complementing the characterization of ZWT's STAN phase I metabolites* ") reactions. Thus, probably this metabolite was not produced due to kinetics issues. An experimental design should be

performed targeting this ZWT's LTM increasing the experiment time course, number of fish and/or temperature in order to tune the model to produce this metabolite.

The comparison between the bioaccumulation of 3'OH-STAN and 3'OH-STAN-G showed that the hydroxylated amount began to decrease after six h (Figure 20.c). Schänzer et al. (SCHÄNZER; OPFERMANN; DONIKE, 1990) noticed that most of 3'OH-STAN are excreted in its glucuronide form in human urine, demonstrating that glucuronidation is the preferable metabolic route to excrete hydrophobic molecules like STAN from the body. Our bioaccumulation curves of 3'OH-STAN and 3'OH-STAN-G from scaled-down ZWT show the opposite since the amount of 3'OH-STAN is fourfold 3'OH-STAN-G amount. This probably happened because 3'OH-STAN has to be excreted in the holding water to be reabsorbed and glycoconjugated. Another evidence for this hypothesis is the plateau observed after seven h of 3'OH-STAN bioaccumulation when 3'OH-STAN began to accumulate. This excretion, resorption, and re-excretion cycle proposed for ZWT could be compared to the enterohepatic circulation in humans, when the substrate is metabolized, cleaved in the gut, re-metabolized, and excreted. Probably, with the increase in the time course of our experiment, the amount of 3'OH-STAN would decrease, and its glucuronide form increase.

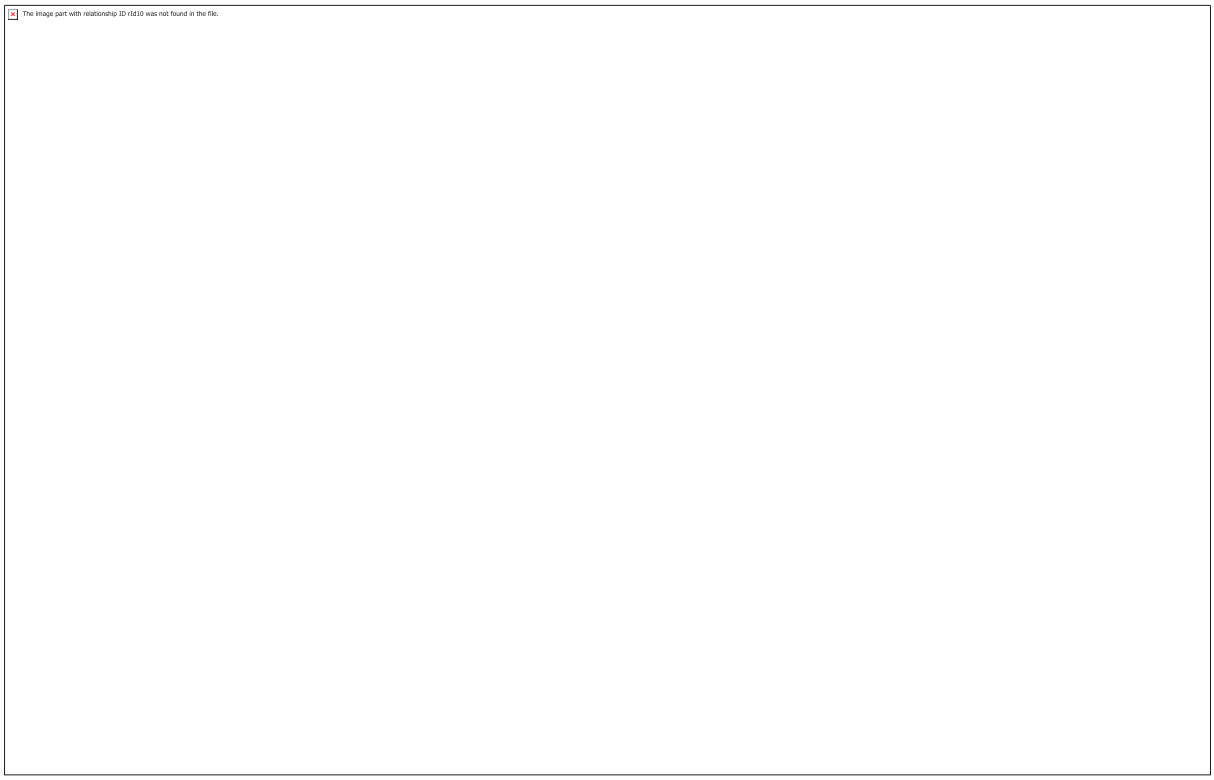

Figure 20 – Six ZWT's phase I and II STAN metabolites accumulation curve monitored through 8 h of the experiment after administration of STAN to the water tank. The charts were elaborated metabolite to IS ratio a) Comparison between putative 4OH-STAN-G (black vertical stripes) and 4OH-STAN-G (white background) of unknown stereochemistry b) Comparison between the confirmed STAN-*N*-G (black background) and putative STAN-*O*-G (white background) and c) comparison between phase I 3'OH-STAN and the confirmed 3'OH-STAN-G.

.

In this scaled-down study, the experimental design had a concentration of fish to the volume of water (40 fish L^{-1}) higher than the used by Anselmo et al. (ANSELMO et al., 2017) (3 fish L^{-1}). Another difference is that the concentration of substance increased four-fold, from 0.25 µg mL^{-1} to 1 µg mL^{-1}. By increasing the fish ratio, the experimental time was reduced from 168 h to 8 h. These differences, along with the sample pretreatment method, could justify that the authors (ANSELMO et al., 2017) did not observe the phase II metabolites of STAN in previous studies. Another advantage of reducing the experimental setup is the cost-effectiveness. Additionally, the biota's influence that naturally occurs in the recipient is reduced. It is noteworthy that, in ZWT experimental design, the whole recipient containing eight fish counts as one organism. This happens because the holding water in which the metabolites are excreted through the gill, urine, and feces are analyzed (FÉLIX et al., 2013). The

Grubbs test for outliers to each metabolite was applied, and the results showed no difference between the three samples.

Using the current ZWT experimental setup, it is expected that the kinetics production of metabolites is accelerated. Interestingly, the production of 16β-OH-STAN, which was the higher hydroxylated metabolite observed by Anselmo et al. 2017 after 168 h after STAN's administration to the fish, was only observed this work after hydrolysis experiments (Figure 11). This indicates that the hydroxylation reaction enzymes may present low substrate affinity to the 17α-hydroxy-17β-methyl moiety (MASSÉ et al., 1989).

5. Conclusion and perspectives

In view of the topics investigated throughout this study, the following questions can be answered, and some perspectives can be contemplated:

- *Can the ZWT model produce phase II metabolites of STAN?*

Yes, after 8 h of the experiment, ZWT produced phase II metabolites found in human urine. Stanozolol metabolites' proposed structures show that the steroid is hydroxylated with a high degree of regioselectivity since only the C-3', C-4, and C-16 positions were hydroxylated. Moreover, our results suggest that ZWT can glycoconjugate in the STAN D ring and pyrazole ring. Therefore, the ZWT experimental setup may be considered a practical approach to investigate the phase II metabolism of other anabolic agents with similar structure features, such as methandienone and methyltestosterone. In the case of doping agents of different structures, extrapolations should be made carefully. In this work a suitable sample preparation DS method is used which could also be applied to the analysis of other steroids metabolites. Further studies using ZWT targeting the LTM of other steroids may use both the sample preparation and the ZWT experimental set up employed in this work. Although glucuronidation and sufation reaction generates the main phase II metabolites used as targets, other reactions as, shows potentials metabolites that have recently being explored as targets for steroids. That this model is able to produce the main phase II metabolic reactions opens perspective to the exploration of these other abovementioned phase II metabolites. In addition, LC-HRMS/MS is a promising analytical tool to be used in this endeavor.

- *Is it possible to characterize the biotransformation products by means of LC-HRMS/MS*?

Yes, it is possible to characterize 3'OH-STAN-G, STAN-*N*-G by means of comparison with the reference standard and matching WADAs identification criterias. 16β-OH-STAN-G presence was indirectly confirmed employing comparison with unconjugated metabolite 16β-OH-STAN. 4-OH-STAN-G, 4-OH-STAN-S, and STAN-*O*-G were characterized by comparing their fragmentation spectrum with literature data. The other two OH-STAN-G and three OH-STAN-S metabolites structures could

not be evaluated. However, by joint efforts of hydrolysis and MS experiments, it is possible infer that all OH-STAN-G are *O*-glucuronides and OH-STAN-S metabolites are *O*-sulfates. The product ion mass spectra exposed in this study provided complementary structural information that may be significant for the future analysis of other glucuronide metabolites. In addition, it is demonstrated the importance of a comprehensive fragmentation from low to high energies exemplified by E_{plots} to understand other phase II metabolites profile.

- *Can the kinetic behavior of STAN be inferred from phase II metabolites bioaccumulation curves be described, and the concentration of phase-II metabolites be estimated against reference material?*

After 8 h of the experiment, STAN-*O*-G was the most intense phase II metabolite from the employed experimental setup accumulation curve while STAN-N-G. This data is the opposite for humans in literature. The sum of OH-STAN-G isomers is higher than OH-STAN-S isomers. From 3'OH-STAN and 3'OH-STAN-G bioaccumulation curves, the hydroxylated amount began to decrease after 6h while the glucuronide increased, suggesting that glucuronidation after hydroxylation occurs, the phase I metabolite has to be excreted in the water first to be reabsorbed. Hence, to target ZWT's phase II metabolites of STAN, more than 8 h of the experiment is desirable. At the end of the experiment, the production of 16β-OH-STAN-G was estimated after 8h of the experiment as approximately 8 ng mL-1, 3'-OH-STAN-G 5 ng mL-1, and STAN-N-G 4 ng mL^{-1}

.

6. References

ALMAZROO, O. A.; MIAH, MOHAMMAD KOWSER RAMAN VENKATARAMANAN, P. Drug Metabolism in the Liver. **Clinical Liver Disposition**, p. 1–20, 2016.

ANSELMO, C. S. et al. Is zebrafish (Danio rerio) a tool for human-like metabolism study? **Drug Testing and Analysis**, v. 9, p. 1685–1694, 2017.

ANSELMO, C. S. et al. Zebrafish (Danio rerio): A valuable tool for predicting the metabolism of xenobiotics in humans? **Comparative Biochemistry and Physiology Part C**, v. 212, p. 34–46, 2018.

AQUINO NETO, F. R. DE. O papel do atleta na sociedade e o controle de dopagem no esporte. **Revista Brasileira de Medicina do Esporte**, v. 7, n. 4, p. 138–148, 2001.

BALCELLS, G.; MATABOSCH, X.; VENTURA, R. Detection of stanozolol O- and N-sulfate metabolites and their evaluation as additional markers in doping control. **Drug Testing and Analysis**, v. 9, n. 7, p. 1001–1010, 2017.

BRANDON, E. F. A. et al. An update on in vitro test methods in human hepatic drug biotransformation research: Pros and cons. **Toxicology and Applied Pharmacology**, v. 189, n. 3, p. 233–246, 2003.

CASTRO, J. DE L. et al. A high throughput approach for determination of dermorphin in human urine using liquid chromatography–mass spectrometry for doping control purposes. **Journal of Mass Spectrometry**, v. 55, n. 10, 2020.

CHEN, L.; FEANY, M. B. α-synuclein phosphorylation controls neurotoxicity and inclusion formation in a Drosophila model of Parkinson disease. **Nature Neuroscience**, v. 8, n. 5, p. 657–663, 2005.

CHIEFFI, C. et al. Metabolic profile of the synthetic drug 4 , 4 ′ - dimethylaminorex in urine by LC – MS - based techniques : selection of the most suitable markers of its intake. **Forensic Toxicology**, n. 0123456789, 2020.

CHNG, H. T. et al. An investigation of the bioactivation potential and metabolism profile of zebrafish versus human. **Journal of Biomolecular Screening**, v. 17, n. 7, p. 974–986, 2012.

DA CUNHA PINTO, A. et al. Electrospray ionization tandem mass spectrometry analysis of isopimarane diterpenes from Velloziaceae. **Rapid Communications in Mass Spectrometry**, v. 30, n. 1, p. 61–68, 2016.

DE SOUZA ANSELMO, C. et al. Zebrafish (Danio rerio): A valuable tool for predicting the metabolism of xenobiotics in humans? **Comparative Biochemistry and Physiology Part - C: Toxicology and Pharmacology**, v. 212, n. May, p. 34–46, 2018.

DEMARQUE, D. P. et al. Fragmentation reactions using electrospray ionization mass spectrometry: An important tool for the structural elucidation and characterization of synthetic and natural products. **Natural Product Reports**, v. 33, n. 3, p. 432–455,

2016.

DIAS, M. H.; DE SOUSA, E. L. A. Esporte de alto rendimento: Reflexões psicanalíticas e utópicas. **Psicologia e Sociedade**, v. 24, n. 3, p. 729–738, 2012.

DUVAL, A. The Russian doping scandal at the court of arbitration for sport: lessons for the world anti-doping system. **International Sports Law Journal**, v. 16, n. 3–4, p. 177–197, 2017.

FABREGAT, A. et al. Use of LC-MS/MS for the open detection of steroid metabolites conjugated with glucuronic acid. **Analytical Chemistry**, v. 85, n. 10, p. 5005–5014, 2013.

FÉLIX, A. S. et al. Noninvasive Measurement of Steroid Hormones in Zebrafish Holding-Water. **Zebrafish**, v. 10, n. 1, p. 1–6, 2013.

FENN, J. B. et al. Electrospray Ionization for Mass Spectrometry of Large Biomolecules. **Science**, v. 246, n. 6, p. 64–71, 1989.

FOGEL, C. A. Manufacturing muscle: an overview of the history and legal aspects of doping in sport. **European Journal of Sport Studies**, n. August, p. 1–9, 2014.

GAMBELUNGHE, C. et al. Effects of Chrysin on Urinary Testosterone Levels in Human Males. **Journal of Medicinal Food**, v. 6, n. 4, p. 387–390, 2003.

GOLDSTONE, J. V et al. Identification and developmental expression of the full complement of Cytochrome P450 genes in Zebrafish. **BMC Genomics**, v. 11, n. 1, p. 643, 2010.

GÖSCHL, L. et al. Development and validation of a simple online-SPE method coupled to high-resolution mass spectrometry for the analysis of stanozolol-N-glucuronides in urine samples. **Drug Testing and Analysis**, v. 12, n. 8, p. 1031–1040, 2020.

GRAEF, V.; FURUYA, E.; NISHIKAZE, O. Hydrolysis of steroid glucuronides with β glucuronidase preparations from bovine liver, Helix pomatia, and E. coli. **Clinical Chemistry**, v. 23, n. 3, p. 532–535, 1977.

HOBERMAN, J. Toward a Theory of Olympic Internationalism Toward a Theory of Olympic Internationalism. **Journal of Sport History**, v. 22, n. 1, p. 1–37, 1995.

HORNE, J. The four “knowns” of sports mega-events. **Leisure Studies**, v. 26, n. 1, p. 81–96, 2007.

JONES, H. S. et al. Oxidative and conjugative xenobiotic metabolism in zebrafish larvae in vivo. **Zebrafish**, v. 7, n. 1, p. 23–30, 2010.

KUROGI, K. et al. The use of zebrafish as a model system for investigating the role of the SULTs in the metabolism of endogenous compounds and xenobiotics. **Drug Metabolism Reviews**, v. 45, n. 4, p. 431–440, 2013.

LEINONEN, A. et al. Screening of free 17-alkyl-substituted anabolic steroids in human urine by liquid chromatography-electrospray ionization tandem mass spectrometry. **Steroids**, v. 69, n. 2, p. 101–109, 2004.

LEVSEN, K. et al. Structure elucidation of phase II metabolites by tandem mass spectrometry: An overview. **Journal of Chromatography A**, v. 1067, p. 55–72,

2005.

LINDHOLST, C. et al. Metabolism of bisphenol A in zebrafish (Danio rerio) and rainbow trout (Oncorhynchus mykiss) in relation to estrogenic response. **Comparative Biochemistry and Physiology Part C**, v. 135, p. 169–177, 2003.

LIU, T.-A. et al. Zebrafish as a Model for the Study of the Phase II Cytosolic Sulfotransferases. **Current Drug Metabolism**, v. 11, n. 6, p. 538–546, 2010.

LOOTENS, L. et al. uPA+/+-SCID mouse with humanized liver as a model for in vivo metabolism of exogenous steroids: Methandienone as a case study. **Clinical Chemistry**, v. 55, n. 10, p. 1783–1793, 2009.

MAKAROV, A.; SCIGELOVA, M. Coupling liquid chromatography to Orbitrap mass spectrometry. **Journal of Chromatography A**, v. 1217, n. 25, p. 3938–3945, 2010.

MASSÉ, R. et al. Studies on anabolic steroids. III. Detection and characterization of stanozolol urinary metabolites in humans by gas chromatography-mass spectrometry. **Journal of Chromatography B: Biomedical Sciences and Applications**, v. 497, n. C, p. 17–37, 1989.

MATOS, R. R. et al. Pharmacokinetic study of xylazine in a zebrafish water tank, a human-like surrogate, by liquid chromatography Q-Orbitrap mass spectrometry. **Forensic Toxicology**, v. 38, n. 1, p. 108–121, 2020.

MATOS, R. R. et al. Phase II stanozolol metabolism study using the zebrafish water tank (ZWT) model. **Journal of Pharmaceutical and Biomedical Analysis**, v. 195, 2021.

MCKINNEY, A. R. et al. Detection of stanozolol and its metabolites in equine urine by liquid chromatography – electrospray ionization ion trap mass spectrometry. **Journal of Chromatography B**, v. 811, n. 2004, p. 75–83, 2006.

MOHAMMED, Y. et al. Identification and Characterization of Zebrafish SULT1 ST9, SULT3 ST4, and SULT3 ST5. **Aquatic Toxicology**, n. 419, p. 11–18, 2013.

PEREIRA, H. M. G. et al. Doping control analysis at the Rio 2016 Olympic and Paralympic Games. **Drug Testing and Analysis**, v. 9, n. 11–12, p. 1658–1672, 2017.

POELMANS, S. et al. Analytical possibilities for the detection of stanozolol and its metabolites. **Analytica Chimica Acta**, v. 473, n. 1–2, p. 39–47, 2002.

POLET, M.; EENOO, P. VAN; COPPIETERS, G. Gas chromatography − mass spectrometry analysis of non - hydrolyzed sulfated steroids by degradation product formation. n. February, p. 1656–1665, 2019.

POZO, O. J. et al. Detection and structural investigation of metabolites of stanozolol in human urine by liquid chromatography tandem mass spectrometry. **Steroids**, v. 74, n. 10–11, p. 837–852, 2009a.

POZO, O. J. et al. Combination of liquid-chromatography tandem mass spectrometry in different scan modes with human and chimeric mouse urine for the study of steroid metabolism. **Drug Testing and Analysis**, v. 1, p. 554–567, 2009b.

PRADO, E. et al. Metabolism of synthetic cathinones through the zebrafish water

tank model: a promising tool for forensic toxicology laboratories. **Forensic Toxicology**, n. 0123456789, 2020.

PROTTI, M.; MANDRIOLI, R.; MERCOLINI, L. Perspectives and strategies for anti-doping analysis. **Bioanalysis**, v. 11, n. 3, p. 149–152, 2019.

REITER, M. et al. Gene expression in hair follicle dermal papilla cells after treatment with stanozolol. **Biomarker Insights**, v. 2009, n. 4, p. 1–8, 2009.

RENSON, R. Fair play: Its origins and meanings in sport and society. **Kinesiology**, v. 41, n. 1, p. 5–18, 2009.

RUBIO, K. Do Olimpo ao pós-olimpismo: Elementos para a reflexão sobre o esporte atual. **Revista Paulista de Educação Física**, v. 16, n. 2, p. 130–143, 2002.

SARDELA, V. F. et al. Comprehensive analysis by liquid chromatography Q-Orbitrap mass spectrometry: Fast screening of peptides and organic molecules. **Journal of Mass Spectrometry**, v. 53, n. 6, p. 476–503, 2018a.

SARDELA, V. F. et al. Zebrafish (Danio rerio) water tank model for the investigation of drug metabolism: Progress, outlook, and challenges. **Drug Testing and Analysis**, v. 10, p. 1657–1669, 2018b.

SARDELA, V. F. et al. Comprehensive Zebrafish Water Tank Experiment for Metabolic Studies of Testolactone. **Zebrafish**, v. 00, n. 00, p. 1–8, 2020.

SARTORI, L. R. et al. A systematic investigation of the fragmentation pattern of two furanoheliangolide C-8 stereoisomers using electrospray ionization mass spectrometry. **Rapid Communications in Mass Spectrometry**, v. 28, n. 7, p. 723–730, 2014.

SCARTH, J. P. et al. The application of in vitro technologies to study the metabolism of the androgenic/anabolic steroid stanozolol in the equine. **Steroids**, v. 75, n. 1, p. 57–69, 2010.

SCHÄNZER, W. et al. Long-term detection and identification of metandienone and stanozolol abuse in athletes by gas chromatography-high-resolution mass spectrometry. **Journal of Chromatography B: Biomedical Applications**, v. 687, n. 1, p. 93–108, 1996.

SCHÄNZER, W. Metabolism of anabolic androgenic steroids. **Clinical Chemistry**, v. 42, n. 7, p. 1001–1020, 1996.

SCHÄNZER, W. et al. Expanding analytical possibilities concerning the detection of stanozolol misuse by means of high resolution/high accuracy mass spectrometric detection of stanozolol glucuronides in human sports drug testing. **Drug Testing and Analysis**, v. 5, n. 11–12, p. 810–818, 2013.

SCHÄNZER, W.; OPFERMANN, G.; DONIKE, M. Metabolism of stanozolol: Identification and synthesis of urinary metabolites. **Journal of Steroid Biochemistry**, v. 36, n. 1–2, p. 153–174, 1990.

SCHÄNZER, W.; OPFERMANN, G.; DONIKE, M. 17-Epimerization of 17a-methyl anabolic steroids iu humans: metabolism and synthesis of 17a-hydroxy-17b-methyl steroid. **Steroids**, v. 57, p. 537–550, 1992.

SEGRAVE, J. O. The sports metaphor in American cultural discourse. n. June 2013, p. 37–41, 2007.

SERRANO-DURÁ, J.; MOLINA, P.; MARTÍNEZ-BAENA, A. Systematic review of research on fair play and sporting competition. **Sport, Education and Society**, v. 0, n. 0, p. 1–15, 2020.

SHARMA, A. K. Doping In Sports : A Review. **International Journal of Physical Education and Sports**, v. 125, n. 1992, p. 51–58, 2017.

SMITH, A. C. T.; STEWART, B. Why the war on drugs in sport will never be won. **Harm Reduction Journal**, v. 12, n. 1, p. 4–9, 2015.

SOBOLEVSKY, T.; RODCHENKOV, G. Journal of Steroid Biochemistry and Molecular Biology Detection and mass spectrometric characterization of novel long-term dehydrochloromethyltestosterone metabolites in human urine. **Journal of Steroid Biochemistry and Molecular Biology**, v. 128, n. 3–5, p. 121–127, 2012.

TESTA, B.; KRÄMER, S. D. The Biochemistry of Drug Metabolism – An Introduction Part 4. Reactions of Conjugation and Their Enzymes. **CHEMISTRY & BIODIVERSITY**, v. 5, p. 2171–2336, 2008.

THEVIS, M. et al. Mass spectrometry of stanozolol and its analogues using electrospray ionization and collision-induced dissociation with quadrupole-linear ion trap and linear ion trap-orbitrap hybrid mass analyzers. **Rapid Communications in Mass Spectrometry**, v. 19, p. 3369–3378, 2005.

THEVIS, M. et al. Analytical challenges in sports drug testing. **Analytical and Bioanalytical Chemistry**, v. 410, n. 9, p. 2275–2281, 2018.

THEVIS, M.; WALPURGIS, K.; THOMAS, A. Analytical Approaches in Human Sports Drug Testing: Recent Advances, Challenges, and Solutions. **Analytical Chemistry**, 2019.

TIERBACH, A. et al. Glutathione S-Transferase protein expression in different life stages of zebrafish (Danio rerio). **Toxicological Sciences**, v. 162, n. 2, p. 702–712, 2018.

TUDELA, E.; DEVENTER, K.; VAN EENOO, P. Sensitive detection of 3'-hydroxy-stanozolol glucuronide by liquid chromatography-tandem mass spectrometry. **Journal of Chromatography A**, v. 1292, n. 2010, p. 195–200, 2013.

VAN CRUCHTEN, S. T. J. et al. Absorption, distribution, and biliary excretion of cafestol, a potent cholesterol-elevating compound in unfiltered coffees, in mice. **Drug Metabolism and Disposition**, v. 38, n. 4, p. 635–640, 2010.

VESSECCHI, R. et al. Re - examination of the anion derivatives of isoflavones by radical fragmentation in negative electrospray ionization tandem mass spectrometry : experimental and computational studies. **Rapid Communication in Mass Spectrometry**, v. 25, n. April 2011, p. 2020–2026, 2020.

WADA. World Anti-Doping Code. **The World Anti-Doping Code**, 2014.

WADA. 2018 Anti-Doping Testing. **Word Anti-doping Agency**, v. 6, p. 2–6, 2018.

WADA. **International Standrad for Laboratories**.

WADA. **Prohibited List**.

WANG, Y.; HUANG, H.; WU, Q. Characterization of the Zebrafish Ugt Repertoire Reveals a New Class of Drug-Metabolizing UDP Glucuronosyltransferases. **Molecular pharmacology**, v. 82, p. 62–75, 2014.

YI, L. et al. Identification of sulfation sites of metabolites and prediction of the compounds' biological effects. **Analytical and Bioanalytical Chemistry**, v. 386, n. 3, p. 666–674, 2006.

Appendix 1 – Rationalization of ZWT's detected metabolites

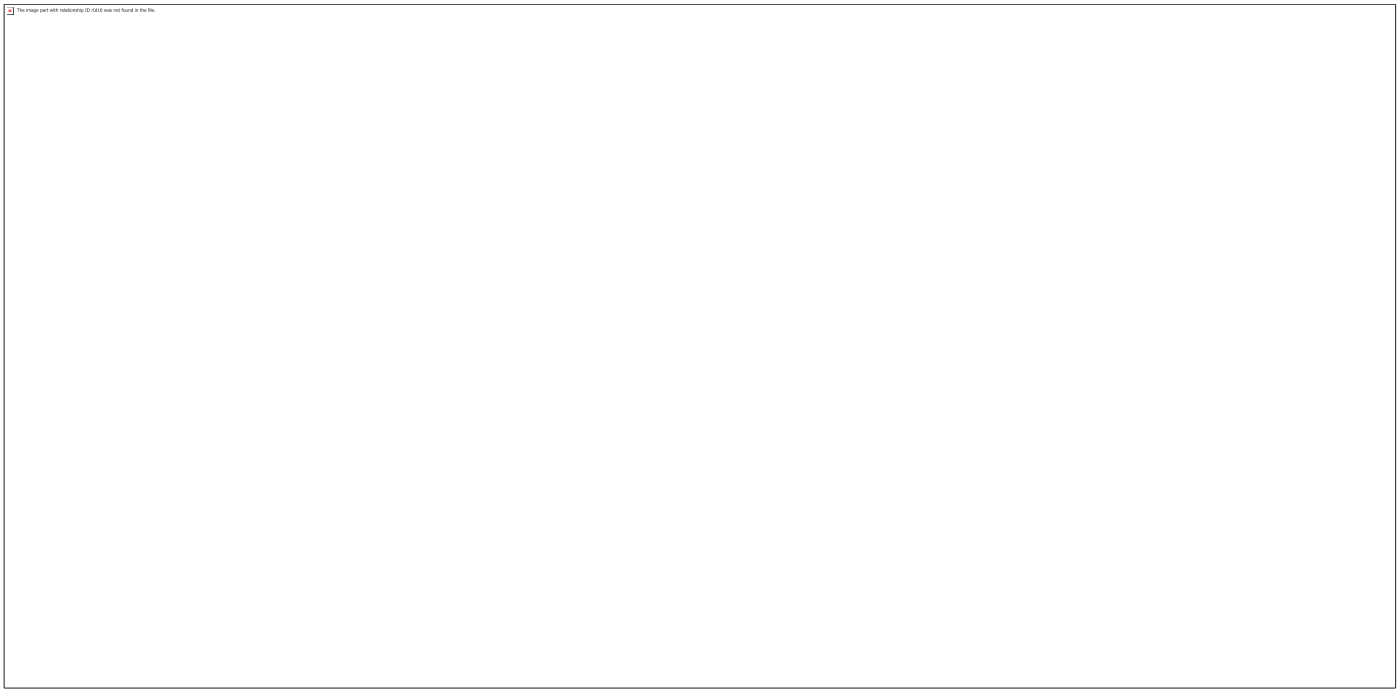
The image part with relationship ID rId10 was not found in the file.

Appendix 2 – Confirmation of 3’OH-STAN-G

Appendix 3 – OH-STAN-G isomer **M2** fragmentations, applying collision energy between 0 and 70 eV using Orbitrap-HCD

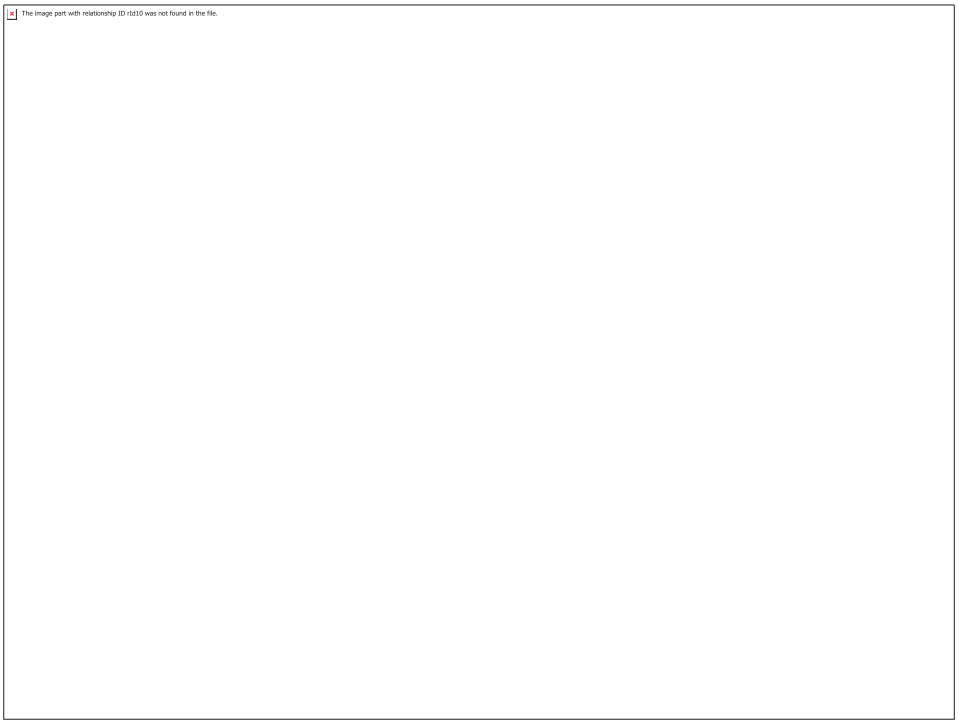

MS/MS spectra of **M2** using Orbitrap-HCD at 10 eV.

MS/MS spectra of **M2** using Orbitrap-HCD at 15 eV.

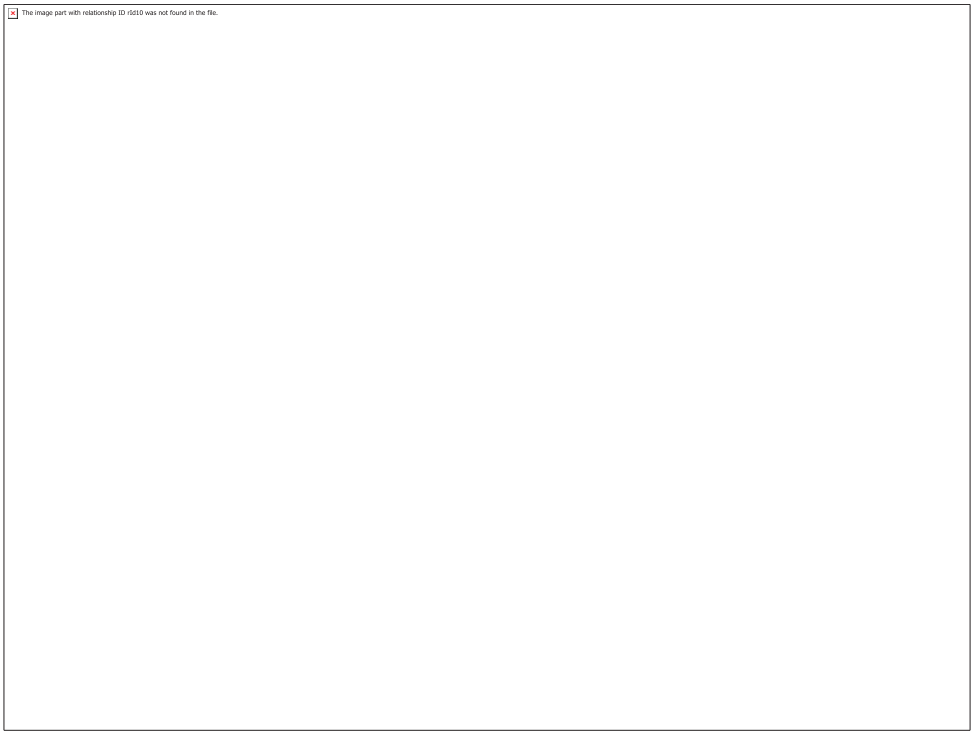

MS/MS spectra of **M2** using Orbitrap-HCD at 25 eV.

MS/MS spectra of **M2** using Orbitrap-HCD at 30 eV.

MS/MS spectra of **M2** using Orbitrap-HCD at 33 eV.

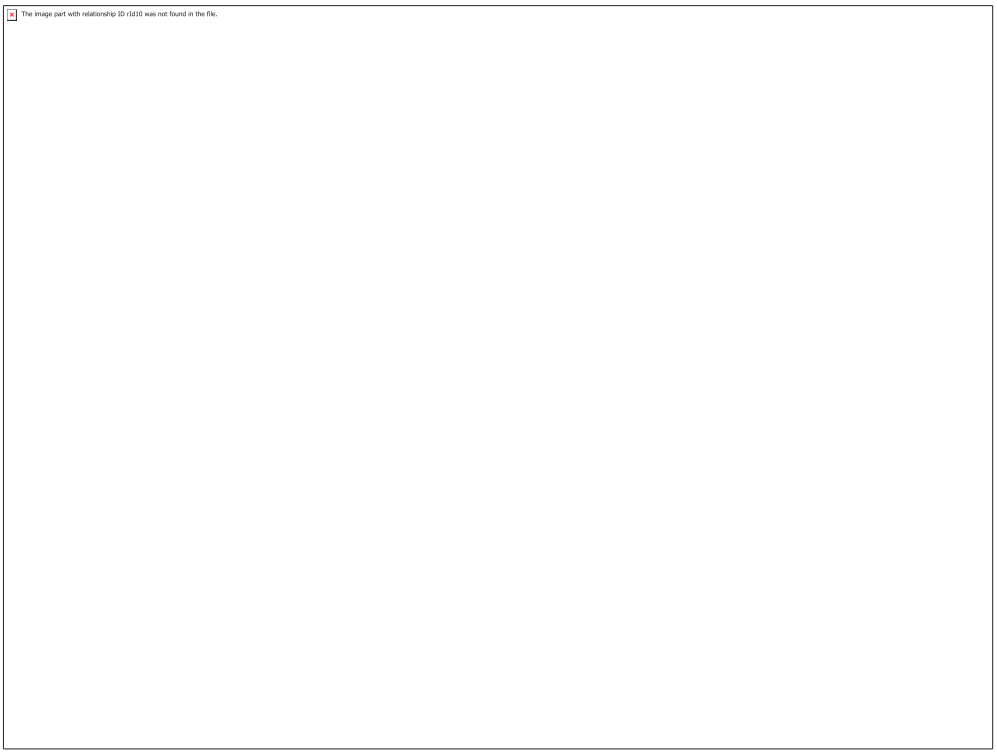

MS/MS spectra of **M2** using Orbitrap-HCD at 35 eV.

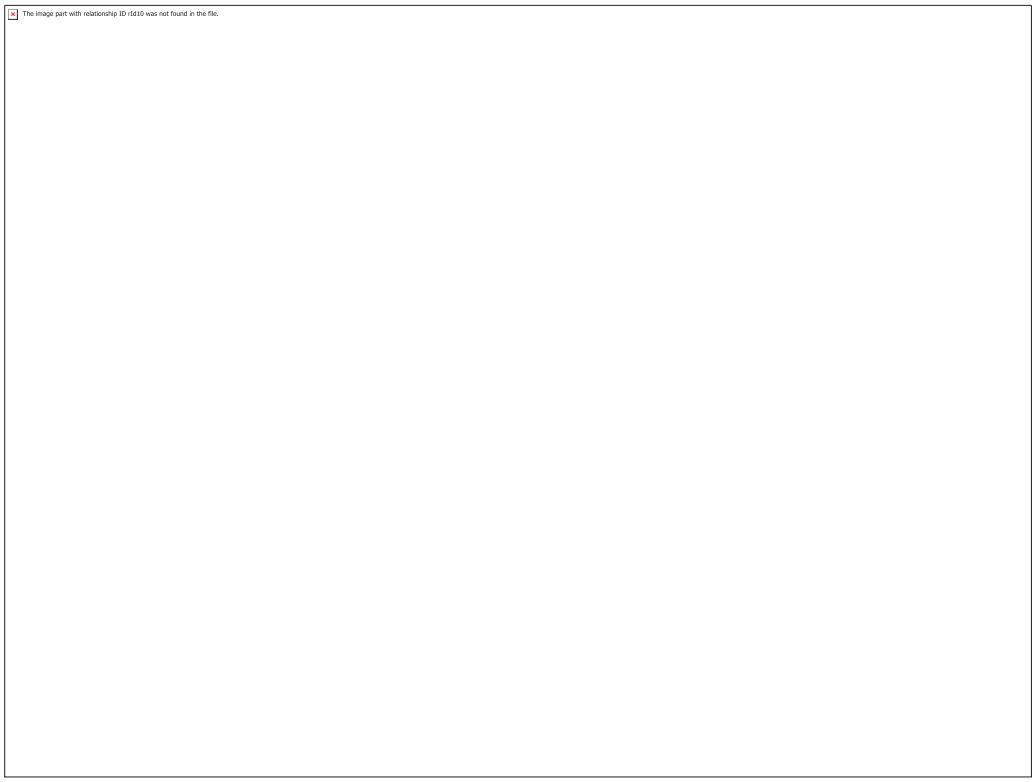

MS/MS spectra of **M2** using Orbitrap-HCD at 40 eV.

MS/MS spectra of **M2** using Orbitrap-HCD at 43 eV.

MS/MS spectra of **M2** using Orbitrap-HCD at 50 eV.

MS/MS spectra of **M2** using Orbitrap-HCD at 55 eV.

MS/MS spectra of **M2** using Orbitrap-HCD at 65 eV.

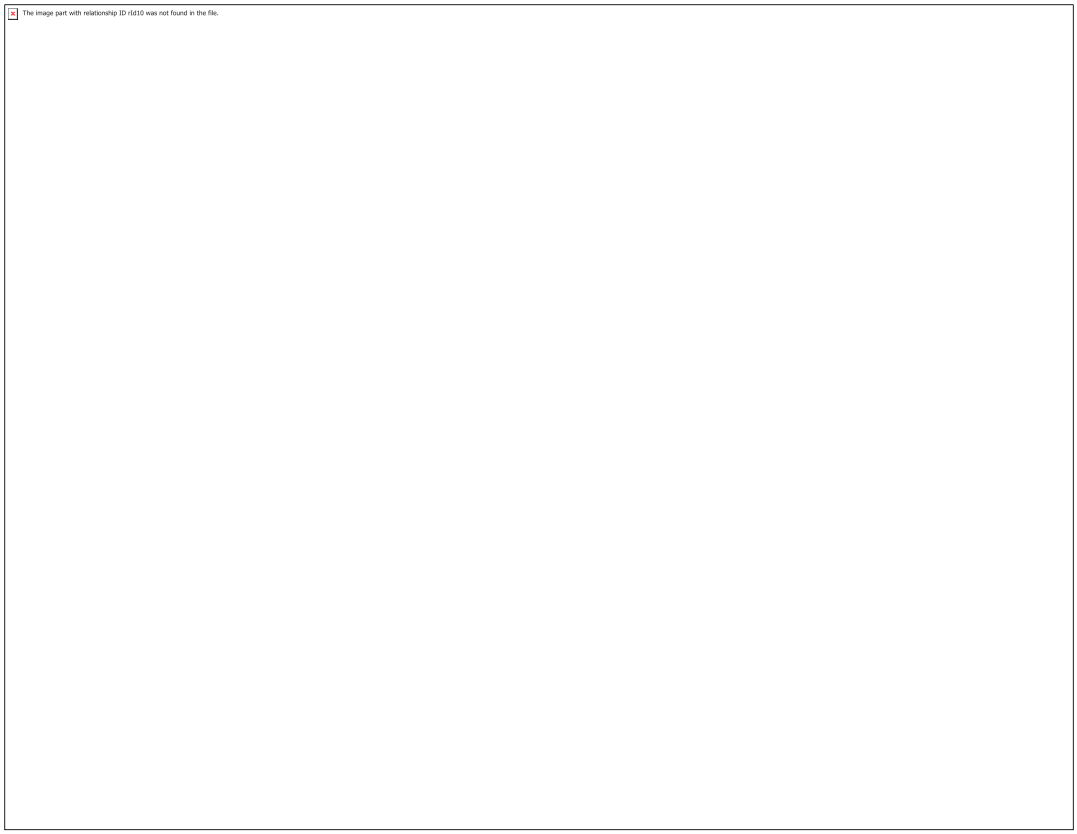

MS/MS spectra of **M2** using Orbitrap-HCD at 65 eV.

Appendix 4 – OH-STAN-G isomer **M3** fragmentations, applying collision energy between 0 and 70 eV using Orbitrap-HCD

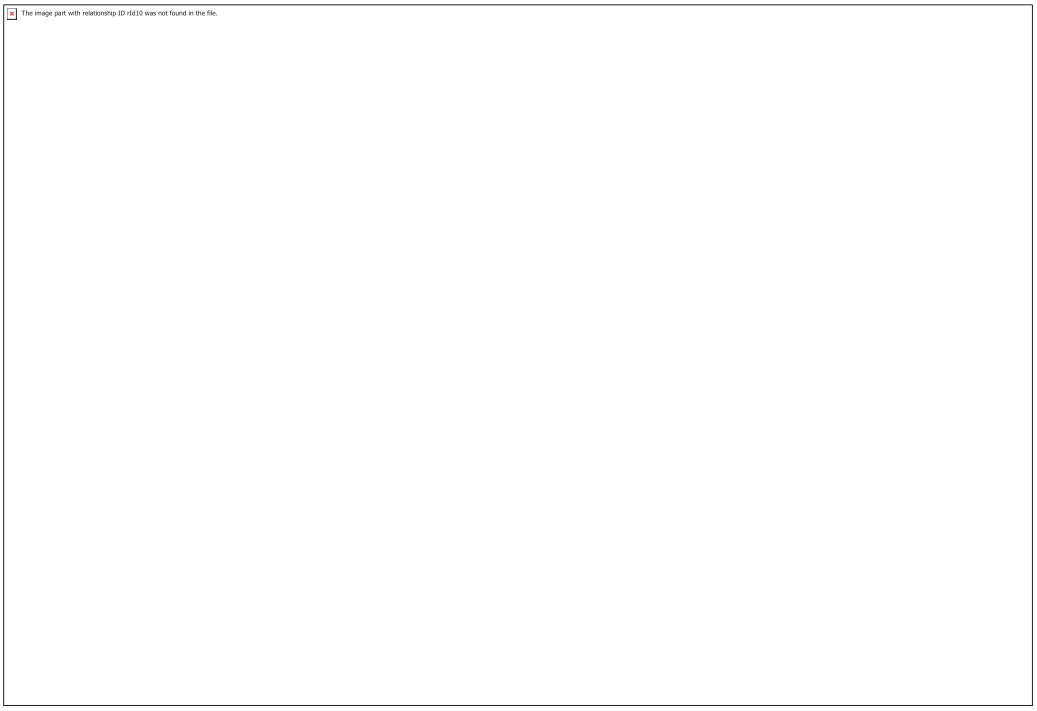

MS/MS spectra of **M3** using Orbitrap-HCD at 10 eV**.**

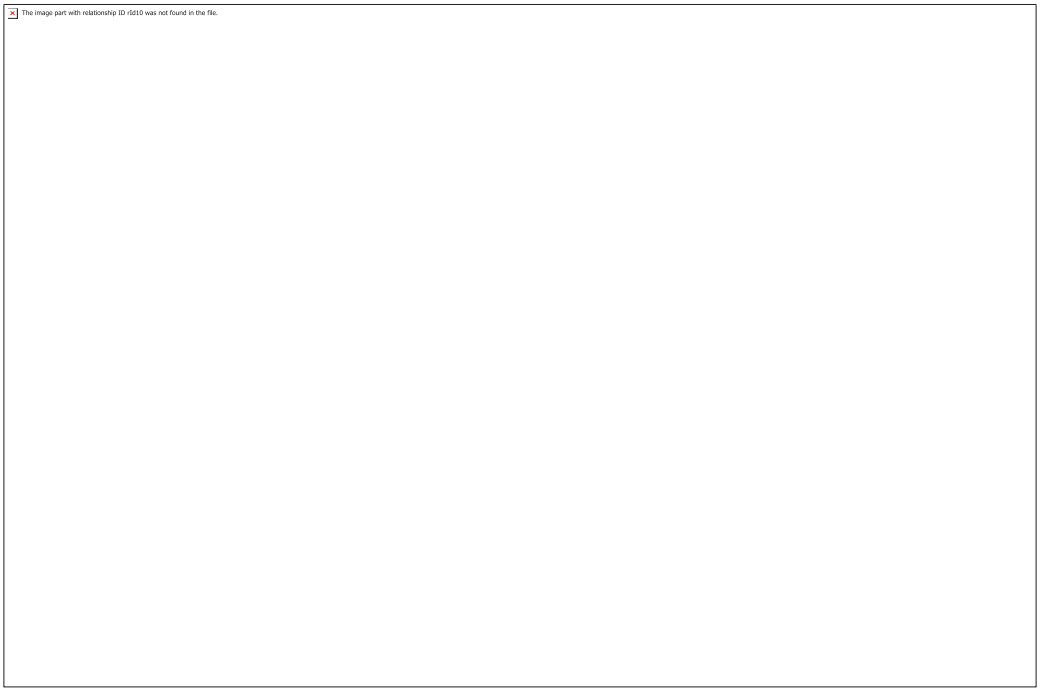

MS/MS spectra of **M3** using Orbitrap-HCD at 15 eV.

MS/MS spectra of **M3** using Orbitrap-HCD at 20 eV**.**

MS/MS spectra of **M3** using Orbitrap-HCD at 25 eV.

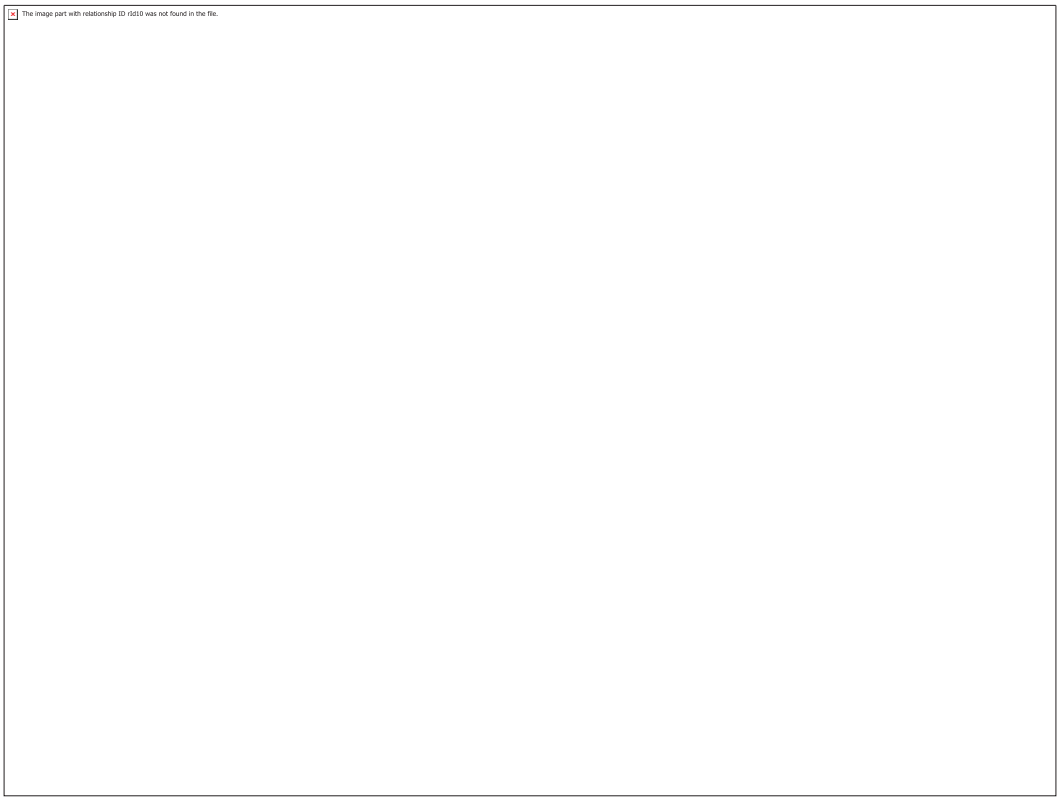

MS/MS spectra of **M3** using Orbitrap-HCD at 30 eV.

MS/MS spectra of **M3** using Orbitrap-HCD at 33 eV.

MS/MS spectra of **M3** using Orbitrap-HCD at 35 eV.

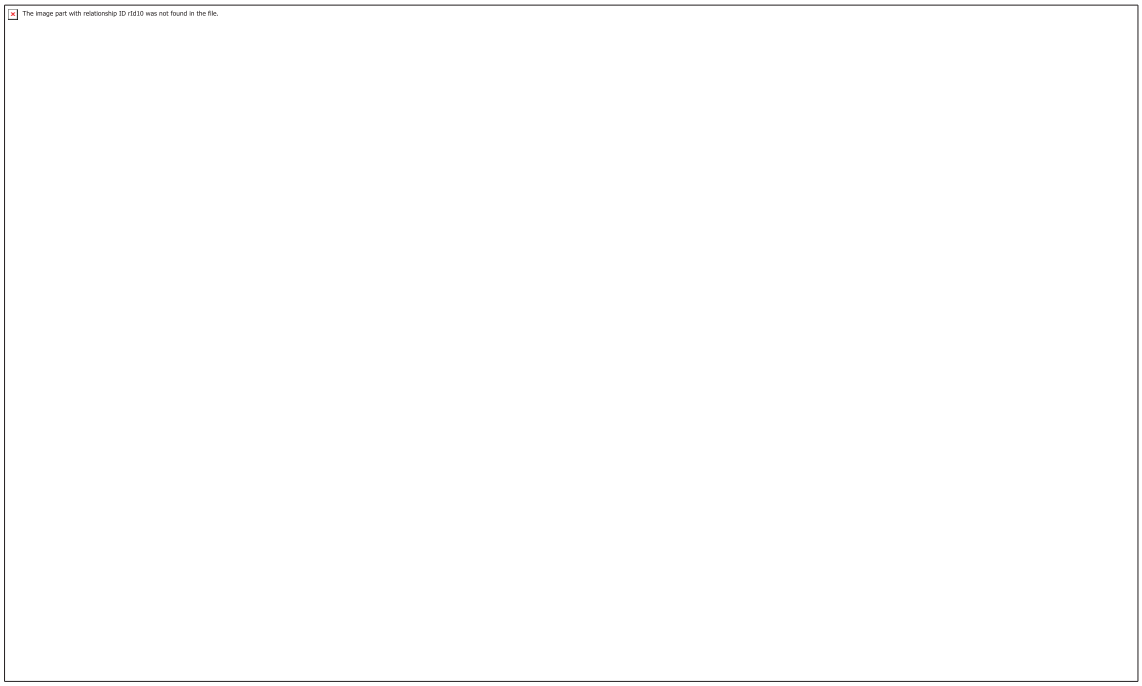

MS/MS spectra of **M3** using Orbitrap-HCD at 40 eV**.**

MS/MS spectra of **M2** using Orbitrap-HCD at 43 eV.

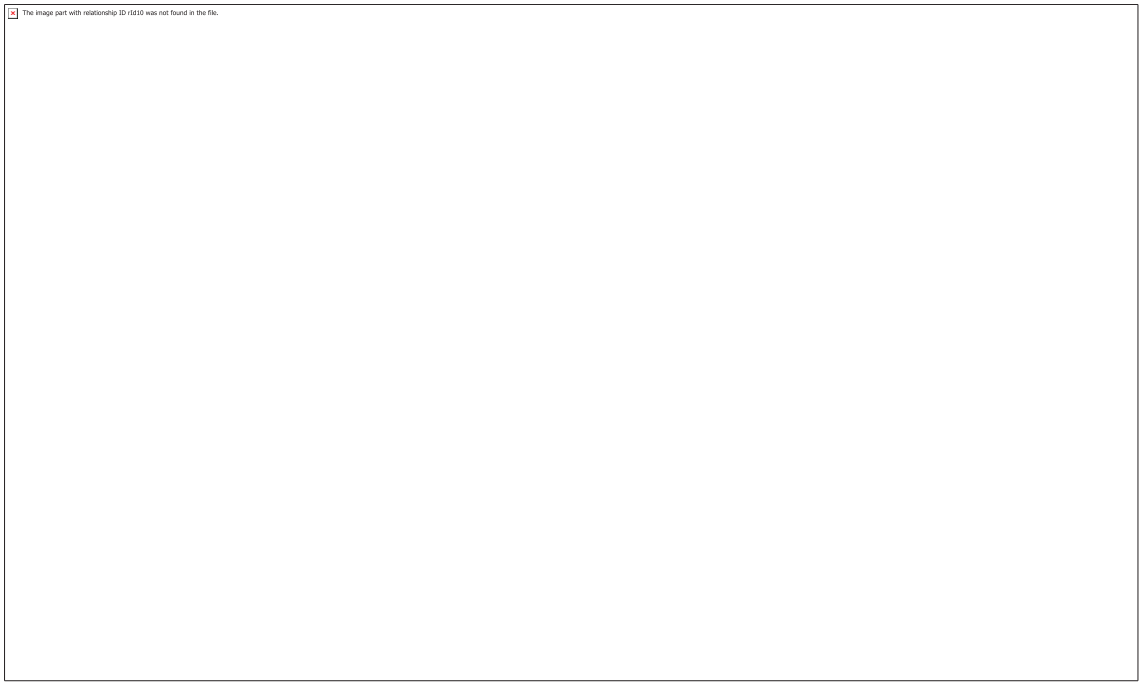

MS/MS spectra of **M3** using Orbitrap-HCD at 45 eV.

MS/MS spectra of **M3** using Orbitrap-HCD at 50 eV.

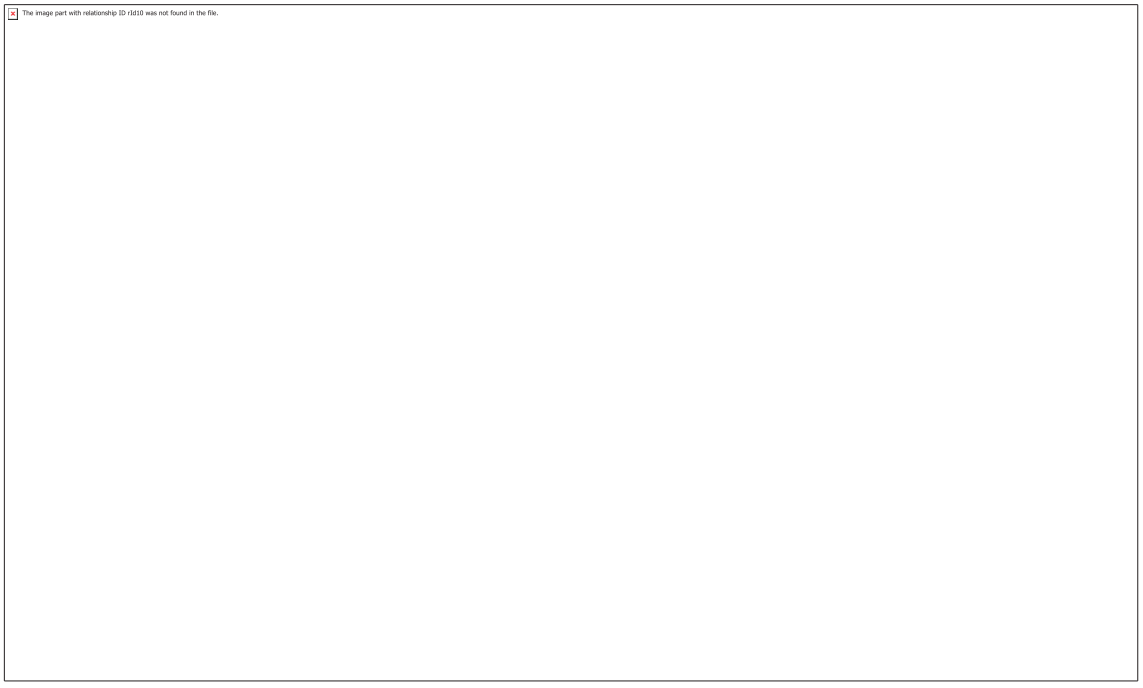

MS/MS spectra of **M3** using Orbitrap-HCD at 55 eV.

MS/MS spectra of **M3** using Orbitrap-HCD at 65 eV.

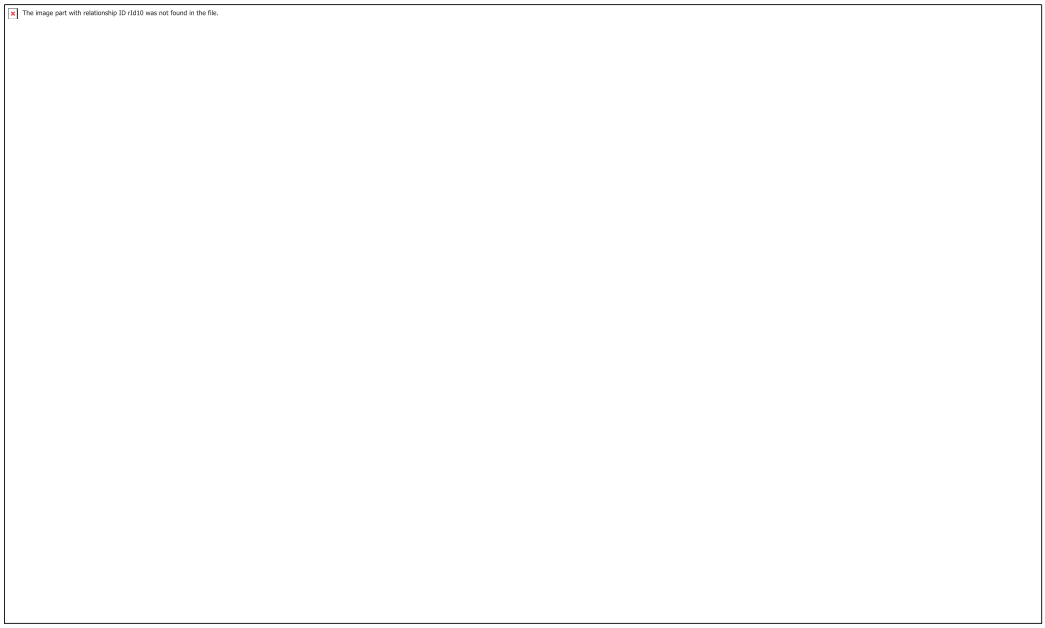

MS/MS spectra of **M3** using Orbitrap-HCD at 70 eV.

Appendix 5 – OH-STAN-G isomer **M4** fragmentations, applying collision energy between 0 and 70 eV using Orbitrap-HCD

MS/MS spectra of **M4** using Orbitrap-HCD at 10 eV.

MS/MS spectra of **M4** using Orbitrap-HCD at 15 eV.

MS/MS spectra of **M4** using Orbitrap-HCD at 20 eV.

MS/MS spectra of **M4** using Orbitrap-HCD at 25 eV.

MS/MS spectra of **M4** using Orbitrap-HCD at 30 eV**.**

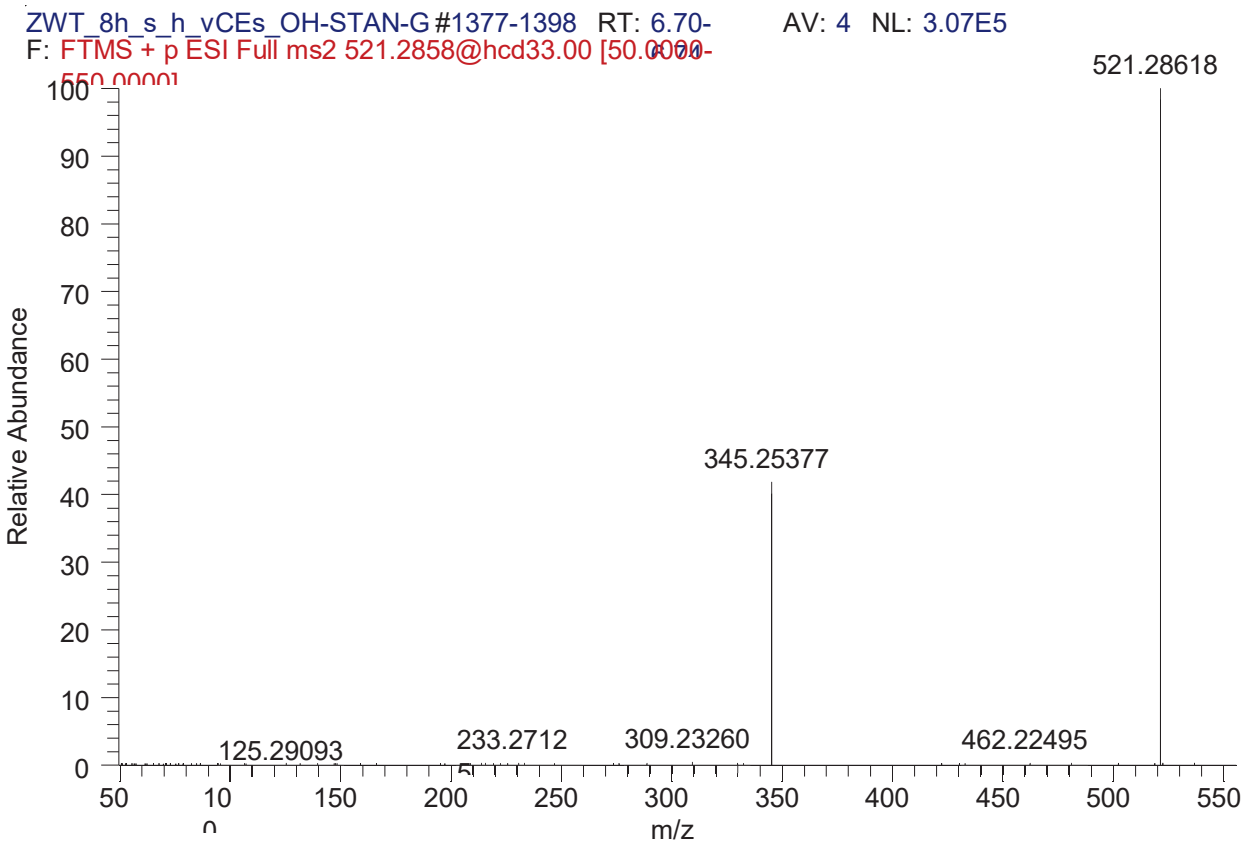

MS/MS spectra of **M4** using Orbitrap-HCD at 33 eV.

MS/MS spectra of **M4** using Orbitrap-HCD at 35 eV.

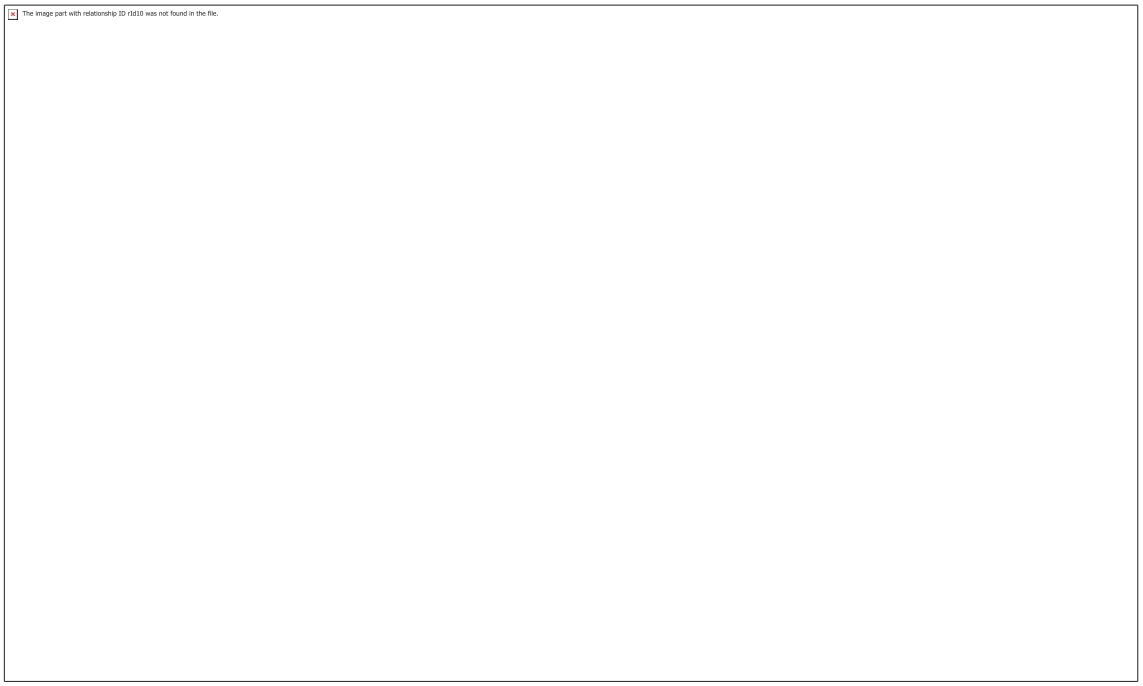

MS/MS spectra of **M4** using Orbitrap-HCD at 40 eV.

MS/MS spectra of **M4** using Orbitrap-HCD at 43 eV.

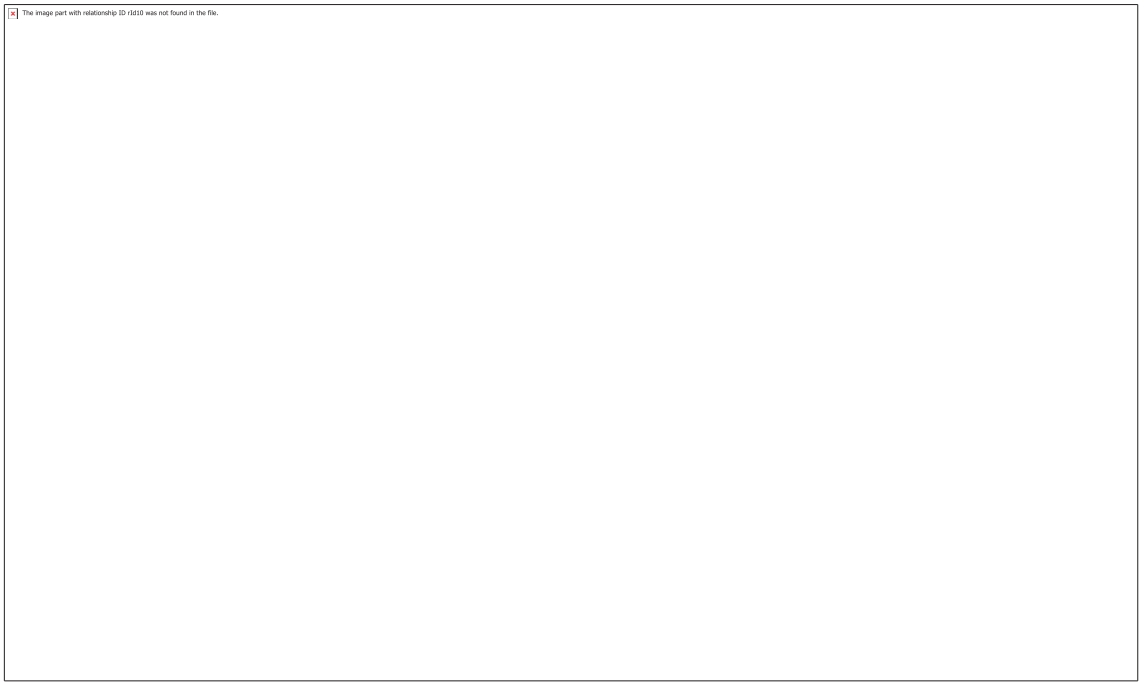

MS/MS spectra of **M4** using Orbitrap-HCD at 45 eV.

MS/MS spectra of **M4** using Orbitrap-HCD at 50 eV.

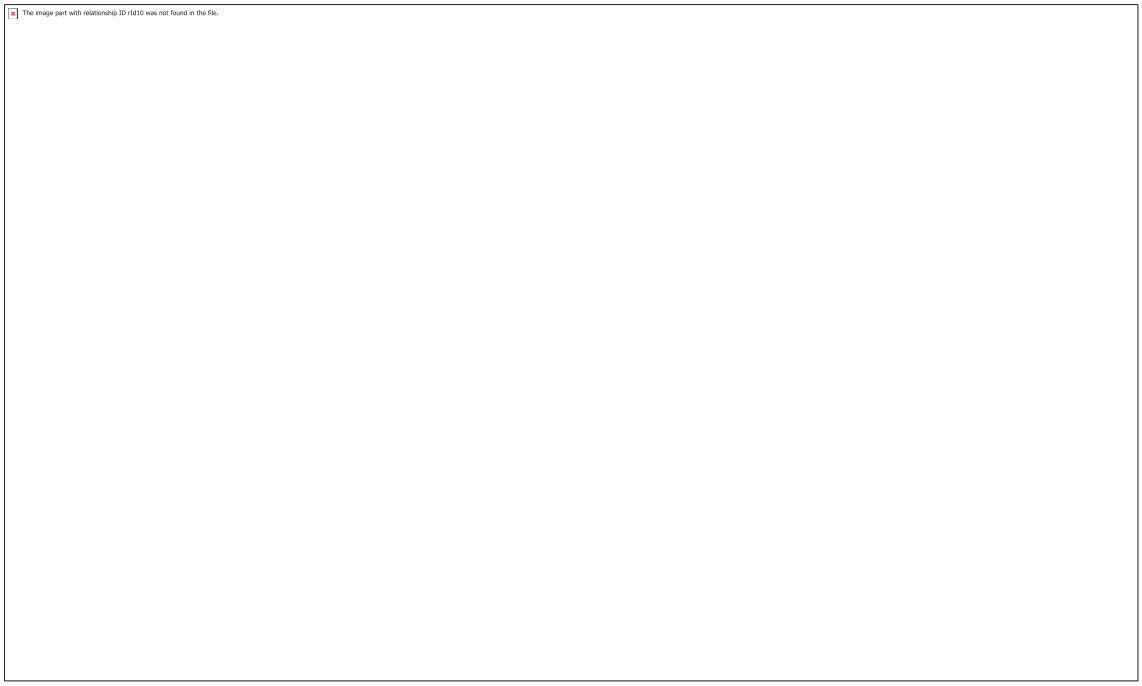

MS/MS spectra of **M4** using Orbitrap-HCD at 55 eV.

MS/MS spectra of **M4** using Orbitrap-HCD at 65 eV.

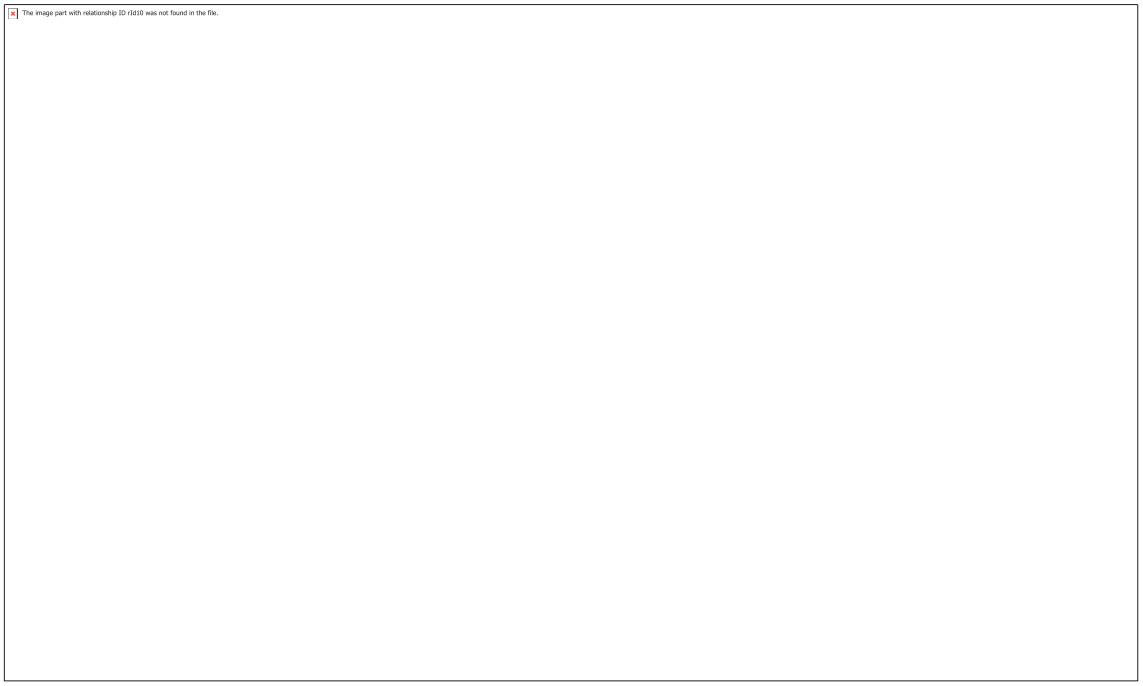

MS/MS spectra of **M4** using Orbitrap-HCD at 70 eV.

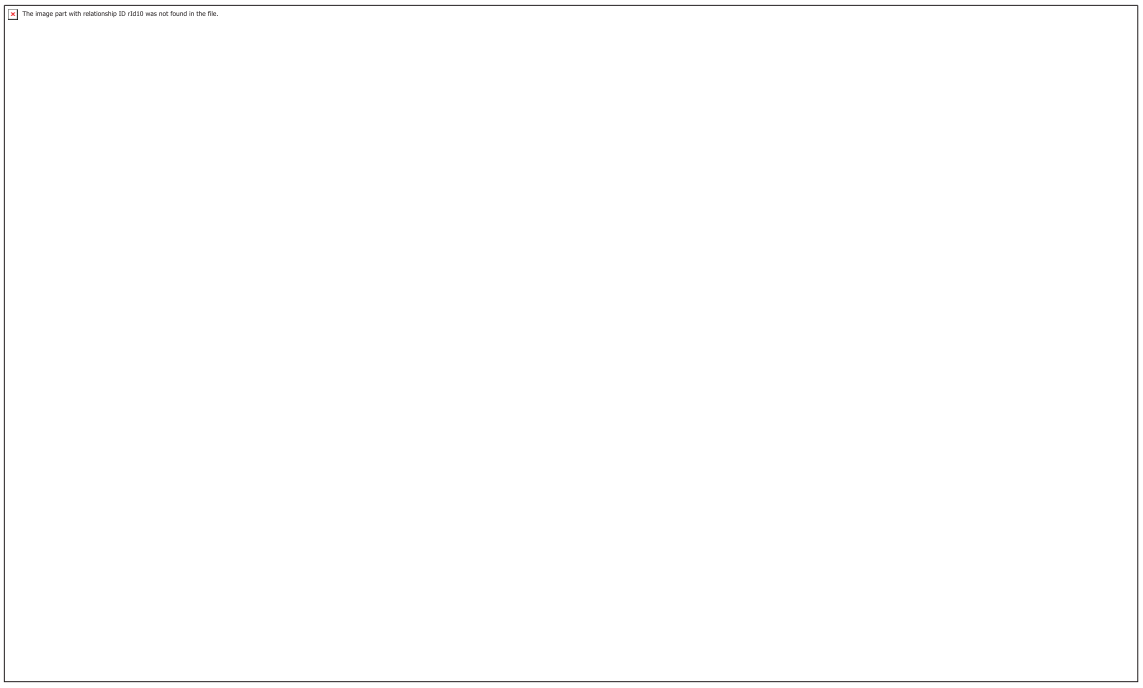

MS/MS spectra of **M4** using Orbitrap-HCD at 75 eV.

Appendix 6 – OH-STAN-G isomer **M5** – confirmed as 3'OH-STAN-G – fragmentations, applying collision energy between 0 and 70 eV using Orbitrap-HCD

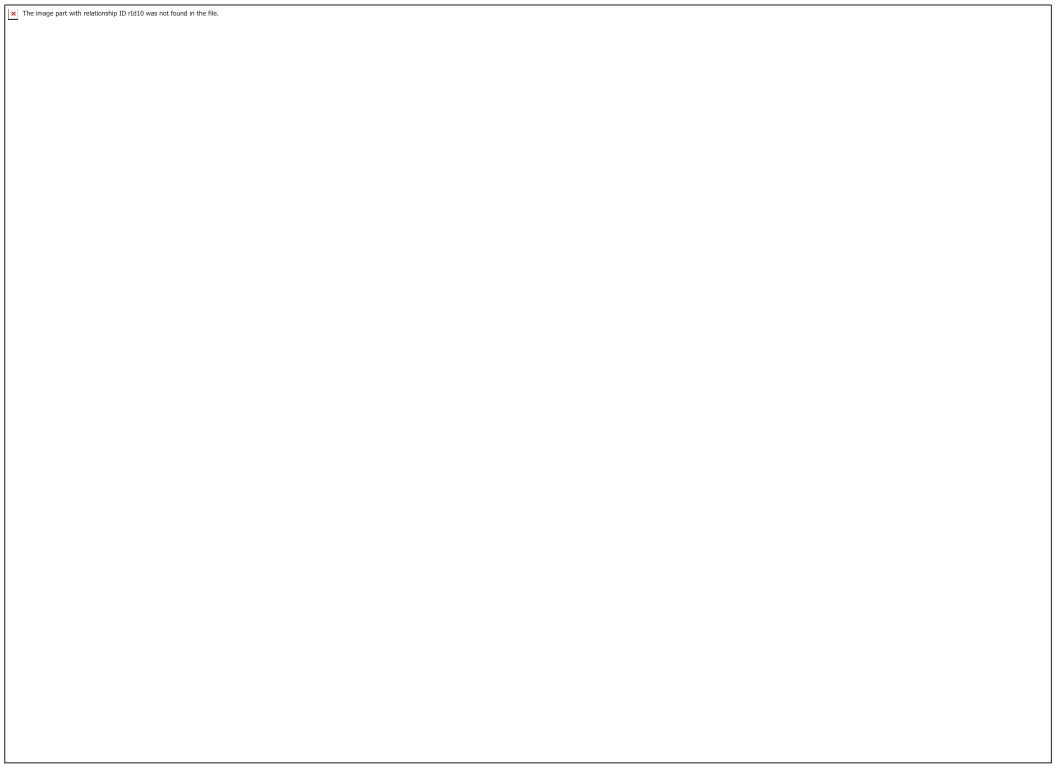

MS/MS spectra of **M5** using Orbitrap-HCD at 10 eV.

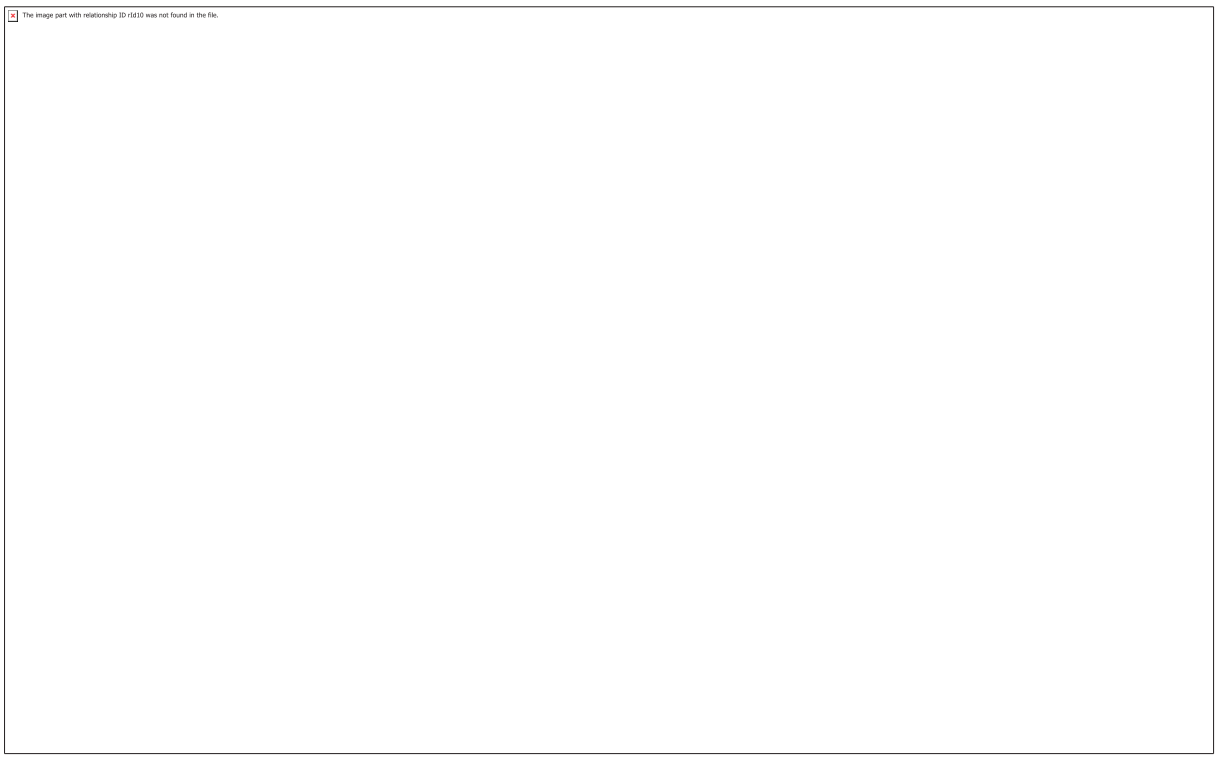

MS/MS spectra of **M5** using Orbitrap-HCD at 15 eV.

MS/MS spectra of **M5** using Orbitrap-HCD at 20 eV.

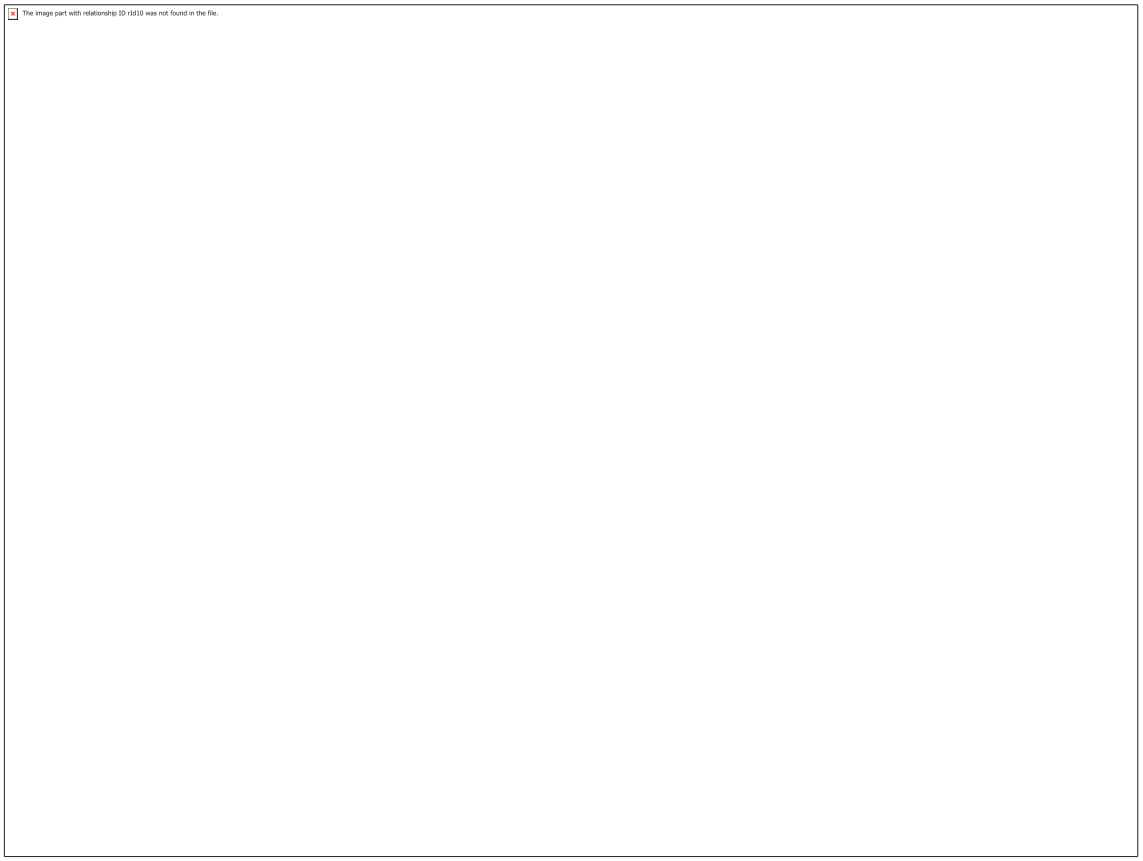

MS/MS spectra of **M5** using Orbitrap-HCD at 25 eV.

MS/MS spectra of **M5** using Orbitrap-HCD at 30 eV.

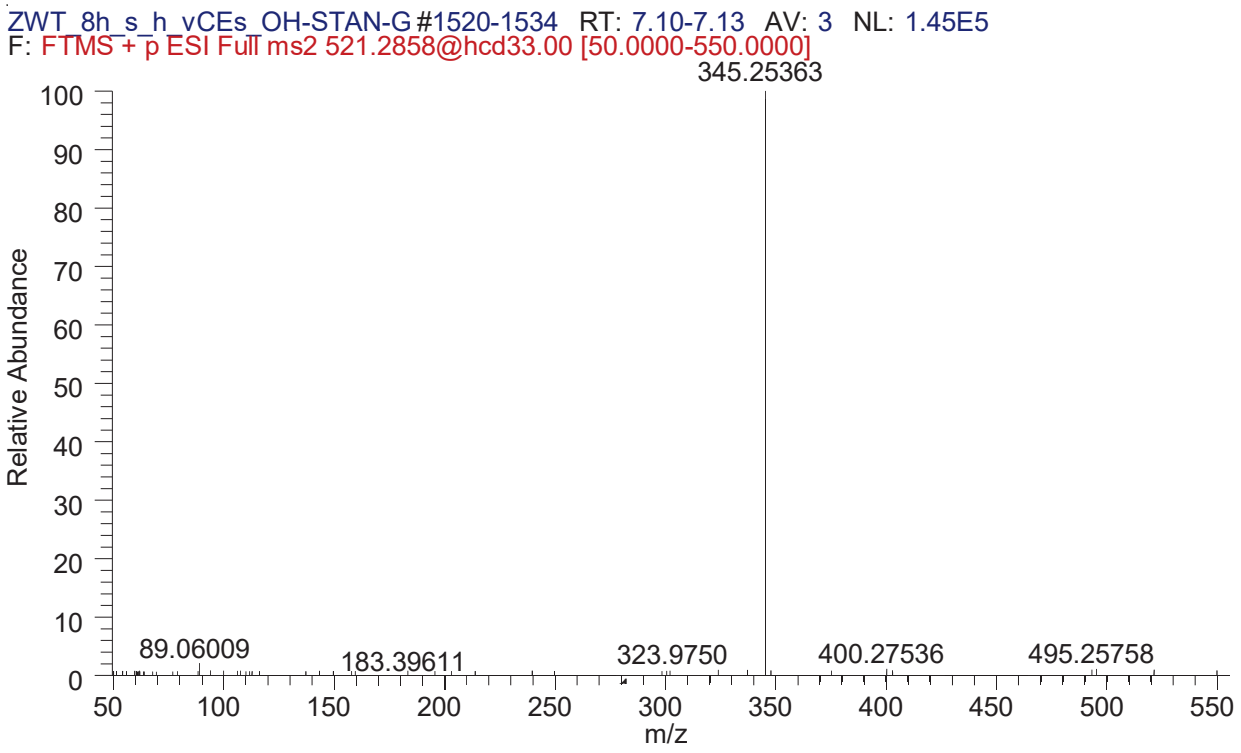

MS/MS spectra of **M5** using Orbitrap-HCD at 33 eV.

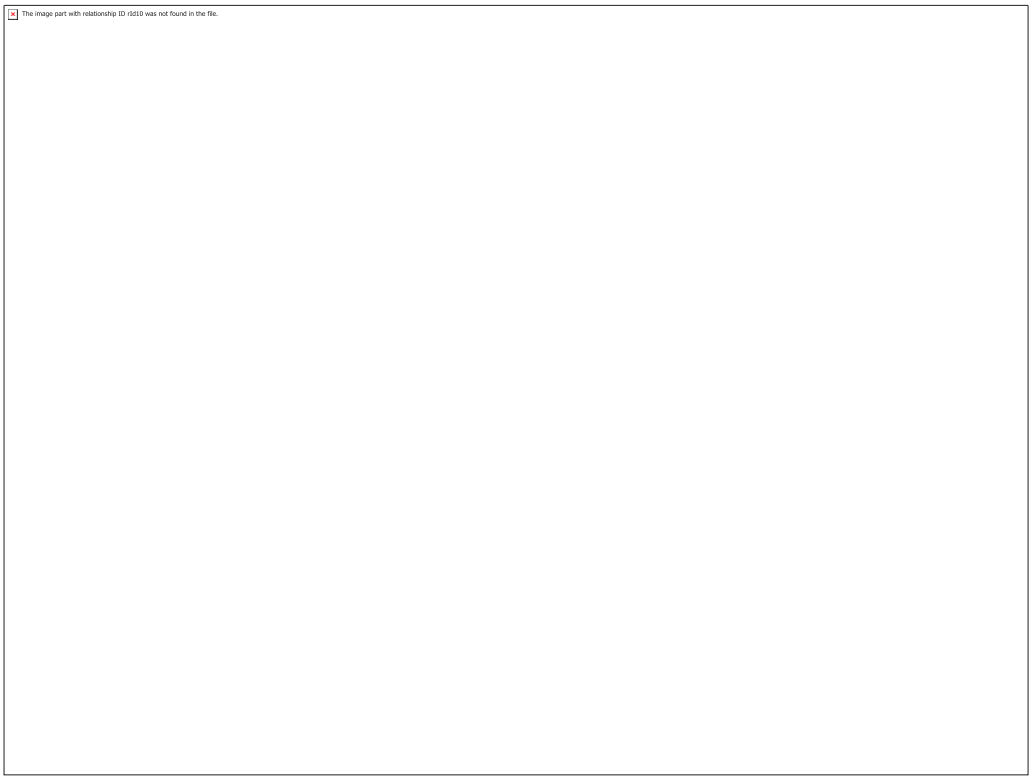

MS/MS spectra of **M5** using Orbitrap-HCD at 35 eV.

MS/MS spectra of **M5** using Orbitrap-HCD at 40 eV.

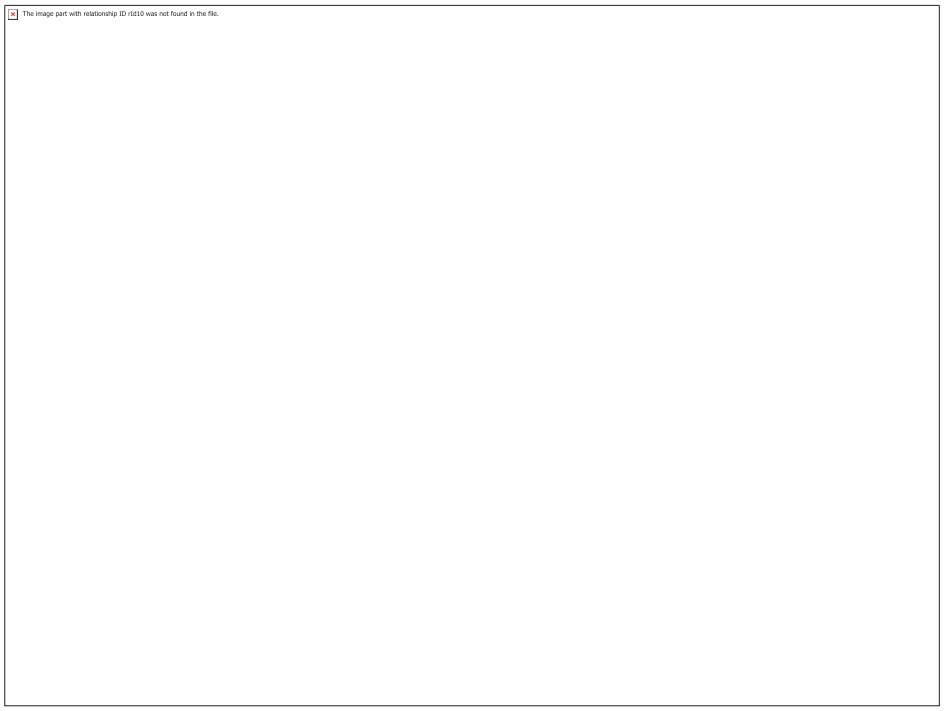

MS/MS spectra of **M5** using Orbitrap-HCD at 50 eV.

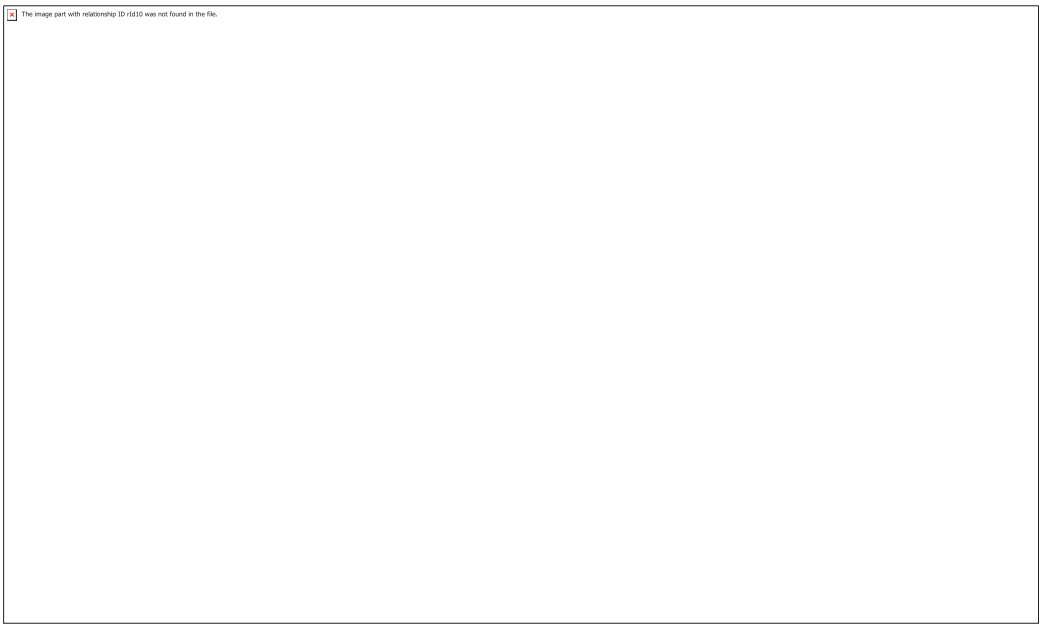

MS/MS spectra of **M5** using Orbitrap-HCD at 65 eV.

MS/MS spectra of **M5** using Orbitrap-HCD at 70 eV.

Appendix 7 – STAN-N-G isomer **M10** fragmentations, applying collision energy between 10 and 70 eV using Orbitrap-HCD

MS/MS spectra of **M10** using Orbitrap-HCD at 10 eV.

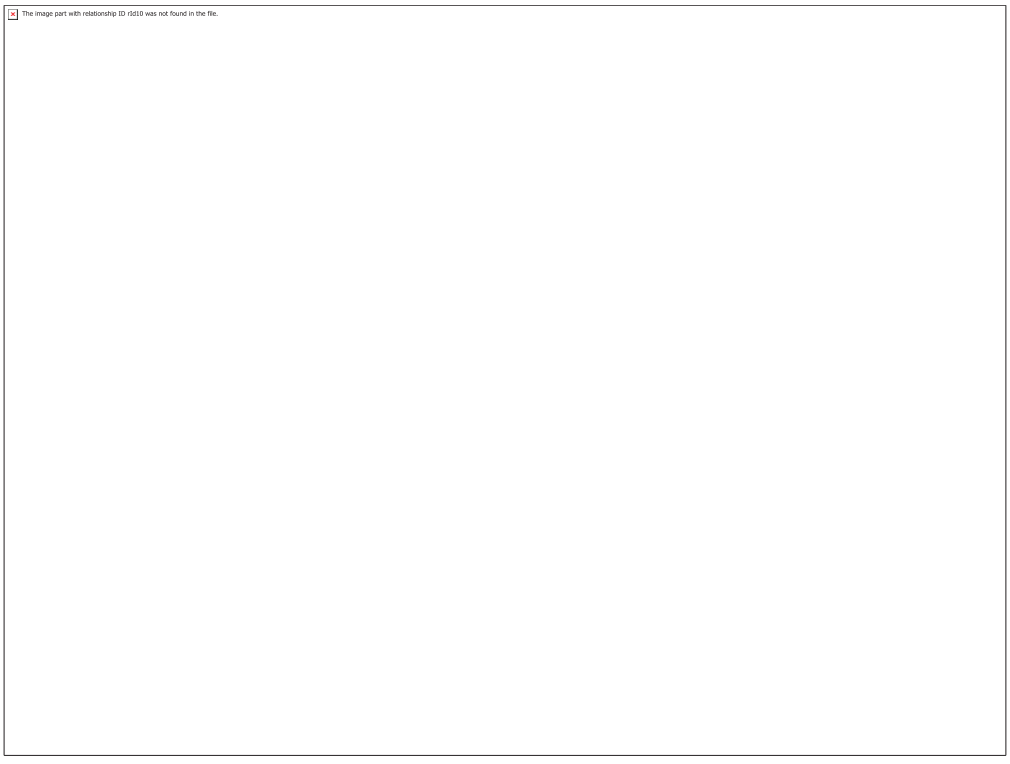

MS/MS spectra of **M10** using Orbitrap-HCD at 15 eV.

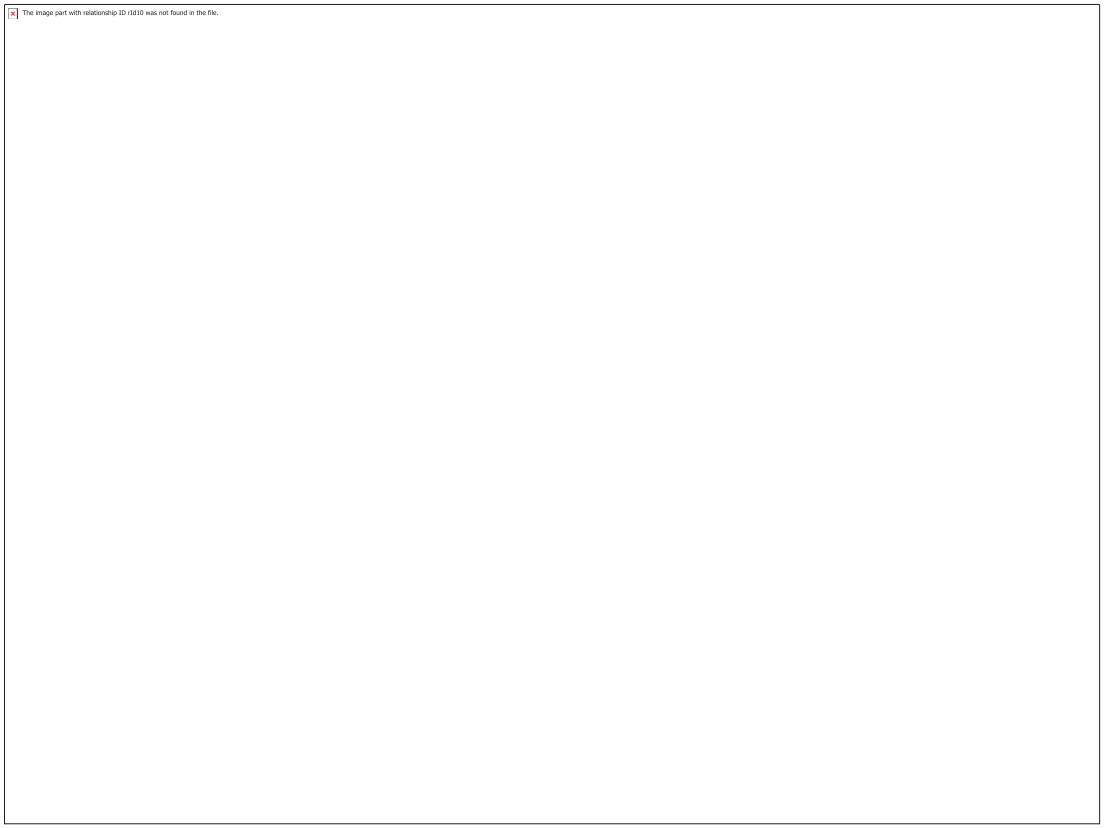

MS/MS spectra of **M10** using Orbitrap-HCD at 25 eV.

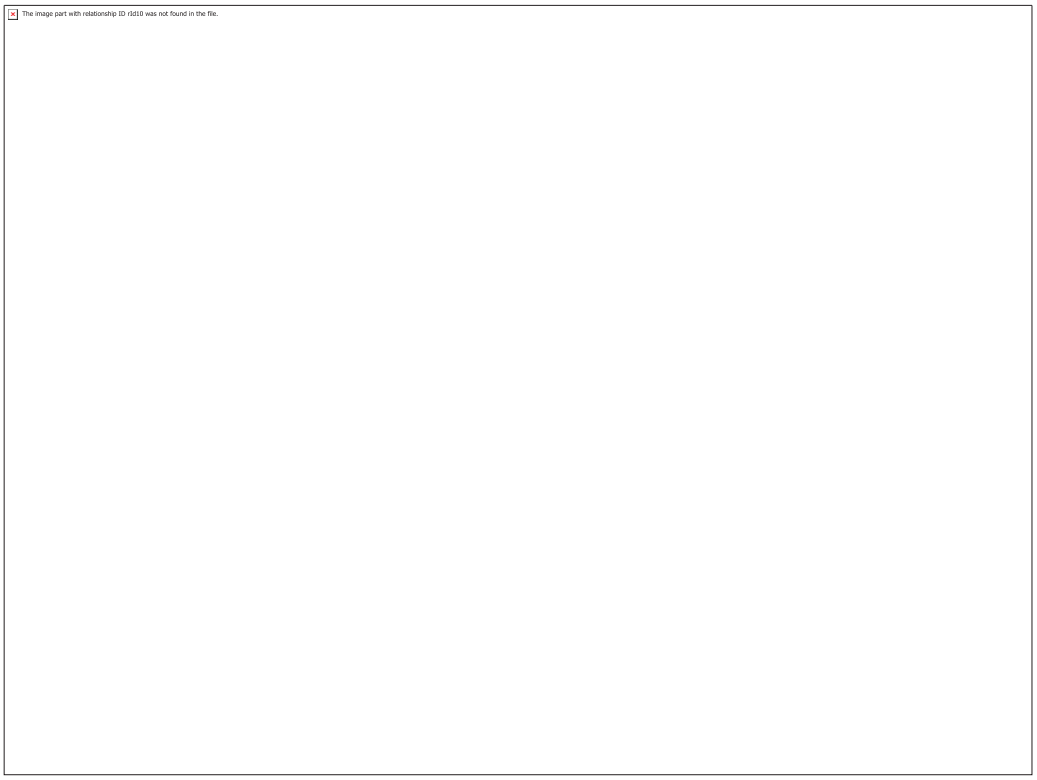

MS/MS spectra of **M10** using Orbitrap-HCD at 33 eV.

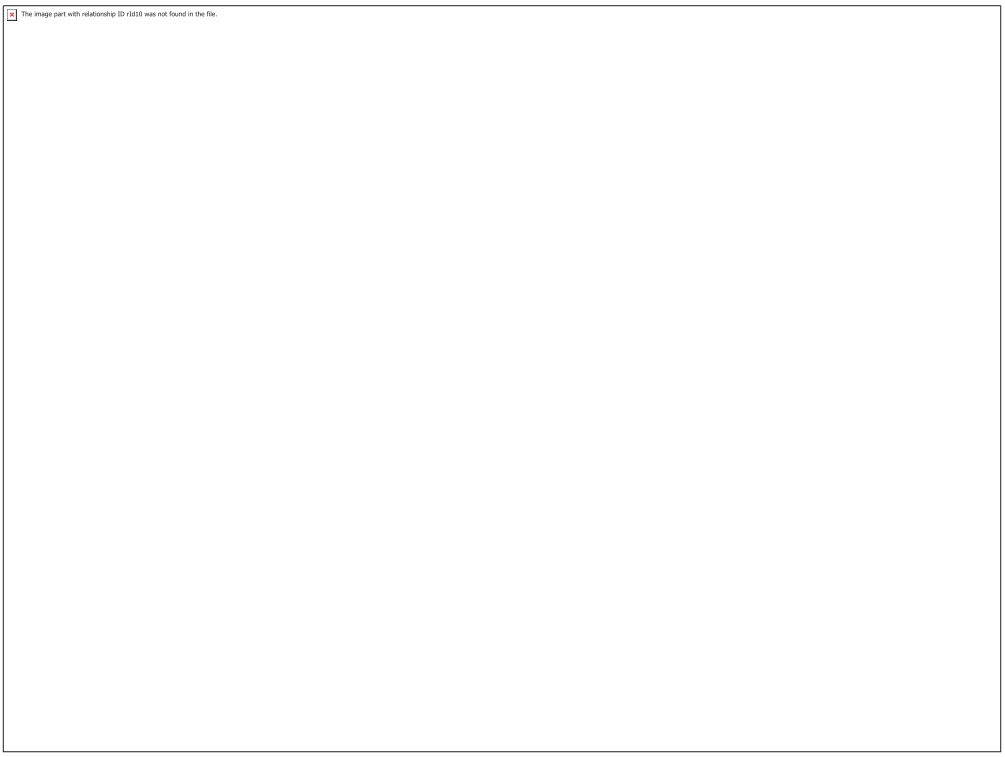

MS/MS spectra of **M10** using Orbitrap-HCD at 40 eV.

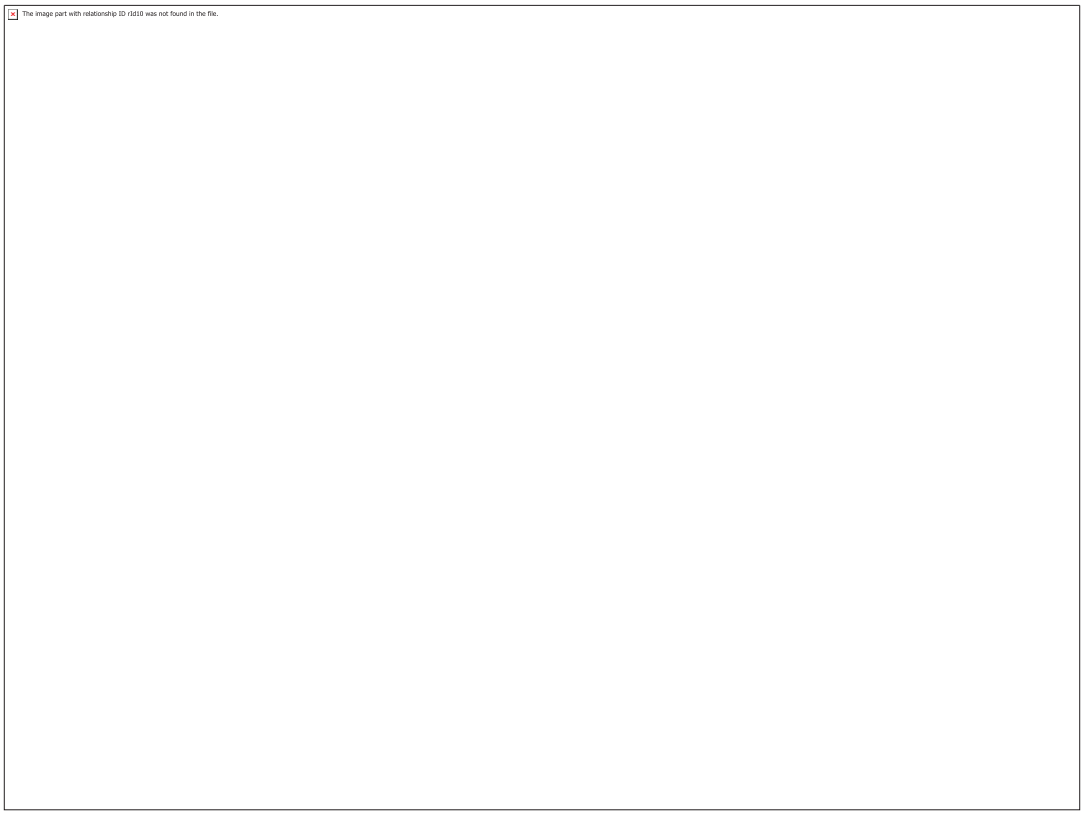

MS/MS spectra of **M10** using Orbitrap-HCD at 45 eV.

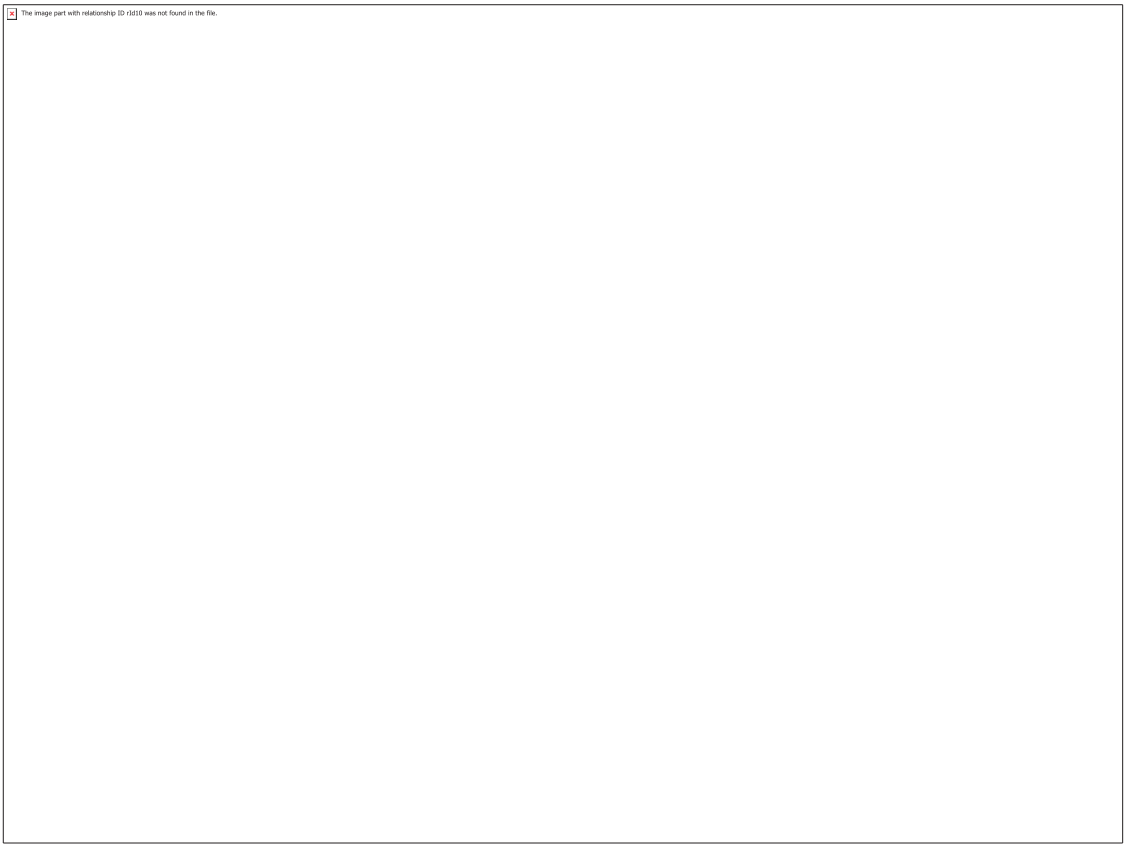

MS/MS spectra of **M10** using Orbitrap-HCD at 55 eV.

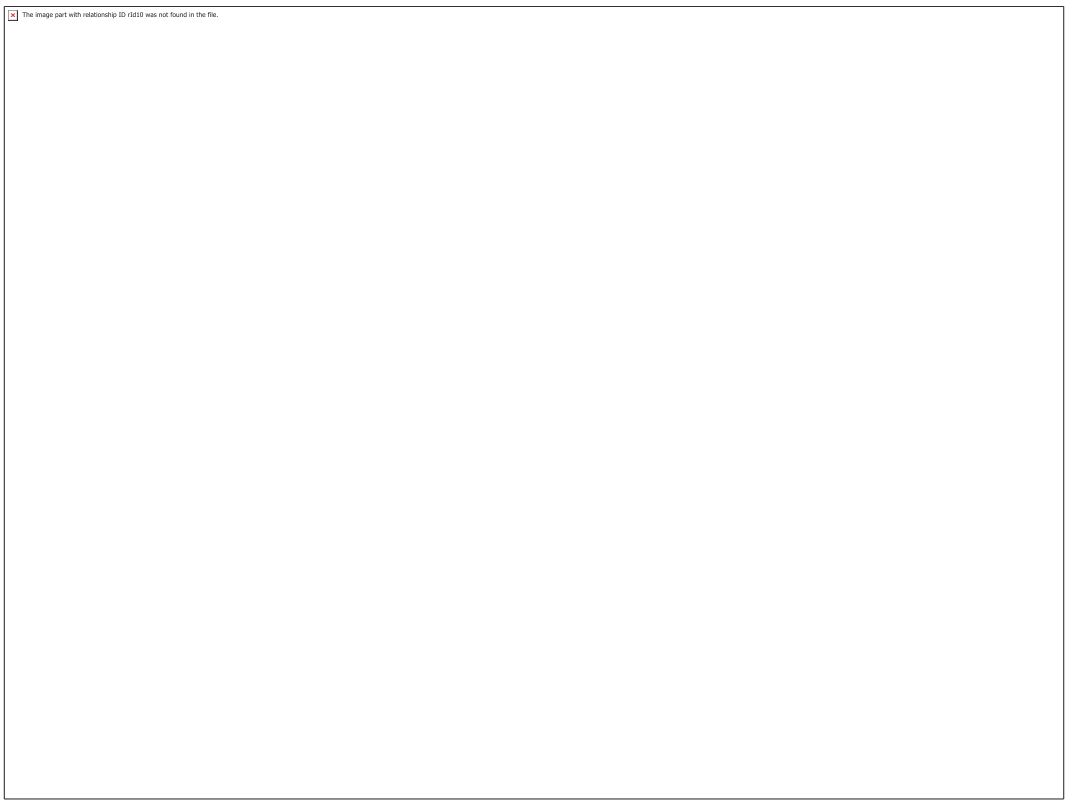

MS/MS spectra of **M10** using Orbitrap-HCD at 65 eV.

MS/MS spectra of **M10** using Orbitrap-HCD at 70 eV.

Appendix 8 – STAN-N-G isomer **M11** fragmentations, applying collision energy between 10 and 70 eV using Orbitrap-HCD

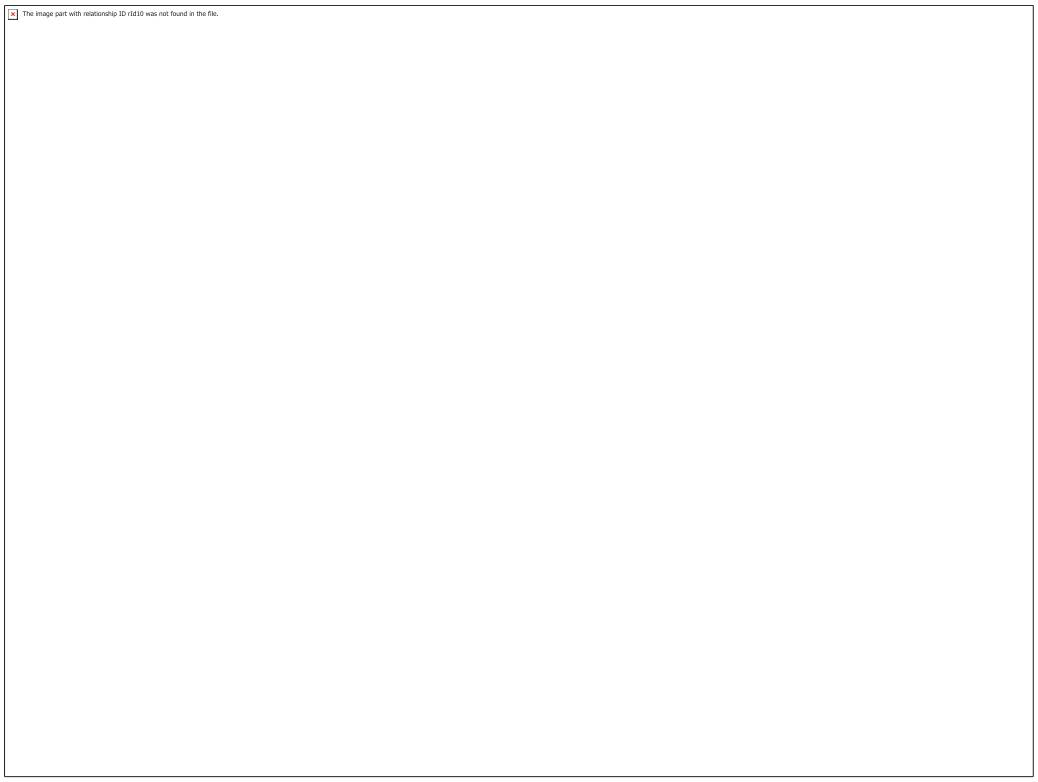

MS/MS spectra of **M11** using Orbitrap-HCD at 10 eV.

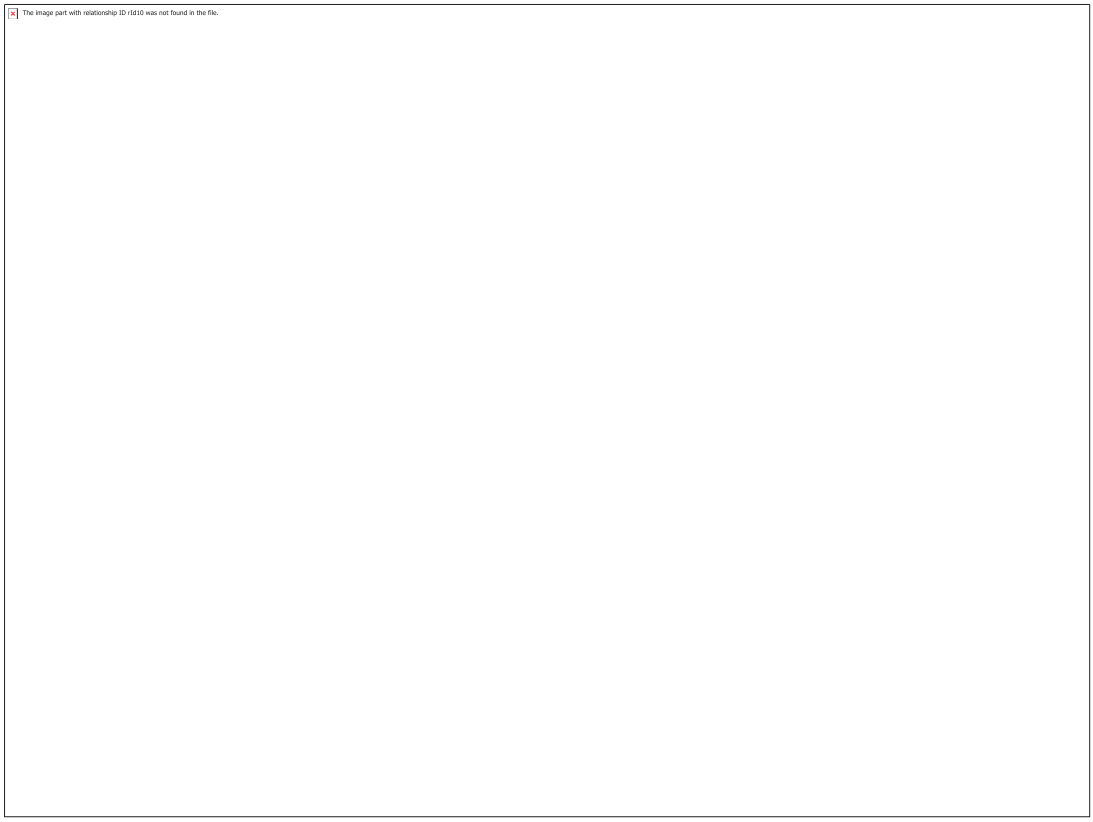

MS/MS spectra of **M11** using Orbitrap-HCD at 15 eV.

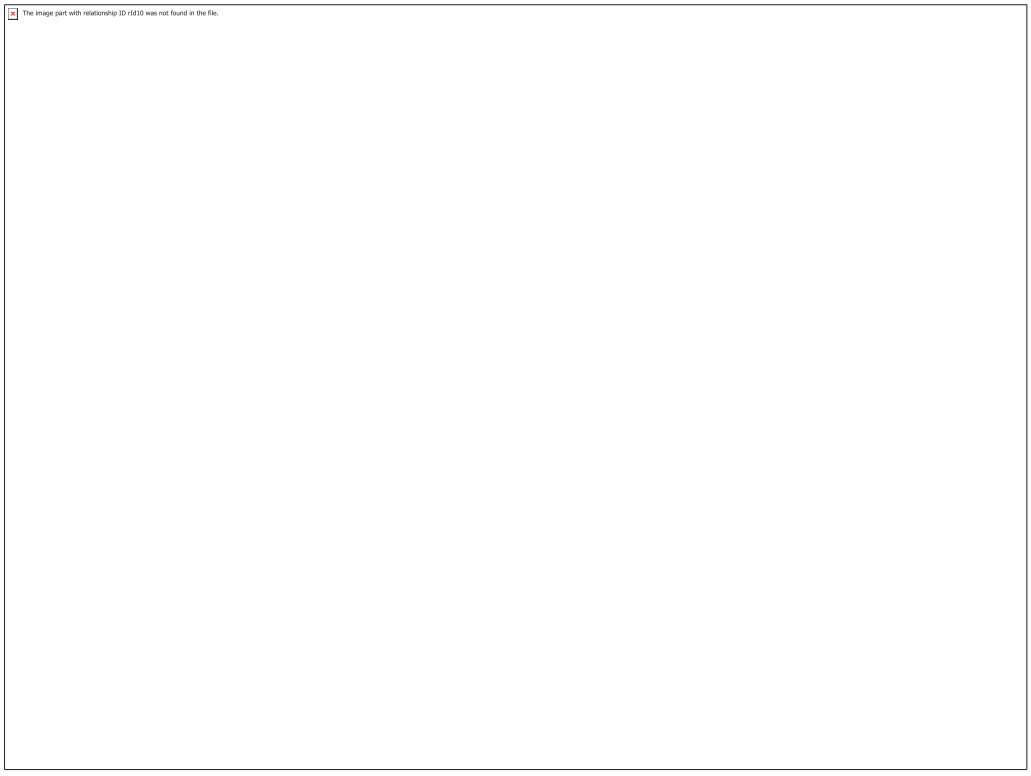

MS/MS spectra of **M11** using Orbitrap-HCD at 25 eV.

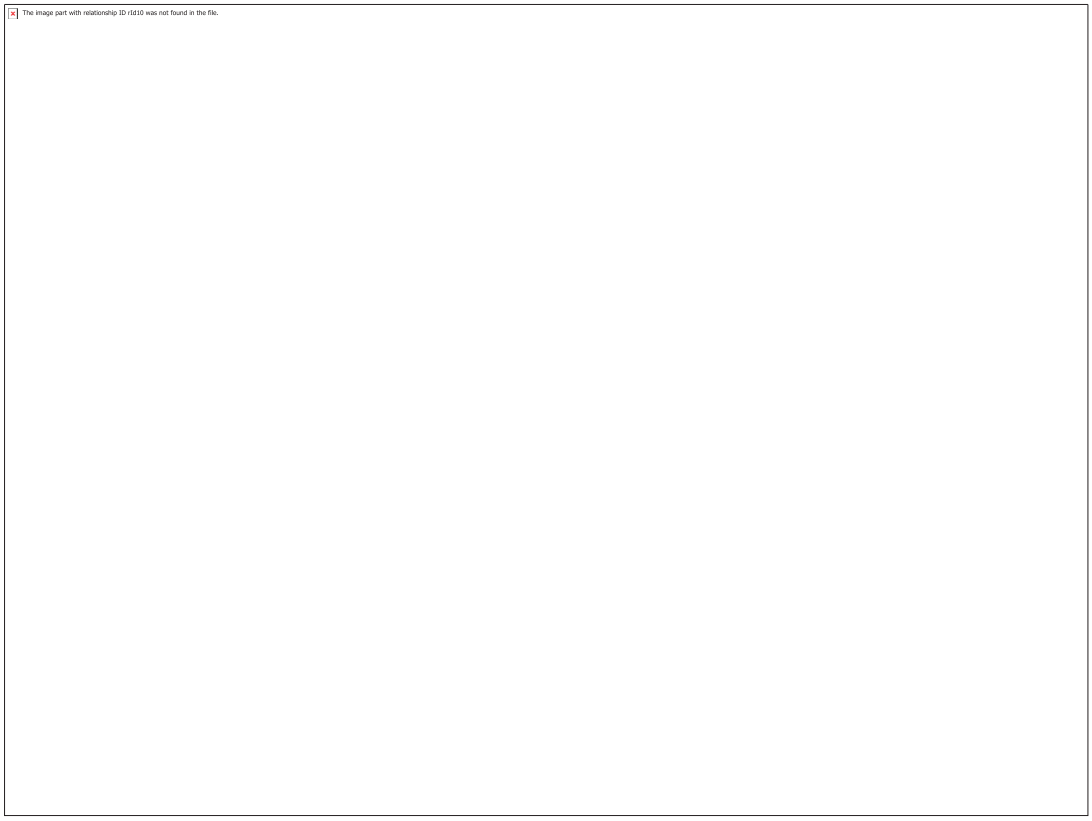

MS/MS spectra of **M11** using Orbitrap-HCD at 33 eV.

MS/MS spectra of **M11** using Orbitrap-HCD at 40 eV.

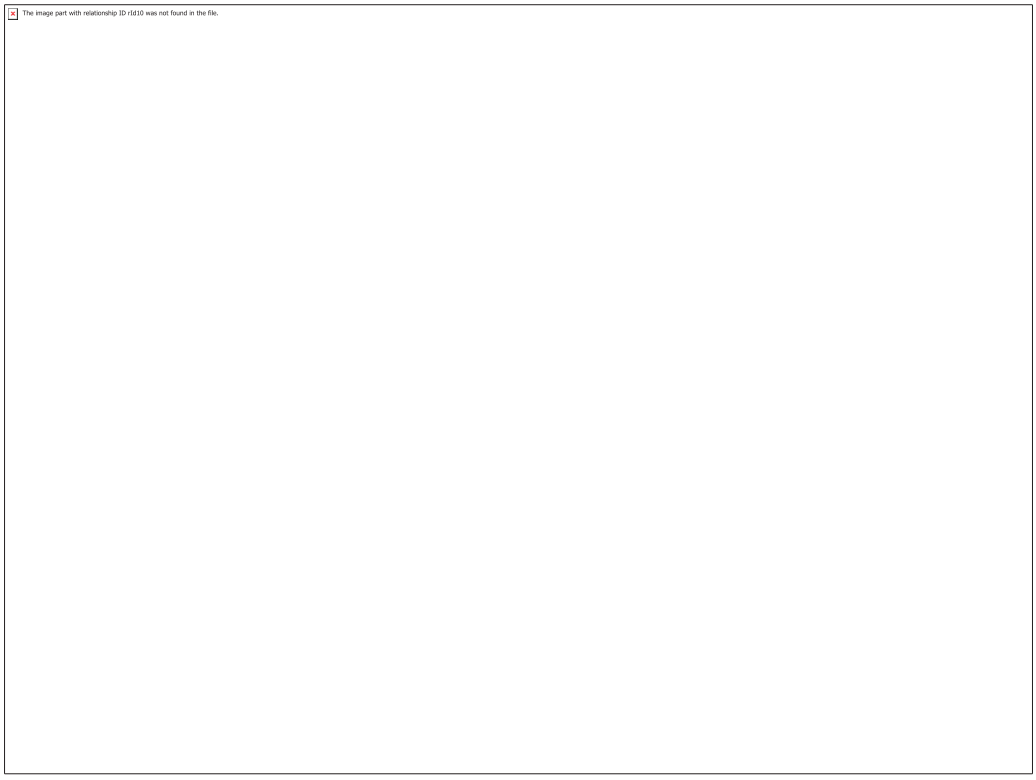

MS/MS spectra of **M11** using Orbitrap-HCD at 45 eV.

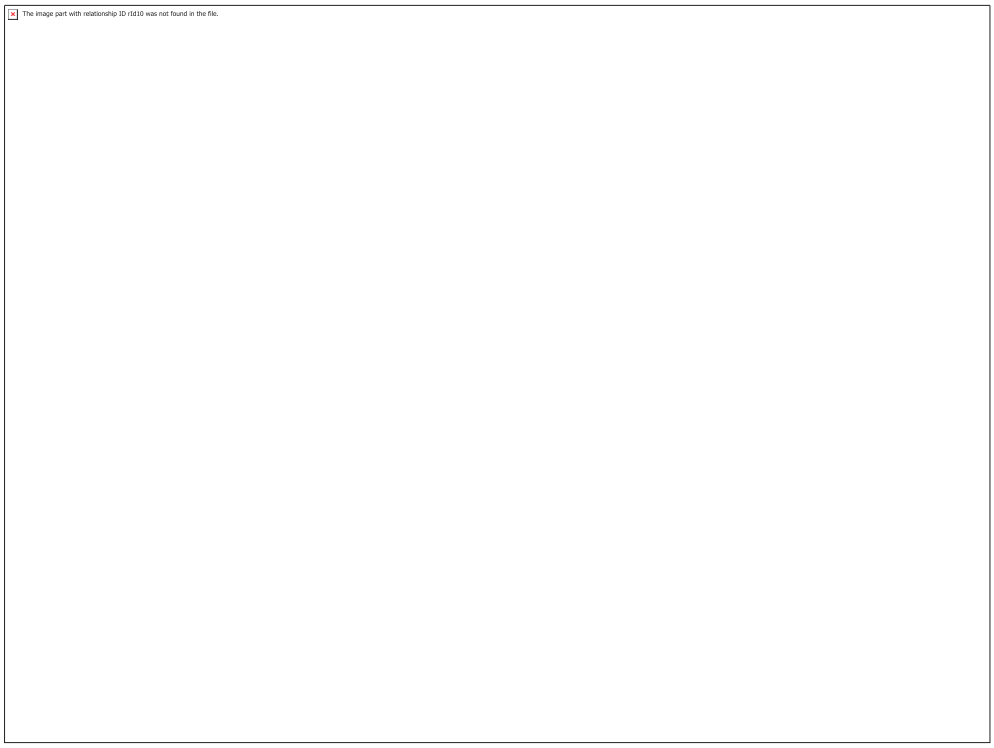

MS/MS spectra of **M11** using Orbitrap-HCD at 55 eV.

MS/MS spectra of **M11** using Orbitrap-HCD at 65 eV.

MS/MS spectra of **M11** using Orbitrap-HCD at 70 eV.